

Operational chemical weather forecasting with the ECCC online Regional Air Quality Deterministic Prediction System version 023 (RAQDPS023) - Part 2: Multi-year prospective and retrospective performance evaluation

5 Michael D. Moran^{1*}, Alexandru Lupu¹, Verica Savic-Jovicic¹, Junhua Zhang¹, Qiong Zheng¹, Elisa I. Boutzis¹, Rabab Mashayekhi², Craig A. Stroud¹, Sylvain Ménard², Jack Chen¹, Konstantinos Menelaou², Rodrigo Munoz-Alpizar², Dragana Kornic², and Patrick M. Manseau²

¹Air Quality Research Division, Environment and Climate Change Canada (ECCC), Toronto, Ontario, Canada

²Canadian Centre for Meteorological and Environmental Prediction, ECC, Montreal, Quebec, Canada

10 *Retired, [ECCC Scientist Emerit](#)

Correspondence to: [Craig Stroud \(craig.stroud@ec.gc.ca\)](mailto:Craig.Stroud@ec.gc.ca)—~~Michael Moran (mike.moran@ec.gc.ca)~~, Alexandru Lupu (alexandru.lupu@ec.gc.ca), or ~~Craig Stroud (craig.stroud@ec.gc.ca)~~[Michael Moran \(mike.moran@ec.gc.ca\)](mailto:Michael.Moran@ec.gc.ca)

Abstract

The operational online version of the Regional Air Quality Deterministic Prediction System (RAQDPS) is a chemical weather forecast system that has been employed ~~operationally~~ by Environment and Climate Change Canada (ECCC) since 2009. It is run twice daily to produce 72 hour forecasts of hourly 10 km abundance fields of three key predictands, NO₂, O₃, and PM_{2.5} total mass, as well as other gas-phase chemical species, PM_{2.5} chemical components, and dry and wet deposition for Canada, the contiguous U.S. and Alaska, and northern Mexico. Version 023 of the RAQDPS (RAQDPS023) went into service at ECCC in December 2021 and was replaced by the RAQDPS025 in June 2024. A companion paper by Moran et al. (2026~~5~~) describes the RAQDPS023 in detail. In this paper we present the results of a five-year performance evaluation of prospective and retrospective annual air quality (AQ) simulations made with the RAQDPS023. The annual simulations considered were the first year of operational RAQDPS023 forecasts in 2021/22 and four years of retrospective annual simulations for the 2013–2016 period that used historical, year-specific emissions. This version of the RAQDPS023, which did not include biomass burning (BB) emissions, is referred to in the text as the RAQDPS-OP023. Forecasts made by the RAQDPS-FW023, a duplicate operational system to the RAQDPS-OP023 except for the addition of ~~near real-time (NRT) time-dependent biomass burning (BB)~~ emissions, were also evaluated for the 2021/22 period. A ~~NRT-near-real-time-~~ measurement data set consisting of hourly NO₂, O₃, and PM_{2.5} surface measurements for Canada and the U.S. was used for the 2021/22 evaluation, whereas a much more extensive set of air-chemistry and precipitation-chemistry measurements was used for the 2013–2016 RAQDPS-OP023 evaluations. Some evaluation results were also compared with results for the 2010–2019 period for forecasts made by earlier operational versions of the RAQDPS and with evaluation results for several peer AQ forecast models. In addition to looking at a number of highly aggregated “headline” scores, many stratified analyses were also performed, including evaluations by network, season, month, hour of day, region, and land-use type. Consideration of simulations for multiple years with the same model ~~but~~ year-specific input emissions helped to identify systematic model errors by reducing the influence of year-to-year variations in meteorology and emissions, and a comprehensive

evaluation for many [additional](#) species for 2013–2016 supported by stratified analyses provided diagnostic insights that allowed the scientific basis for the RAQDPS-[OP023](#) forecasts to be assessed (e.g., were “the right answers [obtained](#) for the right reasons?”). Although one confounding factor for this study was the sizable reduction in the emissions of some pollutants in North America that occurred from 2013 to 2021, it was found that the trends in AQ observations over this period agreed with the year-specific description of emissions used for the five annual simulations from a rank-ordered perspective.

While RAQDPS-[OP023](#) evaluation scores for hourly NO₂ and O₃ volume mixing ratio forecasts were found to be competitive with peer models and often met suggested performance benchmarks for the five simulation years, another key finding was that the RAQDPS-[OP023](#) forecasts consistently underpredicted hourly PM_{2.5} total mass concentrations for all months in 2021/22 and for the majority of months in 2013–2016. The largest underpredictions occurred in summer and at rural stations, whereas overpredictions often occurred in the cold season at urban stations. The model also missed the observed bimodality in monthly PM_{2.5} concentrations and exaggerated the observed diurnal variations in hourly PM_{2.5} concentrations. Additional evaluations with daily PM_{2.5} chemical composition measurements and daily gravimetric PM_{2.5} total mass measurements [from the U.S. PM_{2.5} mass monitoring network](#) were also examined to better understand the hourly PM_{2.5} underpredictions. Consistent overpredictions of elemental carbon and sea salt concentrations and underpredictions of sulfate concentration were identified, but scores for predictions of daily gravimetric PM_{2.5} total mass were better than those for hourly PM_{2.5} total mass, directing attention to differences in measurement methods. SO₂ and HNO₃ levels were also found to be overpredicted in general while NH₃ levels were underpredicted: these three gas-phase species are all PM_{2.5} precursors, which raises concerns about some process representations [in the model](#) such as those for sulfur oxidation and gas-phase dry deposition. As well, springtime O₃ levels were underpredicted while isoprene levels were consistently overpredicted [in all seasons](#). The impact of BB emissions on predictions of NO₂, O₃, and PM_{2.5} was also characterized in detail by comparing evaluation results for the 2021/22 RAQDPS-[OP023](#) and RAQDPS-[FW023](#) forecasts. Negligible impact was found for monthly NO₂ forecasts when BB emissions were included, but monthly O₃ forecast scores [for the RAQDPS-\[FW023\]\(#\)](#) were modestly improved and monthly PM_{2.5} forecast scores were markedly improved from July to September 2021, as well as summer and annual scores. Taken together, the results of this comprehensive multi-year evaluation point to a number of RAQDPS023 system components where improvements are desirable. These results also provide a strong benchmark against which to compare the performance of future versions of the RAQDPS.

1 Introduction

The use of operational short-range air quality (AQ) forecast systems to predict tomorrow’s air quality, also referred to as chemical weather, has expanded rapidly over the last two decades (e.g., Kukkonen et al., 2012; Zhang et al., 2012a,b; WMO, 2020; [Kajino et al., 2018](#); Brasseur and Kumar, 2021; [Wang et al., 2022](#); [Williams et al., 2022](#); [Colette et al., 2025](#); [Li et al., 2025](#)). Environment and Climate Change Canada (ECCC), Canada’s federal environment ministry, which is responsible for operational weather forecasting in Canada, began to make operational regional AQ forecasts

70 in 2001. Since that time, numerous upgrades and improvements have been made to this system (see companion paper
by Moran et al., 2026). Version 23 of the ECCC Regional Air Quality Deterministic Prediction System
(RAQDPS023) became the Canadian operational, continental-scale chemical weather forecast system for North
America on 1 December 2021 (Moran et al., 2021b) and continued in this role until June 2024 (CMC-RAQDPS-025,
2024). One version of the RAQDPS023, which did not include biomass burning (BB) emissions, is referred to in the
75 rest of the paper as the RAQDPS-OP023. There was also a clone of the RAQDPS-OP023 forecast system named the
RAQDPS-FW023, which was identical except for the addition of time-dependent near real time (NRT) biomass
burning (BB) emissions (where “FW”=“FireWork”; Pavlovic et al., 2016; Chen et al., 2019; Chen and Menelaou,
2021). The RAQDPS-OP023 and RAQDPS-FW023 were both run by ECCC twice per day on a 10 km continental
80 grid to produce 72 hour forecasts of hourly surface concentration fields of ozone (O₃), nitrogen dioxide (NO₂),
particulate matter with aerodynamic diameter smaller than 2.5 µm (PM_{2.5}), and other chemical species and compounds.
These forecasts were disseminated internally to ECCC forecast offices and also directly to the public via a public ECCC
website (https://weather.gc.ca/firework/index_e.html, last access: 6 April 2026). This goal of this paper is to present
the results of a multi-year prospective and retrospective performance evaluation of RAQDPS-OP023 AQ predictions,
which both quantifies predictive skill, including the impact of BB emissions, and provides an evaluation benchmark
85 against which the performance of future RAQDPS versions can be compared.

The comparison of AQ model predictions with AQ measurements for a chosen simulation period allows the modelling
system’s performance to be assessed, weaknesses to be identified, and, for some more comprehensive evaluations,
potential improvements to be suggested. Initially, such model performance evaluations considered retrospective
simulations (or hindcasts) for individual or multiple AQ models that were being used in a regulatory environment (e.g.,
90 Dennis and Downton, 1984; Venkatram et al., 1988; Dennis et al., 1993; Tesche et al., 2006; van Loon et al., 2007;
Smyth et al., 2009; Solazzo et al., 2012a,b; Yahya et al., 2014; Im et al., 2015a,b; Appel et al., 2021). In the regulatory
context, however, there is typically interest in both model skill for the simulation period considered and model skill in
predicting AQ changes in response to changes in input emissions or meteorological conditions (e.g., Dennis and
Downton, 1984; Gilliland et al., 2008; Pun et al., 2008; Dennis et al., 2010; Foley et al., 2015; Koo et al., 2015; Colette
95 et al., 2017). For AQ forecasting, by contrast, forecast skill under current conditions is the primary concern (Steyn
and Galmarini, 2008; Dennis et al., 2010).

Zhang et al. (2012a,b) have provided a review of the history of both regional AQ forecasting in North America and
Europe and global AQ forecasting, including performance evaluation approaches, up to 2012. Kukkonen et al. (2012)
provided a similar overview for the same period but focussed on operational European regional-scale AQ forecasting
100 models. Zhang et al. (2012a) noted that the 1998 development in the U.S. of the Aerometric Information Retrieval
Now (AirNow) program (<https://www.airnow.gov>, last access: 8 April 2026), a NRT data repository and dissemination
hub for North American AQ measurements supplied by more than 100 monitoring agencies in the U.S. and Canada,
was revolutionary for North American AQ forecasting since it allowed forecasting teams to obtain immediate feedback
on model performance (e.g., McKeen et al., 2005, 2007, 2009; Eder et al., 2006, 2009, 2010; Mathur et al., 2008;

Field Code Changed

105 Chuang et al., 2011; Chai et al., 2013; Lee et al., 2017; Chen et al., 2021; Campbell et al., 2022; Williams et al., 2022).
A current example of the use of AirNow data for short-term model performance evaluation is ~~in~~ an ongoing multi-
model AQ forecast evaluation for North America that is led by ECCC under the umbrella of the World Meteorological
Organization (WMO) Global Air quality Forecasting and Information System (GAFIS) initiative (see Sect. 4.3).
AirNow data are also used for objective analyses (e.g., Robichaud and Ménard, 2014; Robichaud et al., 2016) and for
110 chemical data assimilation (e.g., Pagowski et al., 2010; Ma et al., 2021).

Formatted: Font: Not Bold

The NRT measurements available from AirNow, however, have three important disadvantages. First, measurements
are only available for six chemical compounds: NO₂, O₃, CO, SO₂, PM_{2.5}, and PM₁₀. Second, AirNow is a “meta-
network” since the multiple agencies contributing measurement data may employ different instruments and sampling
techniques, each with their own biases and errors, to measure the same chemical species. As a consequence, there can
115 be considerable heterogeneity in a combined AirNow measurement data set vs. the uniformity expected of a typical
measurement network data set. And third, the AirNow measurements must be viewed as preliminary since they have
not undergone the quality assurance/quality control (QA/QC) procedures normally applied by the monitoring agencies
before they release new data sets.

The more traditional source of AQ measurement data is to obtain them directly from the lead agency for a monitoring
120 network or from an AQ measurement data clearinghouse such as AQS or NAtChem (see Table S2a in the Supplement).
However, these finalized network data sets suffer from the significant disadvantage of only being available anywhere
from three months to years after ~~samplingsamples were collected~~, since some AQ measurements require post-sampling
calibration while others (e.g., from filterpacks, annular denuders, passive samplers, and precipitation samplers) must
undergo laboratory analysis after collection followed by network QA/QC procedures. But such finalized data sets do
125 have three important advantages over the NRT AirNow data. First, they include measurements of many additional
chemical species, including more trace gases such as nitric acid (HNO₃), ammonia (NH₃), and some individual volatile
organic compounds (VOCs), PM_{2.5} chemical components, and major inorganic ions in precipitation. Second, even for
the six pollutants that are reported to AirNow, not all North American stations that measure these species report to the
AirNow data centre. And third, these finalized data sets have been QA/QCed before release. For example, Chai et al.
130 (2013) compared AirNow and AQS hourly O₃ measurements for 2010 and showed scatterplots of differences between
the two data sets for a one-month period. The issue of availability, however, means that these finalized AQ network
data sets cannot be used for the immediate evaluation of AQ forecasts, that is, for prospective AQ simulations, but they
are preferable for the evaluation of historical or retrospective AQ simulations since they permit more comprehensive
evaluations of predictions of the atmospheric chemical environment using a broader range of QA/QCed measurement
135 data.

Formatted: Font: Not Bold

A paper by Dennis et al. (2010) proposed a framework for evaluating AQ model performance that consists of four
evaluation types: operational; diagnostic; dynamic; and probabilistic. The first two evaluation types are the most
relevant for evaluating deterministic AQ forecasts. Operational evaluations address the basic question of how well
model predictions of chemical concentrations and deposition agree with observations of chemical concentrations and

140 deposition. To do this they use routine measurements of a small set of air-chemistry species, and, infrequently,
additional air-chemistry, precipitation-chemistry, and meteorological parameters, to calculate standard statistical
performance ~~me~~tricasures (e.g., Table A2). Diagnostic evaluations, on the other hand, are less common. They ~~and~~
are used to evaluate model inputs and process representations by considering many additional relevant observations such
as precursor concentrations, pollutant concentrations aloft, PM chemical composition and size distributions, and
145 meteorological parameters that have a direct impact on pollutant concentrations such as temperature, planetary
boundary layer (PBL) height, vertical wind profiles, cloud cover, and precipitation (e.g., Vautard et al., 2012).
Diagnostic evaluations can address three additional important questions. First, is agreement between model predictions
and observations the result of chance or of good scientific understanding and representation of atmospheric dynamics,
physics, chemistry, and emissions? Put another way, is the model getting the right answers for the right reasons?
150 Second, are differences between model predictions and observations due to errors in model input fields or to gaps or
errors in model process representations or to computational ~~facto~~res~~erro~~rs? And third, can the identification of the
sources of differences between the model predictions and observations be used as a guide to improve the model?
Dynamic evaluations, the third of these evaluation types, assess model skill in quantifying the impact of changes in
input emissions or meteorology (e.g., Gilliland et al., 2008; Godowitch et al., 2010; Foley et al., 2015). And fourth,
155 probabilistic evaluations examine the uncertainty and level of confidence in model predictions (e.g., Hanna et al., 2005;
Mallet and Sportisse, 2006; Galmarini et al., 2010; Kioutsioukis et al., 2025).

Many operational evaluations have considered only a small number of observed species even if finalized measurement
data sets were used (e.g., Chai et al., 2013; Pan et al., 2014; Marécal et al., 2015; Wagner et al., 2015; Lee et al., 2017;
Campbell et al., 2022; and Williams et al., 2022). Given the complexity of atmospheric chemistry related to secondary
160 pollutants such as O₃ and to the multiple chemical components of PM (e.g., Sillman, 1999; Meng et al., 1997;
Bachmann, 2013), however, such limited evaluations will not provide insights into the reasons for poor model
performance. A comprehensive operational evaluation, on the other hand, which makes use of the full range of
available AQ measurements, can consider nearly complete mass budgets for some chemical families such as sulphur
species or oxidized nitrogen species and hence may be considered closer to a diagnostic evaluation. Comprehensive
165 operational evaluations, however, are relatively uncommon. For example, Huang et al. (2021) reviewed over 300 peer-
reviewed articles that reported evaluation results from AQ modelling studies for China and found that very few
considered more than seven pollutants. Nevertheless, examples of comprehensive operational evaluations include
publications by Biswas et al. (2001), Hogrefe et al. (2001a,b), Zhang et al. (2006a,b), Cai et al. (2008), Yu et al. (2008),
Zhang et al. (2009a), ~~Hogrefe et al. (2015)~~, Yahya et al. (2014, 2015), Hogrefe et al. (2015), Tessum et al. (2015),
170 Zhang et al. (2016), Chen et al. (2021), and Wang et al. (2021). Lastly, examples of diagnostic evaluations include
Zhang et al. (2006c, 2009b), Godowitch et al. (2011), Gan et al. (2015), Knote et al. (2015), Galmarini et al. (2021),
and Clifton et al. (2023).

This paper presents the results of an operational performance evaluation of both AQ forecasts and AQ hindcasts made
by the RAQDPS-OP023 chemical weather forecast system. Evaluations were performed for five simulation years:

175 (i) the first year of RAQDPS-OP023 (and RAQDPS-FW023) forecasts from 1 June 2021 to 31 May 2022, which used
 projected anthropogenic input emissions files; and (ii) four years of retrospective annual simulations for the 2013–2016
 period performed with the equivalent RAQDPS-OP024 forecast system (same system but ported to a new computer;
 see companion paper by Moran et al., 2026⁵) but using historical, year-specific input emissions files. Note that from
 180 1 June to 30 November 2021 the RAQDPS-OP023 and RAQDPS-FW023 systems were run in a parallel (i.e., pre-
 operational) mode beside the RAQDPS-OP022 and RAQDPS-FW022 systems that were operational at that time before
~~being the former were~~ promoted to operational status on 1 December 2021 (Moran et al., 2026). In addition, the
 performance of a decade of operational forecasts made by earlier RAQDPS versions from 1 January 2010 to 30 June
 2019 is also examined both to show the evolution of forecast skill over this period and to allow comparison with
 RAQDPS-OP023 scores. Note that RAQDPS-FW023 retrospective simulations for 2013–2016 ~~have not been~~
 185 ~~considered here were not available~~ due to the incompatibility ~~with for this~~ earlier period of version 4.1 of the Canadian
 Forest Fire Emissions Prediction System (CFEPEPS), ~~which was~~ used by the RAQDPS-FW023 ~~to calculate BB~~
~~emissions~~. CFEPEPS v4.1, which depends on a satellite instrument launched in 2017, was not introduced until 2021
 (Chen and Menelaou, 2021; Moran et al., 2026⁵). Given that BB emissions also have large year-to-year variations
 (e.g., Table A4), their neglect may complicate identification of systematic model errors, especially for the summer
 190 months. The impact of this omission ~~for 2021/22~~ is examined ~~for 2021/22~~ in Sect. 4.2.

AirNow data have been used for the performance evaluation of the 2021/22 forecasts since not all finalized network
 measurement data sets were available for that period during the preparation of this paper. The use of AirNow data
 does reflect common practice for AQ forecast performance evaluations in the near term and is also consistent with
 evaluation results for previous RAQDPS operational versions for the 2010–2019 period, which also employed AirNow
 195 data (Sect. 4.1). On the other hand, the use of AirNow data limits the number of chemical species that can be
 considered, and 2021/22 analyses were only performed for NO₂, O₃, and PM_{2.5} total mass. For the four years of
 retrospective annual runs, however, a much broader set of finalized AQ measurement data, including PM_{2.5} speciation
 measurements and precipitation-chemistry measurements, was available and was used to carry out as broad and
 comprehensive an evaluation of model performance as possible. The performance evaluation ~~results~~ reported here
 200 ~~includes~~ analyses stratified by different measurement characteristics to identify which network, species, month, hour
 of day, region, and land-use type resulted in the most skillful and the least skillful model predictions. Both Canadian
 and U.S. AQ measurement data sets were considered for all five years in order to expand the spatial coverage of the
 evaluation. This differs from many past evaluations of AQ model performance over North America that have only
 considered U.S. AQ measurements (e.g., Tessum et al., 2015; Yahya et al., 2015; Appel et al., 2017; Toro et al., 2021),
 205 although there are exceptions (e.g., Appel et al., 2021). One complicating factor for this study was that emissions of
 some anthropogenic pollutants decreased materially between 2013 and 2021 (see Sect. 2.2), but this factor was also
~~positive-helpful~~ in that it allowed examination of the representativeness of the input model emissions that were used
 and constituted a dynamic evaluation of opportunity (cf. e.g., Gilliland et al., 2008; Godowitch et al., 2010; Foley et al.,
 2015). The consideration of a total of 15 simulation years facilitated the identification of systematic model biases and

Formatted: Font: Not Bold

210 errors by revealing common patterns across years and reducing the importance of year-to-year variations in emissions
 and in meteorology, including ~~its~~ [the latter's](#) impact on biogenic emissions.

The rest of this paper is organized as follows. Section 2 describes the study methodology, including the model configuration, run setup, and input emissions used to perform the 2013–2016 retrospective annual runs, the AQ measurement data sets used for the evaluation, the data processing and data filtering applied for model-measurement
 215 pairing, and the techniques and evaluation metrics used for the performance evaluation. Section 3 and the Supplement (S) present results of the RAQDPS-~~OP~~023 performance evaluation for 2021/22 and 2013–2016, where Sect. 3 focuses on aggregate annual analyses for air- and precipitation-chemistry measurements and the Supplement presents more detailed analyses ~~ies~~ [results](#) stratified by network, season or month, hour of day, region, or land-use. Section 4 then compares RAQDPS-~~OP~~023 performance relative to 2010–2019 RAQDPS-~~OP~~ forecast performance and ~~to~~ 2021/22
 220 RAQDPS-FW023 performance, summarizes RAQDPS-~~OP~~023 and RAQDPS-FW023 performance vs. four peer AQ forecast systems, and discusses RAQDPS-~~OP~~023 shortcomings revealed by the evaluations. Lastly, Sect. 5 presents a summary and conclusions.

2 Methodology

2.1 Modelling system configurations and setups

225 The model configuration and run setup of the RAQDPS-~~OP~~023 [and RAQDPS-FW023](#) for the 2021/22 forecasts has been summarized in CMC-RAQDPS-023 (2021) and described in detail [in the companion paper](#) by Moran et al. (2026~~5~~), ~~so o-~~ only a short overview will be given here. Some key aspects include the use of the following: (1) version 5.1.0 of the ECCO Global Environmental Multiscale (GEM) numerical weather prediction (NWP) model code and version 3.1.0.0 of the Modelling Air quality and Chemistry (MACH) chemical weather module code, which is
 230 embedded within the GEM code; (2) a ~~rotated~~-limited-area [rotated](#) latitude-longitude grid covering North America and adjacent oceans (e.g., Fig. 13) with 10-km horizontal grid discretization and 84 staggered vertical hybrid levels capped by a model lid at 0.1 hPa; (3) a two-time-level iterative-implicit time integration scheme and three-dimensional semi-Lagrangian advection scheme used with a 300 s meteorological time step and a 900 s chemistry time step; (4) imposed tracer mass conservation with an iterative, locally mass-conserving monotonicity correction and a Bermejo-Conde
 235 (2002) global mass fixer; (5) a simplified two-bin sectional representation of the PM₁₀ size distribution (diameter ranges of 0–2.5 μm and 2.5–10 μm); (6) PM dry chemical composition represented by eight chemical compounds [sulfate (SO₄), nitrate (NO₃), ammonium (NH₄), elemental carbon (EC), primary organic matter (POM), secondary organic matter (SOM), crustal material (CM), and sea salt (SS)]; (7) ~~42~~ prognostic gas-phase chemical compounds and 16 prognostic particle-phase section-compounds (i.e., ~~two~~2 size bins x ~~eight~~8 compounds); (8) ADOM-2 gas-phase
 240 chemistry mechanism, ADOM aqueous-phase chemistry mechanism, HETV inorganic heterogeneous chemistry mechanism, and Instantaneous secondary organic Aerosol Yield (IAY) scheme; (9) parameterizations of aerosol particle nucleation, condensation/evaporation, coagulation, dry deposition and sedimentation, hygroscopic growth, and

activation; and (10) parameterizations of gas-phase dry deposition and in-cloud and below-cloud scavenging of particles and soluble gases.

245 The configuration and setup used for the 2013–2016 retrospective annual runs followed those of the RAQDPS-~~OP023 operational~~-2021/22 forecasts as closely as possible, but some differences could not be avoided as the retrospective simulations were performed later and outside of the operational environment. One major (and deliberate) difference was the replacement of the RAQDPS-~~OP023 operational~~-projected anthropogenic input emissions files (see Moran et al., 2026) with year-specific anthropogenic input emissions files based on historical year-specific emissions inventories
250 for 2013–2016 (see next section). A minor (but unavoidable) difference was the need to use an equivalent modelling system (RAQDPS-~~OP024~~) for the 2013–2016 hindcasts due to the migration with minimum changes of all ECCC operational and research computing applications to a new supercomputer in late June 2022. In addition, there were a few more minor differences related to near-surface vertical diffusion, model initialization and spin-up, meteorological piloting, and simulation run strategy, whose impacts were small.

255 First, the RAQDPS-~~OP023 operational~~-runs for 2021/22 employed two code adjustments related to near-surface vertical diffusion to avoid the possibility of predicting extremely high surface concentrations due to the combination of high surface emissions, an extremely stable PBL, and very low wind conditions such as might occur during northern winter nights under a strong anticyclone. As described in the companion paper by Moran et al. (2026), one pre-emptive adjustment was to impose a minimum PBL height of 100 m when calculating the vertical
260 diffusion of chemical tracers (where free-atmosphere convection applies above the PBL top); the other was to inject surface emissions into the lowest two model layers instead of the lowest layer (61 m thickness vs. 20 m thickness). For the four years of retrospective runs, however, these two adjustments were removed so that whatever PBL height was forecast by GEM was used in defining the vertical diffusivity profile and surface emissions were injected into the lowest (20 m thick) model layer. The reason for doing so was to test over a four-year period whether the two
265 operational adjustments were needed.

A different approach was also used to maximize the dynamical balance between the mass and momentum fields in the meteorological initialization step. The operational forecast runs for 2021/22 employed an hourly incremental analysis update (IAU) approach from T-3 to T+3 hours, where T=0 is the run start time (e.g., Bloom et al., 1996). For the retrospective runs, on the other hand, a digital filter was employed at T=0 (Fillion et al., 1995). This difference was
270 necessary because archived analyses for T-3 hours were not available for the 2013–2016 period.

The hourly meteorological lateral boundary conditions (LBCs) supplied by a meteorological “piloting” model for the retrospective runs also had a different source. For the 2021/22 operational forecasts these were supplied by version 8.0.0 of the operational 10-km Regional Deterministic Prediction System (RDPS), a limited-area-model configuration of GEM v5.1.0 that was run by ECCC to make meteorological forecasts for North America in advance of the RAQDPS-
275 ~~OP023 and RAQDPS-FW023 runs~~ (Moran et al., 2026). The RDPS 8.0.0 horizontal grid was a superset of the RAQDPS-~~OP023~~ horizontal grid and its vertical levels were identical with those of the RAQDPS-~~OP023~~ (CMC-

RDPS-8.0.0, 2021). For the retrospective runs, on the other hand, the meteorological LBCs were supplied from special [hindcast](#) runs of a 15-km global configuration of GEM 5.1.0. This change avoided the need to run both global and regional versions of GEM [for the 2013-2016 period](#), and previous tests had shown that the use of a meteorological piloting model with 10 km vs. 15 km grid spacing had very little impact on RAQDPS forecasts.

Lastly, simulation run length was the source of one more difference. [The twice-daily RAQDPS-OP023 and RAQDPS-FW023](#) operational forecast runs were 72 hours in length and were initialized at T-3 hours using the T+9 hour forecast fields from the previous RDPS [8.0.0](#) run launched 12 hours earlier. To save computer time the [twice-daily RAQDPS-OP023](#) retrospective runs were only 18 hours in length and were initialized at T=0 hours using the T+12 hour forecast [meteorological](#) fields from the previous global GEM run [and T+12 hour forecast chemical fields from the previous RAQDPS-OP023 run](#). In both cases, though, annual sequences of hourly predicted [meteorological and chemical](#) fields were prepared by concatenating hourly predictions for only the first 12 forecast hours of each [RAQDPS-OP023](#) run (i.e., T+1 to T+12 hours).

2.2 Input emissions

The RAQDPS-[OP023](#) and [RAQDPS-FW023](#) 2021/22 forecasts used the SET4.0.0 anthropogenic emissions data set described by Moran et al. (2021b, 2026~~5~~). The SET4.0.0 emissions were based on a projected 2020 Canadian national [annual anthropogenic](#) emissions inventory and projected 2023 U.S. and Mexican national [annual anthropogenic](#) emissions inventories, which were roughly in temporal alignment with the [2021/22](#) forecast period. Note, though, that it was not possible to modify the SET4.0.0 emissions in near-real time to account for rapidly evolving emissions changes in North America associated with [large-scale public-health responses to the global](#) COVID-19 pandemic (cf. Mashayekhi et al., 2021).

To provide year-specific [anthropogenic](#) input emissions files for each of the 2013–2016 retrospective annual runs, however, a concerted effort was made to use recently available and consistent national [annual anthropogenic](#) emissions trend data sets for Canada, the U.S., and Mexico. Each of these national emissions trend data sets provides a multi-decadal sequence of annual anthropogenic national emission inventories that were generated using largely consistent emissions estimation methodologies for all of the years considered by each data set. Four year-specific annual anthropogenic national emission inventories were extracted for the 2013–2016 period for Canada from the ECCC TREND16 emissions trend data set. Similarly, four year-specific annual anthropogenic national emission inventories were extracted for the 2013–2016 period for the U.S. from the U.S. EPA EQUATES (EPA's [Air QUALity Time Series](#)) national emissions trend data set. The EQUATES data set also includes a set of annual anthropogenic national emissions inventories ~~and annual wildfire emissions inventory files~~ for 2002-2019 for Mexico, so that year-specific Mexican inventories for the 2013–2016 period were also available. More details about these [emissions](#) data sets are provided in [Sect. S2.2 of the Supplement](#).

Formatted: Font: Not Bold

310 Model-ready emissions files for the years 2013–2016 were then prepared from these national inventories using version
4.8 of the Sparse Matrix Operator Kernel (SMOKE) emissions processing system
(<https://www.cmascenter.org/smoke/>; last access: 6 April 2026; Zhang et al., 2018b). The use of an emissions
processing system was necessary because while the national inventories of the three countries report annual emissions
of seven criteria air pollutants by jurisdiction (province, county, or state), the RAQDPS-OP023 requires gridded
315 emissions fields for each emitted model species for every hour of every day of the year (e.g., Dickson and Oliver, 1991;
Houyoux et al., 2000; Matthias et al., 2018; Zhang et al., 2018b). ~~D~~Additional details about the processing of these
anthropogenic emission inventories with SMOKE are provided in Sect. S2.2.

Several types of natural emissions were also accounted for. Time-varying biogenic emissions were included in all five
annual simulations, where biogenic emissions were calculated for each time step of the RAQDPS-OP023 simulations
320 using code for a modified version of the Biogenic Emission Inventory System (BEIS) v3.09 biogenic emissions
algorithms. ~~with~~ Inputs of two GEM-predicted meteorological fields were required: surface temperature and solar
insolation (Moran et al., 2026). Time-varying sea-salt emissions were also included for all five annual simulations;
these emissions were calculated for each chemistry time step based on surface wind speed. Hourly BB emissions, on
the other hand, were only considered in the 2021/22 RAQDPS-FW023 forecast runs (Sect. 4.2). Note that some BB
325 emissions might be due to very large prescribed burns or grass fires as well as wildfires if these were detected by
satellite (Moran et al., 2026). Note also that neither system version considered some other types of natural emissions,
namely natural wind-blown fugitive dust emissions, lightning emissions, pollen and other biological emissions, other
marine emissions, and volcanic emissions, but these sources were assumed to be less important for Canada (see Moran
et al., 2026).

330 Table 1 presents a summary of annual inventory emissions of the seven criteria pollutants for Canada, the U.S., and
Mexico for the five years for which annual RAQDPS-OP023 runs were performed. The rows named “Total Anthro”
and “Total Biogenic”, on the other hand, are ~~respectively~~, the annual, SMOKE-processed anthropogenic emissions
and the annual, ~~dynamically~~BEIS-calculated biogenic emissions within the model domain that the model “sees” (i.e.,
responds to). The domain-total “Total Anthro” and “Total Biogenic” values thus include all Canadian emissions but
335 only U.S. emissions from the 48 contiguous U.S. states and part of Alaska and exclude emissions from the rest of
Alaska, Hawaii, and some U.S. territories in the Caribbean and the Pacific Ocean and only include Mexican emissions
from the 340 Mexican counties out of 2,457 that lie completely or partially within the RAQDPS-OP023 domain (e.g.,
Fig. 13). This spatial exclusion of emissions is the reason that the “Total Anthro” values are consistently lower than
the “3 Country EIs” values for all inventory species. In addition, the domain-total SMOKE-processed values for “Total
340 Anthro” PM_{2.5} and PM₁₀ emissions are also considerably lower than total inventory values due to the impact of
adjustments for land-use-dependent, near-source removal due to settling and impaction (i.e., transportable fraction TF),
but further meteorology-dependent emission reductions due to snow cover and wet soil were only applied during the
RAQDPS-OP023 simulations (Moran et al., 2026).

Some significant changes are evident in annual emissions over this nine-year time period in Table 1, first over the four-year period from 2013 to 2016, then from 2016 to 2021/22, and in total from 2013 to 2021/22. For example, North American “Total Anthro” SO₂ emissions decreased by 37% from 2013 to 2016 and then by a further 37% from 2016 to 2021/22, for a total decrease of 60% relative to 2013, while “Total Anthro” NO_x emissions decreased by 19%, 22%, and 36% for the same three periods. “Total Anthro” VOC and CO emissions also decreased over the three periods, by 8%, 1%, and 9% for VOC emissions and by 13%, 14%, and 25% for CO emissions. “Total Anthro” NH₃ emissions, on the other hand, were nearly constant during the 2013–2016 period but then increased in Canada while decreasing in the U.S. and Mexico in 2021/22 for an overall domain-total decrease of 6% from 2013 to 2021/22. ~~Lastly, the domain-total SMOKE-processed values for “Total Anthro” PM_{2.5} and PM₁₀ emissions are considerably lower than total inventory values due to the impact of adjustments for land use dependent, near source removal due to settling and impaction (i.e., transportable fraction), but further meteorology-dependent emission reductions due to snow cover and wet soil are only applied during the RAQDPS023 simulation (Moran et al., 2025).~~

Table 1 also compares SMOKE-processed, domain-total annual anthropogenic emissions with calculated domain-total annual biogenic emissions of NO_x and VOCs. Biogenic NO emissions can be seen to have contributed 4% of domain-total NO_x emissions in 2013, rising to 6% in 2021/22 as anthropogenic NO_x emissions decreased and biogenic NO emissions increased. By contrast biogenic VOC emissions contributed 78% of domain-total VOC emissions in 2013, a considerably much larger percentage, and then rose to 81% in 2021/22 as anthropogenic VOC emissions declined and biogenic VOC emissions increased. In addition, Table S1 compares the seasonal variation of the SMOKE-processed SET4.0.0 anthropogenic emissions for 32 model species and the biogenic emissions of four model species. Seasonal variations depend strongly on both the pollutant and its source types and can have markedly different cycles. For example, NH₃ is primarily emitted by agricultural activities and can be seen to have a pronounced winter minimum and summer maximum, whereas seasonal emissions of two lumped model VOC species, ALD2 (acetaldehyde and higher aldehydes) and CRES (cresols and phenols), have a pronounced winter maximum and summer minimum consistent with their dominant source being residential wood combustion. For most anthropogenic species, however, seasonal variations were considerably smaller, including SO₂, NO, and NO₂. Although fossil-fuel power generation is important for both SO₂ and NO_x emissions, this suggests that at the continental scale the increased power load for space heating in the winter in North America is roughly balanced by the increased power load for air conditioning in the summer. The seasonal variation of biogenic emitted species emissions, on the other hand, was more like NH₃; they had strong seasonal cycles with winter minima and summer maxima. In fact, biogenic isoprene (C₅H₈) emissions were predicted to have the most pronounced domain-level seasonal cycle, increasing from just 2% in the winter to 65% in the summer (Table S1).

Formatted: Subscript

Formatted: Subscript

2.3 Air-chemistry and precipitation-chemistry observations

Routine air-chemistry and precipitation-chemistry measurements are available from multiple measurement networks operating in Canada and the U.S. The hourly measurements of abundances of NO₂, O₃, and PM_{2.5} total mass made by continuous instruments that are reported in near-real time by some agencies to the U.S. EPA’s AirNow program (Dye

et al., 2004; Wayland et al., 2004; Zhang et al., 2012a) have already been mentioned. AirNow hourly measurement data for NO₂, O₃, and PM_{2.5} from U.S. monitors have been combined in this study with NRT NO₂, O₃, and PM_{2.5} hourly measurement data from Canadian National Air Pollution Surveillance (NAPS) monitors that report directly to ECCC's Canadian Meteorological Centre (CMC). This combined NRT data set has been used to evaluate the 2021/22 RAQDPS-OP023 and RAQDPS-FW023 operational forecasts of these species.

The use of these NRT abundance measurements, which are considered to be preliminary, for model evaluation is consistent with the operational nature of the RAQDPS-OP023 forecasts. Two automated data filters were applied by CMC to the AirNow and NAPS NRT measurements upon receipt before they were used for model evaluation or other purposes such as operational air pollutant objective analyses (e.g., Robichaud et al., 2016). The first filter flagged negative abundance values and above-threshold abundance values as suspicious (NO₂ levels over 200 ppbv, O₃ levels over 200 ppbv, PM_{2.5} levels over 300 µg·m⁻³) or invalid (NO₂ levels over 2000 ppbv, O₃ levels over 500 ppbv, PM_{2.5} levels over 1000 µg·m⁻³), while the second filter flagged large jumps in abundances between consecutive hours as suspicious (over 30 ppbv for NO₂, over 60 ppbv for O₃, over 90 µg·m⁻³ for PM_{2.5}). Values flagged as suspicious or invalid were not used for this study. Measurements from stations located near roadways were discarded as well to ensure spatial representativeness. A temporal completeness criterion was also imposed on this NRT measurement data set to ensure temporal representativeness of the evaluation data: individual station data sets were required to have at least 75% valid values out of the total possible values for a one-year evaluation period to be considered complete. More details about these representativeness constraints are provided in Sect. S2.4. Table 2 lists the number of available AirNow and NAPS stations for 2021/22 that measured hourly O₃, NO₂, and PM_{2.5} abundances and the number with complete data records while Figure S2 shows the locations of these all stations measuring each of these three species. Note that some stations only measured one or two of these species.

The evaluation of the retrospective annual simulations for 2013–2016, on the other hand, was based on finalized AQ network data sets. The CAPMoN and NAPS networks in Canada and the AMoN, AQS, CASTNET, CSN, IMPROVE, NATTS, and PAMS networks in the U.S. provide finalized air-chemistry measurement data sets for various chemical species, including hourly NO₂, O₃, and other gas-phase species (e.g., SO₂, CO, HNO₃, ~~and~~ NH₃, ethene (C₂H₄), formaldehyde (HCHO), and C₂H₆), hourly PM_{2.5} and PM₁₀ mass, daily FRM (Federal Reference Method) and FEM (Federal Equivalent Method) PM_{2.5} mass (e.g., Demerjian, 2000; Noble et al., 2001; Gantt, 2022), and daily PM_{2.5} chemical composition, while the CAPMoN network in Canada and the NADP network in the U.S. provide finalized precipitation-chemistry measurement data sets. Details about each of these networks are given in Table S2a, and Sect. S2.3 provides some additional information about daily PM_{2.5} measurements. Note that all network data sets used in this study were accessed on 24 June 2024 (relevant because these data sets are always subject to change even years after their original release). Table 2 and Tables S2b-d list the number of stations for each network for 2013–2016 with available measurements and with complete measurements of various chemical species (~~seeef~~ Sect. S2.4), while Figs. S3–S6 show the locations of available stations by network. It is clear from these four figures that spatial coverage varies widely by the species being measured.

Formatted: Subscript

Formatted: Subscript

Formatted: Subscript

Formatted: Subscript

Although AQ measurements provide important chemical information about the real atmosphere, these measurements, like AQ model predictions, also have biases and errors. For example, NO₂ measurements made with chemiluminescence monitors frequently have positive biases due to interference from other oxidized nitrogen species (e.g., Dunlea et al., 2007; Lamsal et al., 2015; [Dickerson et al., 2019](#)), and NH₃ measurements made with passive monitors have negative biases (Puchalski et al., 2011). Measurements of both PM_{2.5} total mass and semi-volatile PM_{2.5} chemical components are known to have both positive and negative artifacts (e.g., Chow, 1995; Frank, 2006; Watson et al., 2009; Dabek-Zlotorzynska et al., 2011; Malm et al., 2011; Su et al., 2018; Gantt, 2022). Estimates of reconstructed PM_{2.5} total mass based on the sum of PM_{2.5} ~~species-chemical component~~ mass measurements from the CSN, IMPROVE, and NAPS networks often differ from direct measurements of PM_{2.5} total mass (e.g., Malm et al., 2011; Chow et al., 2015; Hand et al., 2019). As well, different networks measuring the same species often do not use the same instruments or follow the same field and laboratory protocols, which can affect comparability across networks. Examples include the use of different instruments to measure SO₂, CO, and O₃ concentrations by different agencies reporting to AQS (e.g., Demerjian, 2000; Parrish and Fehsenfeld, 2000), SO₂ and HNO₃ concentrations measured by the CAPMoN and CASTNET networks vs. the NAPS network (Dabek-Zlotorzynska et al., 2011; Feng et al., 2020), NH₃ concentrations measured by the AMoN and NAPS networks (Dabek-Zlotorzynska et al., 2011; Puchalski et al., 2011), sulphur and nitrogen species measured by the CASTNET and IMPROVE networks (e.g., Ames and Malm, 2001; Lavery et al., 2009), and PM_{2.5} chemical components measured by the IMPROVE and CSN networks (Hand et al., 2012; Solomon et al. 2014). In order to assess measurement comparability between networks some efforts have been made to co-locate instruments used by different networks at one or more locations, including CSN and IMPROVE (Malm et al., 2011; Hand et al., 2012), CASTNET and CAPMoN (Schwede et al., 2011), and CAPMoN and NADP (Sirois et al., 2000; Wetherbee et al., 2010; Feng et al., 2023).

2.4 Pairing measurements with model predictions

The comparison of AQ measurements and AQ model predictions must be done with care since measurements and model predictions never represent exactly the same quantities (e.g., Seigneur and Moran, 2004; Appel et al., 2008). From a temporal perspective, reported AQ measurements may either be instantaneous values or time averages, and the time averages may in turn represent mean values for an averaging period that begins, ends, or straddles the reporting time. Model values, on the other hand, are nominally instantaneous but correspond to a time that is a discrete time step after the previous integration time and after a particular operator calculation step in a repeating sequence of [numerical](#) operators. From a spatial perspective, AQ measurements are typically made at a near-surface “point” location whereas AQ model predictions represent a volume-average value corresponding to the volume of an individual model grid cell. This spatial representativeness discrepancy is sometimes referred to as incommensurability. It is a fundamental source of model uncertainty that can be reduced by reducing model grid spacing but never removed entirely (e.g., Nappo et al., 1982; Venkatram, 1988; McNair et al., 1996; Spicer et al., 1996; Swall and Foley, 2009; Stroud et al., 2011; Schutgens et al., 2016). Estimates of population exposure to air pollutants based on ambient measurements from a small number of AQ measurement stations also suffer from the same problem (e.g., Jerrett et al., 2005; Hystad et al., 2011). And lastly, from a chemical perspective AQ measurements sometimes correspond to a combination of two or

450 more model variables while in other cases they correspond to more detailed chemical species than the AQ model is able to consider. For these reasons some pre-processing is generally required to pair or match AQ measurements and model predictions before they are compared while bearing in mind that some differences will still remain, ~~and~~. It is thus important to document the methodology used to perform this pairing ~~should be documented~~ (Simon et al., 2012).

Temporal pairing was relatively straightforward for this study, although it was necessary to examine AQ network documentation carefully to understand the exact temporal nature of the measurements being reported. Model ~~concentration-abundance~~ predictions were available every chemistry time step, or every 15 minutes in the case of the RAQDPS-OP023 (Moran et al., 2026~~5~~), so it was simple to pair model predictions with instantaneous hourly ~~abundance~~ ~~concentration~~ measurements. On the other hand, to pair model predictions with the mean hourly ~~abundance~~ ~~concentration~~ measurements reported by the NAPS and AQS networks (Fig. S2), multiple consecutive sub-
460 hourly model predictions needed to be combined using one of two approaches: an end-value approach, which averages the model values at the beginning and end of the measurement sampling period; or an integration approach, where the trapezoidal rule is used to combine the five RAQDPS-OP023 values available for the hour. The end-value approach was used in this study. To pair model predictions with mean daily air ~~abundance~~ ~~concentration~~ measurements from the AQS, CSN, IMPROVE, and NAPS networks (Table S2a), all hourly model values for each 24-hour sampling period
465 were averaged. To pair with mean weekly air ~~abundance~~ ~~concentration~~ measurements from CASTNET, all hourly model values for each weekly sampling period were averaged; the same weekly averaging was also performed for daily mean CAPMoN and NAPS air concentrations for temporal consistency in order to be able to compare evaluation statistics between networks properly and to pool measurements for these three networks. Similarly, to pair model predictions with mean biweekly AMoN ~~abundance~~ measurements, hourly model NH₃ values were averaged for each
470 biweekly sampling period, and the same was done for NAPS daily mean NH₃ values for temporal consistency. Finally, to pair model predictions with daily precipitation-chemistry measurements (CAPMoN) or weekly precipitation-chemistry measurements (NADP), hourly model wet deposition forecasts were accumulated for the appropriate period, but then weekly deposition values were also calculated for CAPMoN for temporal consistency with NADP. Weekly precipitation-weighted mean wet concentration values were then calculated from weekly precipitation and weekly
475 deposition values.

More details about pairing related to this study, including spatial and chemical considerations, especially for PM measurements, and completeness screening, are provided in Sect. S2.4. ~~These~~ ~~These details~~ include the nuances of evaluating VOC predictions, handling ambient vs. standard temperature and pressure, the measurement proxies used for some PM chemical components such as NH₄, total organic matter (TOM (=POM+SOM)), CM, and SS, the treatment
480 of aerosol water, and the combined gas-particle phases implicit in precipitation-chemistry measurements. For example, one important consideration related to pairing with VOC measurements is that while measurements of ethene (C₂H₄) are available, the ADOM-2 model VOC species named ETHE is a lumped species that includes additional VOC species (Sect. S2.4). This misalignment must be considered when interpreting evaluation results for ETHE in Sect. 3.3.1 since the measurements are in effect lower bounds on the model predictions of this species rather than direct counterparts.

Formatted: Subscript

2.5 Model performance metrics and evaluation

Once a set of paired observed and model-predicted values is available, model performance metrics can be calculated. For the present study we chose to calculate 12 statistical metrics: observation mean (\bar{O}); model prediction mean (\bar{M}); mean bias (MB); normalized mean bias (NMB); normalized mean absolute error (NMAE); root mean square error (RMSE); Pearson correlation coefficient (R); fraction of predictions within a factor of 2 of observations (FAC2); centered root mean square error (CRMSE); standard deviations of observations (σ_O or SDO) and model predictions (σ_M or SDM); and normalized standard deviation (NSD). Definitions of these metrics are provided in Table A2 and some background information about their selection is provided in Sect. S2.5. Inclusion of the first seven of these metrics is consistent with the recommendation of Simon et al. (2012) for a minimum set of performance evaluation statistics that should always be calculated to promote comparability across separate studies. The eighth metric, FAC2, is a dimensionless and bounded (0–1) measure of error or scatter that is not sensitive to outliers (e.g., Chang and Hanna, 2004; Borrego et al., 2008; Derwent et al., 2010; Savage et al., 2013). CRMSE, unlike RMSE, is insensitive to bias and represents the error due to differences in pattern variation or, alternately, the standard deviation of the error; it has been used in many studies (e.g., Bencala and Seinfeld, 1979; Stanski et al., 1989; Taylor, 2001; Chang and Hanna, 2004; Entekhabi et al., 2010; Sakaguchi et al., 2012; Thunis et al., 2012). NSD has been suggested as a metric by Taylor (2001), Chang and Hanna (2004), and Thunis et al. (2012), but by itself it does not provide information about the magnitudes of σ_O or σ_M (which were recommended by Willmott (1981) and reported by Appel et al. (2021)). Note that CRMSE, R, σ_O , and σ_M (and sometimes NSD) are all linked by the Taylor diagram (Taylor, 2001). One other quantity that should be reported with these 12 metrics is N, the number of measurement-model pairs. Many evaluation studies fail to report this quantity, but it is used explicitly in the calculation of many metrics and it provides valuable information about sample size, representativeness, and significance (e.g., Huang et al., 2021).

Since this is an AQ forecasting evaluation, we have focused here on “native” network sampling duration: that is, hourly, daily, weekly, or biweekly samples, but based on the networks with the longest sampling duration for each species (e.g., biweekly for AMoN for NH₃, but weekly for CASTNET and NADP-NTN) to allow consistent comparisons between networks and pooling of network measurements. Other studies that focused on model performance for regulatory applications have looked at “constructed” predictands such as maximum daily 8-hr average (MDA8) or maximum 1-hourly values of O₃ volume mixing ratios (VMRs), whereas in this study we have only considered network-reported values such as hourly O₃ VMRs. And while we report annual domain-average statistics based on combined network measurements, we also report results for more stratified (i.e., disaggregated) analyses, including network-specific statistics, seasonal statistics, monthly statistics, diurnal statistics, regional statistics, and urban/rural statistics. To calculate urban vs. rural statistics, each measurement site was classified as urban or rural based on its grid-cell population density, where a threshold of 400 persons km⁻² was applied for Canada and 386 persons km⁻² (1000 persons per square mile) for the U.S. as the minimum urban population density. The slightly different thresholds were used for consistency with national censuses. We have also discussed our statistical results contextually in the next two sections by referring to the performance benchmarks proposed by Simon et al. (2012), Emery et al. (2017), Kelly

et al. (2019), Huang et al. (2021), and Zhai et al. (2024) (see Sect. S2.5). Some additional discussion related to model performance metrics ~~can also be found~~ is provided in Sect. S2.5.

3 Results

This section presents ~~performance evaluation results~~ statistics, first for one meteorological parameter important for air quality (Sect. 3.1), then for three key chemical species, NO₂, O₃, and PM_{2.5} total mass (Sect. 3.2), and then for other gas-phase species, PM_{2.5} chemical composition, and wet concentration and deposition of three inorganic species (Sect. 3.3). Annual, seasonal, monthly, diurnal, and regional evaluations for the one-year period from 1 June 2021 to 31 May 2022, the first year of RAQDPS-OP023 forecasts, are presented in this section along with selected evaluation results for the 2013–2016 RAQDPS-OP023 annual simulations. Many additional tables and figures related mainly to the 2013–2016 simulations, which serve to further quantify predictive skill and characterize the temporal and spatial variability of RAQDPS-OP023 ~~system~~ performance, can be found in Sect. S3 of the Supplement.

3.1 Operational evaluation of AQ-relevant meteorological predictands

Meteorological processes affect air quality through their influence on emissions, atmospheric transport and diffusion, chemistry, and wet and dry removal. Near-surface temperature, wind speed, and precipitation are three meteorological parameters important for surface air quality (e.g., Vautard et al., 2012; Gilliam et al., 2015; McNider and Pour-Biazar, 2020; Wang et al., 2021; Campbell et al., 2022). As described in the companion paper by Moran et al. (2026~~5~~), the RAQDPS-OP023 (and RAQDPS-FW023) is a regional chemical weather model configured to produce nearly identical meteorological forecasts to the RDPS 8.0.0, the ECCC regional weather forecast model that was operational at the same time (Fillion et al., 2010; Caron et al., 2015; McTaggart-Cowan et al., 2019; CMC-RDPS-8.0.0, 2021). Performance ~~e~~evaluations of RDPS weather forecasts have been presented in these and other publications. For this paper we have only evaluated RAQDPS-OP023 precipitation forecasts based on precipitation measurements from AQ precipitation-chemistry networks, which are not usually available to or considered in NWP model performance evaluations. This choice also ensures that performance statistics for precipitation are consistent in time and space with those for pollutant concentrations in precipitation and wet deposition (Sect. 3.3.3).

Domain-average annual scores for RAQDPS-OP023 weekly precipitation forecasts at precipitation-chemistry stations for 2013 to 2016 are listed in Table 6. As noted in Sect. 2.4 ~~w~~e have chosen to consider weekly forecasts because the U.S. NADP precipitation-chemistry network only reports weekly accumulated measurements. Interestingly, this set of scores does not show much variation from year to year. For example, annual MB values ranged from -0.1 to 2.2 mm-week⁻¹, NMB values from -0.01 to 0.12~~4~~, NMAE values from 0.49 to 0.54, RMSE values from 17.6 to 20.6 mm-week⁻¹, FAC2 values from 0.56 to 0.57, and R values from 0.71 to 0.78. Appel et al. (2011) reported a comparable NMB range but a markedly lower RMSE range for 12-km MM5 meteorological model simulations for the 2002-2006 period, but those earlier statistics were calculated for accumulated seasonal and annual precipitation predictions as opposed to weekly predictions, which have greater temporal variability.

Seasonal analyses of RAQDPS-OP023 predictions of near-surface temperature, wind speed, and precipitation can be found in Sect. S3.1 as well as individual-network annual and seasonal evaluation ~~results-scores~~ and subregional annual evaluation ~~score-results~~ for weekly precipitation. These additional evaluations showed that model skill in predicting weekly precipitation was highest for the winter season and lowest for the summer season (e.g., Fig. S161). The probable explanation is that organized, synoptic-scale precipitation, which is more predictable, is likeliest to occur in the winter whereas small-scale convective precipitation, which is harder for NWP models to predict, is likeliest to occur in the summer (e.g., Appel et al., 2011; Gilliam et al., 2021). Many of the largest overpredictions of weekly precipitation at individual stations occurred in the Rocky Mountain region of the western U.S., where ~~subgrid-scale (SGS) topographical features and station location are relative to subgrid-scale (SGS) topographical features~~ is likely to be important, whereas underpredictions at stations were common in the flatter terrain of the southeastern and central U.S. (Fig. S121). In addition, the evaluation statistics for an individual network or month or subregion were sometimes qualitatively different from those for the combined networks, combined months, or combined subregions. For example, model skill in predicting annual and seasonal mean weekly precipitation was found to be higher for the Canadian CAPMoN precipitation-chemistry network than the U.S. NADP network (Tables S6A, S6S). This possibility always needs to be kept in mind when interpreting the most highly aggregated performance statistics (e.g., annual statistics and all-network, all-station statistics), which may obscure systematic network differences or be impacted by compensating errors (e.g., Makar et al., 2014).

3.2 Operational evaluation of three key air quality predictands

This section presents operational evaluation results for RAQDPS-OP023 predictions of hourly surface NO₂, O₃, and PM_{2.5} total mass abundances for five years. Results are presented first for 2021/22 NO₂ and O₃ forecasts ~~based on that were compared to~~ NRT measurements, followed by results for 2013–2016 NO₂ and O₃ hindcasts ~~based on that were compared to~~ QA/QCed network measurements, 2021/22 PM_{2.5} forecasts ~~compared to based on~~ NRT measurements, and 2013–2016 PM_{2.5} hindcasts ~~compared to based on~~ QA/QCed network continuous and gravimetric measurements.

3.2.1 NO₂ and ozone

2021/22 operational forecasts of NO₂ and O₃

Figure 1 shows the spatial distribution over North America of annual mean NO₂ and O₃ hourly surface VMR fields predicted by the RAQDPS-OP023 for the 2021/22 period. Coloured “coffee beans” (i.e., divided dots) are superimposed on the contoured fields to show observed and predicted annual mean values at NRT measurement stations for the same period (see Fig. S2 for station locations). Generally good agreement is evident in Fig. 1 between the observed and predicted annual mean values of both pollutants (although viewing the NO₂ panel with higher magnification is helpful); ~~although note that~~ the higher NO₂ VMRs associated with urban centers are smaller-scale features caused by high NO_x emissions over urban centers (cf. Fig. S1a).

More quantitatively, Table 3 lists values of all-station annual model evaluation statistics for hourly NO₂ and O₃ VMR forecasts for 2021/22. These overall performance scores are generally less good for NO₂ than for O₃, including NMB

Formatted: Subscript

(-0.19 vs. -0.07), NMAE (0.56 vs. 0.28), FAC2 (0.52 vs. 0.83), and R (0.65 vs. 0.72). This difference is not surprising given that NO₂ is a primary pollutant whose spatial distribution is dominated by the distribution of emissions with strong spatial gradients whereas O₃ is a secondary pollutant with a smoother spatial pattern and smaller dynamic range.

590 One indicator of the degree of smoothness of a pattern is the coefficient of variation (CV) or relative standard deviation (ratio of standard deviation to arithmetic mean; see Table A2), where a lower value indicates a ~~greater-smoother~~ fieldness (i.e., lower variability) (e.g., Fruin et al., 2014; Lee et al., 2018). The observed and predicted annual CV values for 2021/22 calculated from Table 3 were 1.16 and 1.20, respectively, for NO₂ vs. 0.50 and 0.47 for O₃.

In order to judge the level of model skill suggested by the Table 3 scores, Zhai et al. (2024) have recommended 595 benchmark goals for NMB, NMAE, and R of ±0.20, 0.40, and 0.60 for “good” NO₂ performance scores (i.e., scores above 67th percentile relative to the scores for a historical multi-model ensemble) while Emery et al. (2017) have recommended benchmark goals for NMB, NMAE, and R of ±0.05, 0.15, and 0.75 as good O₃ performance scores. These benchmark goals were met by RAQDPS-OP023 forecasts for 2021/22 for NO₂ except ~~for NO₂~~ annual NMAE scores ~~and-but not for~~ O₃ annual ~~R~~-scores.

600 When interpreting these benchmark comparisons, however, ~~it should be noted that Emery et al. (2017) also recommended that the evaluation period considered should be no more than one month for O₃ and a 40 ppbv cutoff should be used when calculating NMB and NMAE for O₃, whereas no cutoff was considered for Table 3. In addition, it should also be noted that~~ Simon et al. (2012) found performance scores for retrospective model applications to be better on average than those for forecast applications due to the use by the former of year-specific emissions, 605 meteorological reanalyses, day-specific chemical lateral boundary conditions, and other retrospective data sets that are not available to AQ forecasting applications. It was also noted in Sect. 2.3 that most network NO₂ monitors in North America suffer from positive biases due to interference from other oxidized nitrogen species (e.g., Dunlea et al., 2007; Dickerson et al., 2019). These biases, however, vary greatly with time and location. They are expected to be smallest when fresh NO₂ emissions dominate, for example, in urban areas, in the early morning hours (4-9 a.m.) when the PBL is shallow, and in the winter, but largest relatively speaking for aged air, as in rural areas, in the afternoon hours, and in the summer (e.g., Godowitch et al., 2010; Lamsal et al., 2015; Jaeglé et al., 2018; He et al., 2019; Toro et al., 2021). Thus, the annual NMB value for NO₂ of -0.19 would be smaller if these measurement biases were accounted for.

615 Figures 2 and 3 provide an extreme disaggregation of the all-station annual scores from Table 3 by showing spatial distributions of station-specific annual values of four statistics (MB, NMB, CRMSE, and R) for hourly NO₂ and O₃ measurements, respectively, for 2021/22. Such plots can reveal regional patterns in the evaluation statistics. For example, annual NMB values for NO₂ tend to be negative everywhere (again consistent with a positive measurement bias) but they are more negative (i.e., worse) in general at western stations while CRMSE and R values for NO₂ are lower in the continental interior than ~~the-in~~ coastal areas (Fig. 2). Annual MB and NMB values for O₃, on the other hand, are generally negative at western stations but positive at eastern stations, particularly at coastal stations (Fig. 3), 620 while both annual CRMSE and R scores are higher overall across the continent for O₃ than for NO₂.

Formatted: Subscript

Formatted: Subscript

Formatted: Subscript

Figure 5 adds temporal detail to the annual analysis shown in Fig. 1. It shows the corresponding predicted spatial distributions of seasonal mean NO₂ and O₃ hourly surface VMR fields for 2021/22, again with superimposed coloured divided dots to show observed and predicted seasonal mean values at NRT measurement stations for each season. By inspection, predicted domain-scale, seasonal mean NO₂ levels appear to be highest in the winter season (DJF) and lowest in the summer season (JJA), whereas O₃ levels are predicted to be highest in the spring season (MAM) and lowest in the autumn (SON) season.

Another perspective on the temporal variation of ~~model-RAQDPS-OP023~~ performance is provided by Figs. 6 and 7, which show time series of observed and predicted all-station monthly mean VMR values of hourly NO₂ and O₃, respectively, for 2021/22 for all NRT measurement stations in the model domain ~~as well as~~. Time series of monthly NMB, CRMSE, and R scores ~~are also shown in these two figures~~. Observed and predicted monthly mean NO₂ VMRs are both highest in January and lowest in June and July; observed and predicted monthly mean O₃ VMRs are both highest in April and lowest in November. Monthly NMB values for hourly NO₂ are negative for all months ~~but are slightly worse for the winter months even though the NO₂ measurement bias is expected to be smaller in the winter, while~~; monthly CRMSE values for NO₂ peak in January, and monthly R values for NO₂ do not vary much from month to month but are slightly higher in the winter. Monthly NMB values for hourly O₃ are negative for all months except December and January, monthly CRMSE values for O₃ peak in July, and monthly R values for O₃ also do not vary much but are slightly higher in the summer. It should be noted that seasonal variations in NO_x emissions are very small at the domain scale (Table S1), suggesting that the observed and predicted variations in monthly mean NO₂ levels evident in Fig. 6 are controlled by ~~other~~ factors ~~other~~ than emissions, such as monthly variations in temperature, photolysis, PBL height, vegetation phenology, and dry deposition. For O₃, on the other hand, biogenic emissions of VOCs, its other main precursor, have very large seasonal variations (Table S1). Interestingly, although the largest predicted monthly O₃ values occur in April, the model still underpredicts the well-known springtime O₃ maximum in the Northern Hemisphere (e.g., Penkett and Brice, 1986; Monks, 2000; Liudchik et al., 2015) by about 5 ppbv ~~in April~~.

It is also of interest to examine ~~model-RAQDPS-OP023~~ performance by time of day since many emission source sectors and meteorological and chemical processes vary diurnally. Figures 9 and 10 show all-station, annual-mean diurnal time series in local time (LT) of ~~values of five~~ statistics for hourly NO₂ and O₃ surface VMRs, respectively, for the 2021/22 period. The annual-mean diurnal time series of observed and predicted ~~hourly~~ VMRs for both species display a strong dependence on time of day as do the diurnal time series of annual NMB, CRMSE, and R scores. Model predictions of annual-mean hourly values of both NO₂ and O₃ surface VMRs agree well overall with observations, including the times of the observed daily maxima and minima. The annual-mean diurnal time series of ~~hourly~~ NO₂ VMR and the associated ~~hourly~~ evaluation statistics in Fig. 9 display extrema close to the times of morning and afternoon rush hours, suggesting that diurnal variation of on-road NO_x emissions plays an important role in driving the diurnal pattern. ~~Interestingly, hourly NMB values for NO₂ are most negative in the afternoon when, the NO₂ measurement bias is expected to be largest, while~~ By contrast, the maximum annual-mean hourly O₃ VMR occurs at

Formatted: Subscript

Formatted: Subscript

Formatted: Subscript

Formatted: Subscript

655 14 LT and the minimum at 05 LT (Fig. 10). For O₃ the smallest annual-mean hourly NMB and CRMSE values and highest annual-mean hourly R values occur close to the mid-day O₃ peak.

Figures 2–4 showed how model performance can vary geographically. A complementary result is presented in Fig. 12, which compares regional time series of observed and RAQDPS-OP023 predicted monthly means of hourly NO₂ and O₃ VMRs for 2021/22 for the four continental quadrants shown in Fig. S7. Both observed and predicted time series exhibit a regional dependence. For NO₂ the agreement between observed and predicted monthly means was closest for western Canada while for O₃ it was closest for the eastern U.S. Interestingly, peak observed monthly mean NO₂ VMR values were slightly higher in the west than in the east, at least for these regional sets of stations (see Fig. S2). Observed and predicted monthly mean NO₂ VMR peaks also occurred in January in three of the four regions and in December in the eastern U.S., in overall agreement with Fig. 6. Note too that monthly mean NO₂ VMRs were also underpredicted in all months in the western and eastern U.S., in agreement with Fig. 6, but some monthly overpredictions can be seen in western and eastern Canada. Similarly, peak observed monthly mean O₃ VMR values occurred in April in three of the four regions and in May in the western U.S., in overall agreement with Fig. 7, but in July in the western U.S. But peak predicted monthly mean O₃ VMR values, on the other hand, occurred in both March and/or April, and both underpredictions and overpredictions of monthly mean O₃ VMR are evident in Fig. 12 in all four regions. Note too that monthly mean NO₂ VMRs were also underpredicted in all months in the western and eastern U.S., in agreement with Fig. 6, but some monthly overpredictions can also be seen in western and eastern Canada.

2013–2016 hindcasts of NO₂ and O₃

The RAQDPS-OP023 annual hindcasts for 2013–2016 can also be evaluated to look for consistencies in model performance across multiple years. Figure 13 shows plots of predicted spatial distributions of annual mean NO₂ and O₃ surface VMR fields for 2013–2016 and 2021/22. For both species the broad spatial patterns are very similar over land for the five years despite year-to-year variations in meteorology and the monotonic decrease of 18% in domain-total NO_x emissions over the 2013–2016 period and the further decrease of 20% from 2016 to 2021/22 (Table 1). Nevertheless, year-to-year decreases in annual NO₂ levels are visible over this near-decadal period, including in Texas, the Ohio Valley, and the Washington, D.C.–Boston corridor. Latitudinal gradients in the spatial distributions of O₃ surface VMR can be seen over land in Fig. 13 for all five years, with a east–west band of elevated values stretching across the continental U.S. and peaking in the elevated terrain of the U.S. Rocky Mountain and Great Basin regions. A recent analysis of winter and spring surface O₃ observations over North America for 2010–2014 showed a similar pattern (Gaudel et al., 2018). However, trends in O₃ from 2013 to 2021/22 are not obvious in this figure, unlike those for NO₂.

Table 3 lists values of observed and RAQDPS-OP023-predicted all-station annual mean NO₂ and O₃ surface VMRs for 2013–2016 as well as 2021/22. Note that the statistics for the 2013–2016 period are based on quality-assured, retrospective observation data sets released by individual agencies rather than the NRT measurements used to evaluate

2021/22 forecasts (see Fig. S3 for station locations). Consistent with Fig. 13, observed and predicted all-station annual mean NO₂ VMR values both exhibit a monotonic decrease from 2013 to 2021/22, though for a smaller set of U.S. stations in 2021/22 (Table 2), whereas observed all-station annual mean O₃ VMR values exhibit little change over this period vs. a small upward trend for predicted all-station annual mean O₃ VMR. Table 3 also lists ~~domain-wide-all-station~~ annual values of 10 other model performance statistics for the five years. Statistics for the hindcasts might be expected to be better than the forecasts due to the use of year-specific emissions. In fact, the scores are mixed and are comparable overall for the five years. For example, annual NMB values for NO₂ VMR are negative for 2021/22 but positive and smaller in magnitude for the other four years, annual RMSE and NMAE values for NO₂ VMR are better for 2021/22 than for 2013–2016, but FAC2 and R values for NO₂ VMR are better for 2013–2016 than for 2021/22. The annual NMB and R values for NO₂ VMR for 2013–2016 all ~~meet/exceed~~ the benchmark goals of ± 0.20 and 0.60 for good performance recommended by Zhai et al. (2024), similar to 2021/22, but annual NMAE scores for 2013–2016 do not meet either of their recommended thresholds (0.40 or 0.55). Annual NMB values for O₃ VMR, on the other hand, are more negative for 2013–2016 than for 2021/22 and FAC2 scores are also lower while NMAE and R scores are comparable. In addition, the annual NMB and R scores for O₃ VMR for 2013–2016 are all ~~above-meet~~ the acceptable benchmarks of ± 0.15 and 0.50 for these statistics recommended by Emery et al. (2017), similar to 2021/22, but fall below the more stringent benchmark goals of ± 0.05 and 0.75, while NMAE scores for 2013–2016 do not meet either recommended threshold (0.15 or 0.25).

Additional analyses

Results from additional data analyses for NO₂ and O₃ with a focus on the 2013–2016 RAQDPS-OP023 hindcasts can be found in Sect. S3.2.1. These results include tables of separate annual and seasonal scores for the AQS and NAPS networks as well as ~~seasonal and regional diurnal analyses for 2021/22~~, regional scores for all five years, spatial plots of both annual station scores and predicted seasonal mean surface VMR fields for 2013–2016, ~~seasonal and regional diurnal analyses~~, and monthly time series, monthly density scatterplots, and urban vs. rural monthly time series for 2013–2016. One finding from these supplemental analyses is the high level of consistency between the aggregated annual statistical scores across years for both species for the AQS and NAPS networks individually (Table S3A) and annual scores at the individual station level (e.g., Fig. S42). Another is the clear consistency across the 2013–2016 hindcasts of the seasonal variations in the NO₂ and O₃ seasonal mean VMR fields, statistical scores, ~~diurnal time series~~, and monthly mean time series (e.g., Table S3S, Fig. S1140), which helps to identify systematic model errors. Third, the overall agreement in observed and predicted temporal trends also provides support for the representativeness of the year-specific emissions used for these hindcasts (e.g., Fig. S1404). Fourth, there are some striking differences between the time series of monthly NO₂ and O₃ statistics for urban stations vs. rural stations that underline the importance of emissions forcing, including higher NO₂ levels and lower O₃ levels in urban areas (e.g., Fig. S209 vs. Fig. S210). Fifth, the larger annual, seasonal, and monthly negative biases for NO₂ that were found in the 2021/22 forecasts for U.S. regions vs. Canadian regions (e.g., Fig. S168) suggest that the U.S. NO_x emissions used for these forecasts may have been too low whereas the Canadian NO_x emissions that were used were more representative of 2021/22 conditions. The same pattern was not seen in the 2013–2016 hindcasts, which used different emissions. To detect this possible

Formatted: Space Before: 6 pt

Formatted: Subscript

Formatted: Subscript

725 ~~issue, however, statistics for the individual networks had to be computed and then compared (Table S3A). Sixth, the~~
 annual regional analysis found that the two western regions had the largest negative NMB values for O₃, consistent
 with Fig. 12 and pointing to possible issues with the O₃ lateral boundary conditions for the western boundary (Table
 S7). ~~And seven~~Sixth, the monthly density scatterplots reveal an obvious precision limitation (only whole numbers) in
 the reported hourly NO₂ measurements (Fig. S169).

730 A seventh finding was that annual, seasonal, and monthly negative NMB values were considerably larger for NO₂ in
the 2021/22 forecasts for the two U.S. regions (-0.31, -0.25) vs. the two Canadian regions (-0.06, -0.03). The same
pattern was not seen in the 2013-2016 hindcasts, which used retrospective rather than projected emissions (Table S7).
This is one example of the value of computing and then comparing statistics for the individual networks as well as the
combined networks (e.g., Tables S3A, S3S). The differences in biases between countries found for the 2021/22
 735 forecasts might suggest that the U.S. NO_x emissions used for these forecasts were too low, whereas the Canadian NO_x
emissions that were used were more representative of 2021/22 conditions. Since some time has passed since 2021
when the RAQDPS-OP023 became operational, retrospective national emissions inventories are now available for
2021 for both Canada and the U.S. (ECCC, 2025a; U.S. EPA, 2025). Interestingly, a comparison of these inventories
with Table 1 showed that the projected annual NO_x inventory emissions considered for both countries were in fact
 740 higher than the actual inventory values for 2021: 8% higher for the U.S. and 13% higher for Canada. Other explanations
must thus be sought.

Formatted: Not Highlight
 Formatted: Not Highlight
 Formatted: Not Highlight
 Formatted: Not Highlight
 Formatted: Not Highlight
 Formatted: Subscript

3.2.2 PM_{2.5} total mass

2021/22 operational forecasts of PM_{2.5} total mass

745 Figure 1 also shows the spatial distribution over North America of the annual mean PM_{2.5} hourly surface concentration
 field (without sea-salt component) predicted by the RAQDPS-OP023 for 2021/22. Coloured divided dots are again
 superimposed to show observed and predicted annual values at NRT hourly PM_{2.5} measurement stations for the same
 period (see Fig. S2 for station locations). It is clear from this figure that the RAQDPS-OP023 underpredicts annual
 PM_{2.5} levels for 2021/22 at a majority of measurement stations.

750 Table 3 lists values of observed and RAQDPS-OP023-predicted all-station annual mean PM_{2.5} surface concentrations
 (including the sea-salt component) and 10 other annual evaluation statistics for hourly PM_{2.5} forecasts for all stations
 measuring hourly PM_{2.5} (including both Class III FEM and non-FRM/FEM monitors: see Sect. S2.3 for more details)
 for 2021/22. All-station annual MB and NMB values for forecast hourly PM_{2.5} concentrations were -2.5 µg·m⁻³
 and -0.31, respectively, consistent with Fig. 1. Other statistics in Table 3 for PM_{2.5} were also poorer (e.g., NMAE=0.66,
 FAC2 =0.46, R=0.24, NSD=0.69) than corresponding scores for NO₂ and O₃. Emery et al. (2017) proposed
 755 “acceptable” score benchmarks (i.e., above 33rd percentile for a historical multi-model ensemble) for predicted PM_{2.5}
 total mass for NMB, NMAE, and R scores of ±0.30, 0.50, and 0.40, but none of these benchmarks were met for the
2021/22 hourly PM_{2.5} forecasts.

Formatted: Not Superscript/ Subscript
 Formatted: Subscript

Figure 4 shows the spatial distribution of station-specific annual values of MB, NMB, CRMSE, and R for hourly PM_{2.5} total mass for 2021/22 based on NRT hourly measurements at AirNow and NAPS stations. Consistent with Fig. 1 and Table 3, annual MB was negative for most stations, but values were small at a minority of stations and even positive at a handful of stations. Annual NMB values, on the other hand, were greater than -0.240 at the majority of stations, especially in the west. Annual CRMSE values were highest in the western U.S away from the coast; as discussed in Sect. 4.2 these western scores were influenced by the lack of BB emissions in the RAQDPS-OP023 runs. Lastly, annual R scores were highest in the northeast and along the U.S. west coast and were lowest for many Rocky Mountain, Great Plains (central U.S.), and Prairie (central Canada) stations.

Figure 5 shows the predicted spatial distributions of seasonal mean PM_{2.5} hourly surface concentration fields (without sea-salt component) for 2021/22 predicted by the RAQDPS-OP023, again with superimposed divided dots that show observed and predicted seasonal mean PM_{2.5} concentration values at NRT hourly measurement stations. Similar to Fig. 1, observed seasonal mean values were higher in general than predicted seasonal mean values, especially in the summer and in the west (see Sect. 4.2 for a discussion of the impact of the inclusion of wildfire-BB emissions).

Figure 8 adds further temporal detail by showing time series of observed and RAQDPS-OP023-predicted all-station monthly mean PM_{2.5} concentration values for 2021/22 as well as time series of monthly NMB, CRMSE, and R values based on all NRT measurements of hourly PM_{2.5} surface concentration in the model domain. The observed all-station monthly mean PM_{2.5} concentration time series has a large August peak and a lower January peak but the reverse is true for the predicted all-station monthly mean PM_{2.5} time series. The RAQDPS-OP023 also underpredicted monthly mean PM_{2.5} concentrations in all months, with the largest underpredictions occurring in the summer and the smallest in the winter. While monthly NMB was negative for all months, it was most negative for spring and summer, with an extreme value close to -0.6 in August. Monthly CRMSE was quite variable, but with a pronounced primary peak in August and a secondary peak in January. Monthly R values did not vary much for winter and spring, but they were considerably lower for summer and autumn and were close to zero for July and August. The poor summer scores were in large part due to the neglect of BB emissions (Sect. 4.2).

Figure 11 shows all-station annual-mean diurnal time series of five statistics for hourly PM_{2.5} surface concentration for 2021/22. RAQDPS-OP023 model performance for PM_{2.5} clearly varied with time of day. Predicted annual-mean hourly concentrations were biased low at all hours of the day, and they displayed more diurnal variability than the measurements. The largest negative annual-mean hourly NMB value occurred in the early afternoon (14 LT) while the smallest values occurred at the beginning of the morning rush hour (06 LT) and towards the end of the evening rush hour (20 LT). Annual-mean hourly CRMSE and R values, on the other hand, exhibited relatively small diurnal variations.

It is also of interest to examine how RAQDPS-OP023 model performance varied with geography. Figure 12 compares regional time series of observed and predicted regional monthly means of hourly PM_{2.5} surface concentration for 2021/22 for the four continental quadrants (Fig. S7). Peak observed monthly mean PM_{2.5} concentrations occurred in

Formatted: Font: Not Italic

July or August and were higher in the west than in the east, but as in Fig. 8 there was also a secondary peak in the cold season in December or January for all four regions (cf. Fig. 5). In contrast the predicted monthly mean PM_{2.5} concentrations had a primary cold-season peak in December or January and a weak warm-season secondary peak in July or August, again consistent with Fig. 8. Note that the RAQDPS-OP023-predicted warm-season peak occurred without any contribution from BB emissions (see Sect. 4.2), suggesting a second warm-season emissions source such as biogenic secondary organic aerosol (SOA). Another regional difference is that predicted monthly mean PM_{2.5} concentrations were higher than the observed values in early winter for eastern Canada but were lower for all months for the other three regions.

800 2013–2016 hindcasts of PM_{2.5} total mass

Figure 13 shows the RAQDPS-OP023-predicted spatial distributions of annual mean PM_{2.5} surface concentration fields (including the sea-salt component) over North America the model domain for 2013–2016 and 2021/22. The spatial patterns of annual mean PM_{2.5} concentration for these five years are broadly similar, although some minor interannual variations between years can be seen over the ocean regions due to variations in sea-salt emissions due to that result from interannual differences in near-surface wind speed (cf. Fig. S9). Over North America, a annual mean PM_{2.5} surface concentrations, like annual mean NO₂ surface VMRs, are highest over the eastern U.S. and California and lower over most of Canada and the rest of the western U.S., with the exception of isolated urban areas in the western U.S. and a tongue of elevated PM_{2.5} levels over the Canadian province of Alberta. The impact of the large decreases in domain-total anthropogenic emissions of two PM_{2.5} precursors, SO₂ and NO_x, of 60% and 364% from 2013 to 2021 (Table 1) is also reflected in this figure by a decrease in PM_{2.5} levels with time over North America (see also the multi-year plots of annual mean PM_{2.5}-SO₄ and PM_{2.5}-NO₃ concentration fields in Fig. 14).

Table 3 lists annual values of 12 evaluation statistics for PM_{2.5} hourly surface predictions for all stations measuring hourly PM_{2.5} for the 2013–2016 RAQDPS-OP023 hindcasts in addition to the 2021/22 forecasts. The values of predicted annual mean PM_{2.5} surface concentrations show a noticeable downward trend across the five simulation years: the observed annual mean surface concentrations also show a downward trend but it is much weaker. This difference might be due in part to the impact of BB emissions of PM_{2.5} on observed ambient PM_{2.5} values that is missing from the predicted ambient PM_{2.5} values. Overall, the 2013–2016 scores for each statistic were very similar amongst themselves, suggesting consistent behaviour in RAQDPS-OP023 PM_{2.5} predictions from year to year, but some differences are evident between the 2013–2016 scores and the 2021/22 scores. Annual NMB values were negative for all five years, but the range for 2013–2016 was -0.06 to -0.09, considerably better than the 2021/22 value of -0.31. Annual NM_AE scores, on the other hand, were slightly worse for 2013–2016 (0.71–0.73) than 2021/22 (0.66), while annual FAC2 scores were slightly better (0.48–0.50 vs. 0.46) and annual R scores were comparable (0.17–0.29 vs. 0.24). Note that all of the annual NMB scores for 2013–2016 (unlike 2021/22), but none of the NM_AE and R scores, met the PM_{2.5} benchmarks for acceptable performance recommended by Emery et al. (2017).

Formatted: Underline

Formatted: Subscript

825 In addition to hourly continuous PM_{2.5} total mass concentration measurements, there are also roughly 900 daily PM_{2.5}
monitors operating in North America that make 24-hour PM_{2.5} total mass measurements using a filter-based,
gravimetric approach (see Sect. S2.3 and Table S2c). These daily gravimetric PM_{2.5} measurements mainly support
regulatory and human health applications and are not available in near-real time, but they are notable because they
represent an independent data source for model evaluation that can supplement the Class III FEM and non-FRM/FEM
830 hourly continuous PM_{2.5} concentration measurements used for NRT evaluations and the Table 3 statistics. Daily
gravimetric PM_{2.5} measurements also have different uncertainties than the hourly continuous PM_{2.5} measurements,
including negative artefacts due to the volatilization of semi-volatile species such as ammonium, nitrate, and particle
water during transport to and inside the controlled laboratory environments where filter analyses are performed (e.g.,
Frank, 2006; Dabek-Zlotorzynska et al., 2011; Malm et al., 2011; Chow et al., 2015; Hand et al., 2019). Gravimetric
835 PM_{2.5} monitor locations from the AQS, IMPROVE, and NAPS networks are shown in Fig. S6a (vs. Fig. S3c for
continuous PM_{2.5} monitors). Note that these combined networks include monitors with every-day, one-day-in-three,
and one-day-in-six sampling frequencies, but roughly 65% of the daily gravimetric PM_{2.5} mass measurements in the
U.S. are made by non-speciation, mass-only monitors (Tables 5 and S2c; Malm et al., 2011).

Table 5 lists all-station annual evaluation statistics for gravimetric measurements of daily PM_{2.5} mass for the 2013–
840 2016 hindcasts. First, note that observed annual PM_{2.5} total mass concentration values for the gravimetric data set in
Table 5 have a range from 7.2 to 8.2 $\mu\text{g}\cdot\text{m}^{-3}$, similar to but smaller than the corresponding range of 7.4 to 8.7 $\mu\text{g}\cdot\text{m}^{-3}$
for the hourly continuous PM_{2.5} data set from Table 3. The range of annual NMB scores for the gravimetric data set,
however, is 0.0 to 0.07, slightly better and of opposite sign to the range of -0.09 to -0.06 range for the continuous PM_{2.5}
measurements in Table 3. Other annual scores for the 2013–2016 hindcasts are also better for the gravimetric
845 measurement data set. The range of annual NMAE scores for the gravimetric PM_{2.5} measurements is 0.51 to 0.54 (vs.
0.71 to 0.73 for the continuous PM_{2.5} measurements), the range of annual FAC2 scores is 0.68 to 0.70 (vs. 0.48 to 0.50),
and the range of annual R scores is 0.43 to 0.47 (vs. 0.17 to 0.29). Note the narrow range of each of these annual
statistics for the four years, suggesting a high level of consistency in model performance. Note too that the range of
annual NSD scores for the gravimetric measurements is 1.41 to 1.61, higher than the range of 0.78 to 1.36 for the
850 continuous PM_{2.5} measurements.

Some differences in scores for these two independent data sets are to be expected due to differences in monitor
locations, in temporal aggregation (daily vs. hourly), and in measurement technologies. One reason for some of the
better scores for the gravimetric PM_{2.5} mass measurements may be their daily sampling period, which will reduce the
influence of short-term model errors compared to the hourly continuous measurements (e.g., Appel et al., 2008, 2021).
855 The sampling period would not, however, affect annual means or MB and NMB scores. One technical difference
between the daily gravimetric PM_{2.5} mass measurements and the continuous mass measurements is that the filter
analysis for the former is performed under constant-temperature, low-humidity conditions in a laboratory after transport
from the field and storage prior to analysis whereas the hourly continuous mass measurements are made under ambient
conditions where temperature and humidity can vary widely. This means that daily gravimetric PM_{2.5} mass values are

860 likely to be lower than daily continuous PM_{2.5} mass values due to loss of some semi-volatile mass from ammonium nitrate, organic matter, or particle water from the sample filter, especially for filters exposed under high-humidity or low-temperature ambient conditions. The fact that annual NMB scores for gravimetric PM_{2.5} mass measurements are more positive than those for continuous PM_{2.5} measurements is thus somewhat surprising.

Additional analyses

865 The results of additional analyses for hourly continuous and daily gravimetric PM_{2.5} total mass measurements with a focus on the 2013–2016 hindcasts are presented in Sect. S3.2.2. These results include tables of separate annual and seasonal scores for the individual AQS, IMPROVE, and NAPS networks as well as regional scores for all five years, spatial plots of both annual station scores and predicted seasonal mean PM_{2.5} surface concentration fields for 2013–2016, seasonal and regional diurnal analyses for 2021/22, and monthly time series, monthly density scatterplots, and urban vs. rural monthly time series for 2013–2016. One insight from these additional analyses are the considerable variations between seasons that are evident across all five years in the seasonal mean PM_{2.5} mass fields, in the seasonal statistical scores, and in monthly mean time series (e.g., Figs. S13, S142). Another is the high level of consistency between seasonal scores for PM_{2.5} for the 2013–2016 hindcasts (and in many cases for the 2021/22 forecasts) at the aggregated all-station level and annual scores at the individual station level, which allows systematic model errors to be identified. For example, all-station monthly NMB scores were most negative in summer for all four years (Figs. S142 and S198). Third, some of the analyses suggest that the neglect of BB emissions by the RAQDPS-OP023 was an important contributing factor to its overall underpredictions of PM_{2.5} total mass. Fourth, there were some striking differences for 2013–2016 between the time series of monthly PM_{2.5} statistics for urban stations (Fig. S213) vs. rural stations (Fig. S214) that underline the importance of emissions forcing. For example, monthly NMB values for the urban stations were positive for some months whereas they were uniformly negative for the rural stations, suggesting that PM_{2.5} underprediction is mainly a rural issue. Fifth, additional differences are shown between evaluation statistics for 2013–2016 for daily gravimetric PM_{2.5} total mass measurements vs. hourly continuous PM_{2.5} measurements. These differences include positive monthly NMB scores for the cold-season months for the gravimetric measurements (Fig. S198) vs. lower scores for the continuous measurements (Fig. S142). And sixth, some of the evaluation scores between individual networks were also very different, and certain differences in the overall characteristics of the individual networks, in particular the dominance of either urban stations or rural stations, can help to explain why ~~network-the~~ scores between network were different. For example, for the daily gravimetric PM_{2.5} measurements the seasonal MB and NMB scores for one measurement network (NAPS) were positive for all seasons and for a second network (AQS) they were positive for most seasons (Table S5S). For the hourly continuous PM_{2.5} measurements, on the other hand, the seasonal MB and NMB scores were negative for both networks for all seasons. The fact that some scores point to model overpredictions of PM_{2.5} make it clear that the negative all-station MB and NMB scores presented in Table 3 and Figs. 5, 8, and 11 do not tell the whole story. Multiple factors must be considered in addition to model formulation to explain these different scores, including the magnitude and distribution of emissions, seasonal and regional variations in meteorology, differences in network composition, and differences in measurement instrument characteristics.

895

Formatted: Space Before: 6 pt

3.3 Expanded evaluation for additional species and processes

As described in [the companion paper by Moran et al. \(2026\)](#), the RAQDPS023 predicts abundances of 47 [individual and lumped](#) gas-phase chemical species and 16 size bin-chemical components. While direct atmospheric measurements are not available for all of these species and components, this section describes evaluation results based on 2013–2016 QA/QCed measurements of nine atmospheric gases in addition to NO₂ and O₃, seven PM_{2.5} chemical components, and three aqueous-phase inorganic ions.

3.3.1 Other gases

Table 4 extends the all-station annual statistical scores reported in Table 3 for two gas-phase species, NO₂ and O₃, to nine other individual or lumped ADOM-2 gas-phase species predicted by the RAQDPS-OP023 for 2013–2016: NO, NO_x, HNO₃, NH₃, SO₂, CO, ETHE, HCHO, and ISOP, [where ETHE is a lumped species \(Sect. S2.4\)](#). The measurements considered were provided by five networks: AMoN, AQS, CAPMoN, CASTNET, and NAPS. As discussed in Sect. 2.3 and illustrated by Figs. S4 and S5, the available sets of measurements for these other gas-phase species are different from those for NO₂ and O₃ in terms of the numbers and the locations of surface monitors, and also, in some cases, the sampling period, which ranged from hourly to biweekly (see also Tables S2a and S2b). Looking at values of N, the number of complete measurements per year, in Table 4, we see that NO, NO_x, and CO have the most measurements [by far](#), followed by ETHE and ISOP, then SO₂, HCHO and HNO₃, and lastly NH₃ with the fewest measurements. However, due to the different sampling period lengths, the number of measurements does not necessarily reflect the number of measurement stations. For example, there are more monitors measuring HNO₃, NH₃, and HCHO than there are [for measuring](#) ETHE and ISOP (Table S2b) even though N is smaller for the first three species. [In fact, only 8 to 13 stations have complete annual measurements for ETHE and only 6 to 13 stations have complete annual measurements for ISOP for 2013–2016.](#) Note that the evaluation scores for HNO₃, NH₃, and SO₂ will also be referred to in the next section, since these three species are precursors to three PM_{2.5} chemical components.

Compared to the annual model performance for NO₂ and O₃ predictions for 2013–2016 summarized in Table 3, the overall model skill for these other gas-phase species presented in Table 4 is more varied. For example, all-station annual mean NO VMRs, like those for NO₂, were overpredicted for all four years ([by 9% to 32%](#)). All-station annual NMB, NMAE, FAC2, and R scores for hourly NO VMR, however, were less good than those for hourly NO₂ VMR for all four years, but this difference is at least partly due to the limited precision at which NO VMR measurements were reported (see Sect. S3.3.1). All-station annual NMB, NMAE, FAC2, and R scores for hourly CO and daily HCHO VMRs, on the other hand, were comparable to those for NO₂. All-station annual mean [SO₂, HNO₃, SO₂, and ISOP](#) VMRs were overpredicted for all four years (and [also all months: see Sect. S3.3.1, by 16% to 33%, 43% to 60%, and 227% to 271%, respectively](#)), whereas all-station annual mean NH₃ VMR was underpredicted for all four years (and all months: Fig. S145), [by 42% to 47%](#). All-station annual [NMB scores for hourly mean ETHE predictions vs. hourly ethene measurements was also overpredicted for all four years, by ranged from 0.68% to 1.19% \(i.e., overpredictions\)](#), but these scores were confounded by the [model's](#) inclusion of isoprene oxidation products [in addition to ethene](#) in this lumped VOC species ([Sect. S2.4 Moran et al., 2025](#)), [which suggests](#) that overpredictions should be expected. The

impact of decreasing SO₂ and NO_x emissions in 2013–2016 (Table 1) can also be clearly seen in corresponding decreases in Table 4 in both observed and predicted all-station annual mean SO₂ and HNO₃ VMR values.

Additional analyses

More evaluation results for 2013–2016 for these other gas-phase species are provided in Sect. S3.3.1, including tables of annual and seasonal scores for individual Canadian and U.S. networks as well as all-station regional scores, spatial plots of both annual station scores and predicted seasonal mean surface VMR fields, time series of all-station monthly statistics, and monthly density scatterplots. It is clear from these additional analyses that all nine species exhibit strong seasonal variations: four species (HNO₃, NH₃, HCHO, ISOP) were observed and predicted to have summer maxima, four (NO, NO_x, SO₂, CO) were observed and predicted to have winter maxima, and ETHE was observed to have a winter maximum but predicted to have a summer maximum (Table S4S). As noted above, the disagreement for ETHE was not surprising due to the inconsistency between measured ethene (C₂H₄) and lumped model ETHE_{1,7} and However, winter ETHE scores, when isoprene emissions were low (Table S1), were better than those for the other three seasons, when isoprene emissions were higher (Table S4S). For example, winter NMB values ranged from -6% to 13%, suggesting that predictions of pure ethene VMR driven by pure ethene emissions demonstrated skill. As the case for NO₂ and O₃, there were also marked similarities in the scores for these other gas-phase species across the four annual hindcast simulations, which supports identification of systematic model errors. For example, HNO₃, SO₂ and ISOP were consistently overpredicted and NH₃ was consistently underpredicted in all seasons and months (Table S4S; Figs. S146, S150, and S145).

The consistency in annual, seasonal, and monthly scores for the four years also suggests that the year-specific emissions used for these hindcasts were representative. However, some scores discussed in Sect. S3.3.1 raised concerns that Canadian SO₂ emissions and biogenic ISOP emissions may have been too high and North American NH₃ emissions too low for the 2013–2016 period. The decreases in SO₂ and NO_x emissions from 2013 to 2016 were also reflected in time series of both observed and predicted monthly mean VMRs for NO, HNO₃, and SO₂ (Figs. S143, S144, S146) as well as NO₂ (Fig. S140). Performance benchmarks for CO and SO₂ proposed by Zhai et al. (2024) are also discussed in Sect. S3.3.1, and more CO scores than SO₂ scores met these benchmarks. Scores for individual networks can also be quite different owing to different network characteristics. SO₂ provides a good illustration of this behaviour as SO₂ measurements were available from four networks: scores for the CAPMoN and CASTNET networks were significantly better overall than those for the AQS and NAPS networks for both annual and seasonal evaluations (Tables S4A, S4S). It was noted that evaluation scores also tended to be similar for species with similar characteristics, such as primary species vs. secondary species and species having similar emissions sources (e.g., combustion). Observed and predicted annual and seasonal CV values for the other gas-phase species were also considered. Based on CV values, they fell naturally into three groups, depending on whether the pollutants were primary, secondary, or mixed primary-secondary in nature. Lastly, it was noted that a few scores for 2016 appeared to be outliers and that monthly density scatterplots for hourly NO and CO revealed obvious precision problems with reported measurements for these two species (Figs. S172, S176).

Formatted: Space Before: 6 pt

3.3.2 PM_{2.5} chemical composition

As emphasized by Bachmann (2013), PM_{2.5} is a multi-pollutant. This means that accurate forecasts of PM_{2.5} total mass require accurate forecasts of its underlying chemical components, each of which has different emissions sources and different formation pathways. Forecast errors for PM_{2.5} total mass can thus be better understood by examining forecast errors for its underlying chemical components. Fortunately, three North American networks (CSN, IMPROVE, NAPS) make measurements of PM_{2.5} composition (Sect. 2.3 and Table S2a). Station locations for these three networks are plotted in Fig. S6b, while Table S2c summarizes the number of stations for 2013–2016 for which PM_{2.5} speciation measurements were available and the smaller number for which temporally representative seasonal and annual measurements were available (see Sect. S2.4).

Figure 14 shows plots of the spatial distributions of annual mean surface concentrations of nine PM_{2.5} chemical components over North America for 2013–2016 and 2021/22 predicted by the RAQDPS-OP023. Note that the sets of contour intervals used vary by component, with PM_{2.5}-EC, PM_{2.5}-NH₄, and PM_{2.5}-CM having the smallest ranges and PM_{2.5}-SS and PM_{2.5}-TOM (= PM_{2.5}-POM + PM_{2.5}-SOM) having the largest ranges. It is clear from this figure that the predicted spatial distributions vary markedly between PM_{2.5} chemical components. It is also clear that the predicted annual spatial distributions of each of these chemical components for these five years are broadly similar, pointing to the anchoring effect of relatively constant emissions to the atmosphere of primary PM_{2.5} chemical components and PM_{2.5} gas-phase precursors (e.g., Fig. S1), which for most pollutants changed relatively little from year to year (Table 1). The annual mean surface concentrations of PM_{2.5} total mass shown in Fig. 13 also displayed this were also broadly similar from year to yearity. However, a comparison of the spatial distributions of annual mean PM_{2.5}-SO₄ and PM_{2.5}-NO₃ surface concentrations from 2013 to 2021/22 in Fig. 14 does suggest decreasing concentrations of these two chemical components over this period, consistent with the large decreases in domain-total anthropogenic emissions of SO₂ and NO_x from 2013 to 2021/22 (Table 1). Interestingly, annual mean PM_{2.5}-NH₄ surface concentration fields can also be seen to decrease from 2013 to 2021/22 despite nearly constant NH₃ emissions over this period. This downward trend is due instead to the reduced availability of gaseous H₂SO₄ and HNO₃ in the atmosphere, which form sulfate and nitrate particulate salts with NH₃. Domain-wide primary PM_{2.5} emissions also decreased by 8% from 2013 to 2016 (Table 1), and some decline is evident from 2013 to 2016 for PM_{2.5}-EC and PM_{2.5}-POM in Fig. 14. The annual mean spatial distributions of other PM_{2.5} components display only small year-to-year variations with the exception of sea salt, for which interannual variations in mean surface concentration are driven by interannual variations in surface wind speed (see Fig. S9).

Although the above discussion suggests the close connection between the spatial distributions of emissions of primary PM_{2.5} components and PM_{2.5} gas-phase precursors and the resulting spatial distributions of PM_{2.5} chemical components in the atmosphere, it is not a simple relationship since many chemical and physical processes in the atmosphere modulate the chemical transformation and removal pathways of these multiple chemical components. For example, the annual spatial distributions of PM_{2.5}-SO₄ shown in Fig. ure-14 are quite smooth, which reflect its origin as a secondary pollutant resulting from gas-phase or aqueous-phase oxidation of North American SO₂ emissions, even

Formatted: Not Superscript/ Subscript

though the SO₂ emissions shown in Fig. S1d are largely emitted by isolated point sources (e.g., ECCC, 2018; Foley et al., 2023). The spatial distribution in Fig. 14 of PM_{2.5}-SOM, another secondary pollutant, is also smooth, but its maximum is located further south over the southeastern U.S., where biogenic VOC emissions are high, especially in the summer season (cf. Fig. S27). It is also clear from Fig. S1 that there are marked differences in the spatial distributions of some of the anthropogenic emissions associated with different PM_{2.5} chemical components. For example, the majority of NO_x emissions are located in the eastern half of North America, but the locations of some major highways and large urban areas in western North America are visible in the PM_{2.5}-NO₃ surface concentration panels in Fig. 14, which suggests the important contributions of on-road mobile sources and population centres to NO_x emissions. Emissions of primary PM_{2.5} and of NH₃ gas, the precursor to PM_{2.5}-NH₄, on the other hand, are stronger over the North American interior (Figs. S1e,f). Elevated NH₃ emissions from agricultural activities in the midwestern U.S. are visible in Fig. S1e as well as fertilizer application in the San Joaquin Valley of California, large animal feedlot operations in Texas and Oklahoma, and extensive swine production in North Carolina. While NH₃ emissions are dominated by agricultural activities, some NH₃ emissions are also associated with population centres due to on-road mobile emissions (e.g., Toro et al., 2024). In addition, the chemical composition of primary PM_{2.5} emissions depends on the emissions source type. Combustion sources dominate PM_{2.5}-EC and PM_{2.5}-POM emissions, as ~~can be seen~~suggested in Fig. 14 by their association with major highways and population centres, while the PM_{2.5}-TOM surface concentration field displays characteristics of both the PM_{2.5}-POM and PM_{2.5}-SOM fields. Fugitive dust emissions from paved and unpaved roads are the main source of PM_{2.5}-CM, and PM_{2.5}-CM surface concentrations can be seen in Fig. 14 to be elevated in both urban centres and rural areas. Lastly, the spatial distribution of PM_{2.5}-SS is dominated by its oceanic sources, but the limited transport of sea salt from the oceans inland over most of North America that is evident in Fig. 14 should also be noted.

Table 5 presents all-station annual scores for seven PM_{2.5} chemical components for 2013–2016 for the three PM_{2.5} speciation networks combined. The scores for each component tend to be similar from year to year, but ~~these~~ scores can also vary considerably between components. For example, all-station annual NMB scores for PM_{2.5}-SO₄ and PM_{2.5}-NO₃ were negative for all four years whereas all-station annual NMB scores for PM_{2.5}-NH₄, EC, CM, and SS were positive for all four years. Only PM_{2.5}-TOM had small all-station annual NMB values of both signs for this period. Note that the PM_{2.5}-NH₄ overpredictions are inconsistent with the underpredictions of both PM_{2.5}-SO₄ and PM_{2.5}-NO₃ given the inorganic salts formed by these three components. One possible explanation is that this is an artefact due to the lack of available IMPROVE PM_{2.5}-NH₄ measurements (e.g., Solomon et al., 2014) so that only CSN and NAPS measurements were considered for PM_{2.5}-NH₄ in Table 5. However, the same inconsistency can be seen in Table S5A for just CSN measurements. Another possible explanation is that the RAQDPS-OP023 does not consider the neutralization of PM_{2.5}-SO₄ and PM_{2.5}-NO₃ by base cations, which would reduce PM_{2.5}-NH₄ concentrations and increase NH₃ VMR (e.g., Vasilakos et al., 2018; Miller et al., 2024; Semeniuk et al., 2025). All-station annual NMAE scores in Table 5 for 2013–2016 were lowest for PM_{2.5}-SO₄ (~0.47), followed in ~~rank-ascending~~ order by annual NMAE scores for PM_{2.5}-NO₃, TOM, EC, NH₄, CM, and SS (~1.45). All-station annual FAC2 scores were highest for PM_{2.5}-SO₄ (~0.64), followed in ~~decreasing-descending~~ order by those for PM_{2.5}-EC, TOM, NH₄, NO₃, SS, and CM (~0.31).

All-station annual R scores were also highest for PM_{2.5}-SO₄ (~0.66), followed in ~~decreasing~~ descending order by those for PM_{2.5}-NO₃, EC and SS, NH₄, TOM, and CM (~0.17). Based on the annual NMAE, FAC2, and R scores taken together, the RAQDPS-OP023 showed the most skill for PM_{2.5}-SO₄ followed in descending order by PM_{2.5}-NO₃, EC, TOM, NH₄, SS, and CM.

Note also that all-station annual NSD scores fell into two groups: values for PM_{2.5}-SO₄, NO₃, and NH₄ were less than ~~one~~ 1.0 whereas values for PM_{2.5}-EC, TOM, CM, and SS were greater than ~~one~~ 1.0. The three components in the first group are all secondary components whereas those in the second group are all primary components or a mixed primary-secondary component in the case of PM_{2.5}-TOM. While this difference might appear to suggest that the model is overemphasizing the contribution of temporal variations due to emissions, the PM_{2.5} speciation measurements are 24-hour samples so that the observed and predicted temporal variation at measurement locations can only be due to interday and longer variations. For anthropogenic emissions this would point to the day-of-week and month-of-year temporal profiles that have been assumed by the emissions processing system for different source sectors (Sect. S2.2), but emissions for the two primary components that had the largest NSD values, PM_{2.5}-CM and SS, are also the ones most affected by meteorology.

It is worth noting that downward trends can be seen in Table 5 in the values of both observed and predicted annual mean concentrations for PM_{2.5}-SO₄, NO₃, and NH₄, consistent with the monotonic decreases in SO₂ and NO_x emissions that occurred over this period and with Fig. 14. For the PM_{2.5}-SO₄ evaluation statistics, the values of annual RMSE and R also decreased from 2013 to 2016. This is similar to decreases in these two statistics reported by Kelly et al. (2019) for the CMAQ model over the 2007 to 2015 period, which they attributed to decreasing SO₂ emissions and lower summertime PM_{2.5}-SO₄ peaks, which in turn reduced the PM_{2.5}-SO₄ “signal” (e.g., Chan et al., 2018). Note also that 2016 annual \bar{O} , \bar{M} , MB, NMB, RMSE, R, σ_O , and σ_M scores for PM_{2.5}-SO₄, NO₃, EC, and OC for two recent versions of the CMAQ model (with wildfire emissions) were ~~given-reported~~ in Appel et al. (2021). Although minor methodological differences such as inclusion or exclusion of NAPS measurements are suggested by comparisons of the 2016 \bar{O} and σ_O scores ~~for the two models in Table 5 and in Appel et al. (2021)~~, there is rough agreement between the 2016 RAQDPS-OP023 scores and CMAQ scores and the RAQDPS023 2016 scores in Table 5 for PM_{2.5}-SO₄, NO₃, and EC while RAQDPS-OP023 PM_{2.5}-TOM scores CMAQ PM_{2.5}-OC scores cannot be compared directly with CMAQ PM_{2.5}-OC scores RAQDPS023 PM_{2.5}-TOM scores.

PM_{2.5} reconstructed mass

PM_{2.5} speciation measurements can also be used to calculate PM_{2.5} reconstructed dry mass (i.e., excluding aerosol water) as a weighted sum of the individual PM_{2.5} chemical ~~species-components~~ (e.g., Malm et al., 2011; Chow et al. 2015; Hand et al., 2019). This is often done ~~using-with~~ the IMPROVE formula, which uses some measured ~~components-species directly and some measured components~~ as proxies for the TOM, CM, and SS components, which are not measured directly. The RAQDPS-OP023 PM_{2.5} total mass forecasts, on the other hand, which are the sum of the seven predicted PM_{2.5} ~~speciated~~ chemical components shown in Table 5 (including SS but excluding aerosol water),

Formatted: Underline

Formatted: Space After: 6 pt

Formatted: Space Before: 0 pt

Formatted: Not Superscript/ Subscript

are thus also a reconstructed dry mass but do not require the use of any proxies. A slightly modified version of the IMPROVE formula has been used in this study to calculate PM_{2.5} reconstructed mass from speciation measurements (see Sect. S3.3.2 for more details).

Figure 15 compares observed and RAQDPS-OP023-predicted all-station seasonal mean PM_{2.5} reconstructed dry mass and chemical composition for 2013–2016 based on combined CSN, IMPROVE, and NAPS measurements that were mass-complete (Sect. S3.3.2). There is good agreement overall between the seasonal means of observed and predicted PM_{2.5} reconstructed dry mass—seasonal means. Predicted PM_{2.5} total mass was greater than observed PM_{2.5} reconstructed total mass for all four winters, while the opposite was true for all four summers, with closer agreement for spring and autumn. This good agreement might seem surprising given the consistent model underpredictions of hourly PM_{2.5} mass measurements described in Sect. 3.2.2, but it is more consistent with the better evaluation results for daily gravimetric PM_{2.5} mass measurements also discussed in that section. Similar comparisons for the CMAQ model against CSN and IMPROVE measurements have been presented for 2011 and 2016 simulations by Appel et al. (2017, 2021). Interestingly, both models overpredicted PM_{2.5} total mass in winter 2016 and underpredicted it in summer 2016.

In addition, the stars plotted in Fig. 15 indicate the seasonal means of observed gravimetric PM_{2.5} total mass for 2013–2016. It is natural to compare gravimetric PM_{2.5} total mass and PM_{2.5} reconstructed mass since they both attempt to measure of the same quantity. Good agreement can be seen in the observations between these two measurements for three seasons but not for the summer, for which the gravimetric total mass was larger. This is consistent with previous findings by Malm et al. (2011) for the CSN and IMPROVE networks. Predicted seasonal means of PM_{2.5} total mass, on the other hand, were greater than the gravimetric seasonal means in winter and autumn but were even smaller than the observed PM_{2.5} reconstructed mass in summer. A closely related quantity, the PM_{2.5} residual mass, is defined to be the difference between gravimetric PM_{2.5} mass and reconstructed PM_{2.5} mass (e.g., Hand et al., 2019). Observed seasonal mean PM_{2.5} residual mass was greater than 0.5 µg·m⁻³ for summer but was small otherwise, whereas predicted seasonal mean PM_{2.5} residual mass was greater than 1 µg·m⁻³ for summer but was negative for winter, with values ranging from -1.47 to -0.90 µg·m⁻³ (see Table S55-mr). Hand et al. (2019) found observed seasonal PM_{2.5} residual mass to be mostly positive after 2011 with a strong summer peak, consistent with Fig. 15. Given the marked model RAQDPS-OP023 underpredictions of summer mean gravimetric PM_{2.5} total mass but overpredictions of winter mean gravimetric PM_{2.5} total mass (Sect. S3.2.2), the factors that contribute to the non-negligible observed summer PM_{2.5} residual mass may be of interest because they may also be relevant to the model performance. Malm et al. (2011), Chow et al. (2015), and Hand et al. (2019) have suggested that some of these factors may be the neglect of particle-bound water in calculating PM_{2.5} reconstructed mass, ammonium and nitrate volatilization under laboratory conditions, and seasonal variations in the OM:OC scaling ratio (lower in winter, higher in summer) in the OM:OC scaling ratio needed to scale observed OC concentration to ambient TOM concentration. Note too that the volatilization of PM_{2.5}-NO₃ and PM_{2.5}-NH₄ during the transport, storage, and analysis of filter samples, a negative measurement artefact, will create spurious positive model biases for these two PM_{2.5} components (cf. Table 5).

Formatted: Font: Not Bold

1105 Figure 15 also shows good agreement overall between observed and RAQDPS-OP023-predicted seasonal mean PM_{2.5} chemical composition. Looking component by component, the dominant contribution of the PM_{2.5}-EC and TOM carbonaceous components to PM_{2.5} total mass is evident in both the observed and predicted stacked bar graphs as are the anticorrelated seasonal variations in PM_{2.5}-SO₄ and PM_{2.5}-NO₃. Overpredictions of PM_{2.5}-TOM concentration in the winter but underpredictions in the summer can be seen for all four years. The decrease in the observed and predicted contribution of the three major inorganic ions (SO₄, NO₃, NH₄) to PM_{2.5} total mass from 2013 to 2016 due to decreases in annual SO₂ and NO_x emissions can also be seen. Some of the annual mean biases for the PM_{2.5} chemical components noted in Table 5 are also reflected in almost all seasons in Fig. 15, including the underpredictions of PM_{2.5}-SO₄ and NO₃ and overpredictions of PM_{2.5}-EC and SS. In fact, the reduction of bias for predictions of PM_{2.5} total mass that is associated with the summation of these components, with their individual underpredictions and overpredictions is an example of the positive impact that compensating errors can have on model skill, and it demonstrates the value of a more comprehensive evaluation of model performance, in this case evaluating the prediction of PM_{2.5} chemical components in addition to PM_{2.5} total mass.

Since Fig. 15 is based on measurements from sampling sites located mainly over the continental U.S. (see Fig. S6b), it does not account for PM_{2.5} composition over northern Mexico and most of Canada. Figure 16, by contrast, shows a monthly time series of the RAQDPS-OP023-predicted mean PM_{2.5} chemical composition averaged over the land portion of the domain and the 2013–2016 simulations, with PM_{2.5}-TOM separated into POM and SOM (not possible for the measurements). Seasonal variations of PM_{2.5}-SO₄, NO₃, POM, SOM, and SS can be clearly seen, whereas seasonal variations of PM_{2.5}-NH₄, EC, and CM are less pronounced. PM_{2.5}-NO₃ and POM are predicted to have winter maxima and summer minima, whereas PM_{2.5}-SO₄ and SOM are predicted to have winter minima and summer maxima. Note that the total inorganic component (sum of PM_{2.5}-SO₄, NO₃, and NH₄) only has a relatively small monthly variation with a minimum in November. The predicted peak monthly mean PM_{2.5} total dry mass occurs in August, driven by monthly maximum values of PM_{2.5}-SO₄ and SOM. This is different from Figs. 8 and 15, where the highest PM_{2.5} total mass was predicted to occur in the winter, but note that predicted PM_{2.5} total mass in Figs. 8 and 15 is roughly 65 µg·m⁻³ vs. 1.5 µg·m⁻³ in Fig. 16, which suggests that the former overweights the influence of urban areas. One other interesting feature in Fig. 16 is the SS maximum in August, which is in apparent contradiction to the SS wintertime maximum evident in Fig. S30. However, while Fig. S30 showed that inland penetration of sea salt over North America is limited, some seasonal variations are evident near California, Florida and the U.S. Gulf coast, and Florida that may be associated with the occurrence of sea-land breezes in the warm season (and observed seasonal-mean SS values in Table S5S are largest in the spring and summer). Lastly, Fig. S203 presents a similar analysis to Fig. 16 but for averaging over the full domain. Unlike Fig. 16 (The SS component clearly dominates PM_{2.5} bulk total dry mass in this figure, unlike Fig. 16, reflecting predicted high levels of sea salt over the Pacific and Atlantic Oceans. In addition, the largest monthly mean SS concentrations in Fig. S203 occur in the cold season, consistent with Fig. S30.

It is also informative to look at the diurnal variation of the PM_{2.5} chemical components. Figure 17 shows the predicted diurnal variation of eight PM_{2.5} chemical components for each season after averaging over the 2013–2016 simulations

1140 and all North American continental grid cells. It is clear from this figure that both PM_{2.5} total mass and chemical
composition are predicted to vary with time of day. PM_{2.5} total mass has a maximum for three seasons at 12 UTC (=7
EST), near sunrise and morning rush hour, and a minimum in all seasons at 21 UTC (=16 EST). The wintertime
maximum, on the other hand, occurs at 04 UTC (i.e., near local midnight), pointing to a different balance between
surface emissions and vertical stability and mixing. Note too that the individual PM_{2.5} chemical components display
1145 different diurnal behaviours. Hourly PM_{2.5}-SO₄ concentration is predicted to be effectively constant, consistent with a
nonvolatile, secondary regional pollutant. Hourly PM_{2.5}-NO₃ and NH₄ concentrations, by contrast, are lowest in the
afternoon when near-surface temperature is highest, and highest at night, especially before sunrise when near-surface
temperature is often lowest. This behaviour is consistent with the semi-volatile nature of ammonium nitrate, for which
lower temperatures favour the particle phase (e.g., Malm et al., 2004; Yu et al., 2005). Hourly PM_{2.5}-EC, POM, and
1150 CM concentrations are also predicted to be highest during the night and lowest in the afternoon, but this behaviour is
likely due to greater vertical mixing of local emissions during the day, which reduces the near-surface buildup of these
three primary species. Hourly PM_{2.5}-SOM, which is assumed to be nonvolatile in the RAQDPS-OP023 (see companion
paper by Moran et al., 20265), behaves like PM_{2.5}-SO₄ and displays little diurnal variation. Finally, sea-salt
concentrations tend to be higher at night and lower during the day, likely due to diurnal variations in surface wind
1155 speed and hence in sea-salt emissions.

Note that the daily measurements made by the PM_{2.5} speciation networks are not able to confirm these diurnal variations
of PM_{2.5} chemical components in Fig. 17 predicted by the RAQDPS-OP023 model. However, the all-station, annual-
mean diurnal analyses of observed and predicted hourly PM_{2.5} total mass shown in Fig. 11 for North America for
2021/22, in Fig. S167 for four seasons, and in Fig. S168 for four sub-continental regions, all suggest that measured
1160 diurnal variations were smaller than the predicted variations. Two contributing factors to this difference might be the
diurnal allocation of primary PM_{2.5} emissions used by the RAQDPS-OP023 and the parameterization of PM_{2.5} chemical
volatility, including ammonium, nitrate, and water components. Interestingly, Fig. S167 shows that the observed
diurnal variation was largest in the winter and smallest in the summer, which is consistent with Fig. 17. In addition,
both the observed and predicted all-station seasonal-mean diurnal curves of PM_{2.5} total mass in Fig. S167 have one
1165 peak at about the time of morning rush hour and sunrise and a second peak at about the time of evening rush hour and
sunset. By contrast the seasonal continent-wide diurnal time series in Fig. 17 only have one peak, in the morning near
sunrise, but the majority of grid cells sampled for this figure will contain little vehicular activity, unlike the urban areas
in which many monitors are located.

Additional analyses

1170 More evaluation results for the daily PM_{2.5} speciation measurements and gravimetric PM_{2.5} total mass measurements*
for 2013–2016 can be found in Sect. S3.3.2. These results include tables of annual and seasonal scores for the
individual CSN, IMPROVE, and NAPS networks as well as regional scores, spatial plots of annual MB, NMB,
CRMSE, and R station scores for each PM_{2.5} chemical component, spatial plots of predicted seasonal mean PM_{2.5}
component concentration fields (cf. Fig. 14), monthly time series of PM_{2.5} component statistics, monthly density

1175 scatterplots, and additional stacked bar graphs stratified by network and by region. The discussion of Table 5 noted
 consistent annual underpredictions or overpredictions for some of the seven PM_{2.5} chemical components for the 2013–
 2016 hindcasts. Similarly consistent biases were found throughout the year by season or month for the combined
 networks for three PM_{2.5} components, namely underpredictions for PM_{2.5}-SO₄ (Fig. S151) and overpredictions for
 PM_{2.5}-EC (Fig. S154) and PM_{2.5}-SS (Fig. S157). In addition, PM_{2.5}-TOM, the component found to have the smallest
 1180 annual biasNMB values, was shown to have pronounced seasonal biases consistent with Fig. 15, with marked
 overpredictions in winter and underpredictions in summer (Fig. S155). Nevertheless, performance benchmarks for
 five PM_{2.5} chemical components (SO₄, NO₃, NH₄, EC, TOM) proposed by Emery et al. (2017) were also compared
 with both annual and seasonal scores. Nearly all PM_{2.5}-SO₄, NO₃, NH₄, and TOM annual NMB scores and many
 seasonal scores met acceptable NMB benchmarks, all PM_{2.5}-SO₄ and NO₃ annual and most seasonal NMAE scores met
 1185 acceptable NMAE benchmarks, and all PM_{2.5}-SO₄, NO₃, NH₄, and EC annual and seasonal R scores met acceptable R
 benchmarks. Some annual and seasonal biases were also shown to be network-dependent. Annual NMB values for
 2013–2016 for PM_{2.5}-TOM ranged from 0.20 to 0.31 for CSN and from 0.52 to 0.80 for NAPS vs. -0.46 to -0.30 for
 IMPROVE (Table S5A). For PM_{2.5}-CM the network-dependent biases were even more pronounced: annual NMB
 values ranged from 1.23 to 1.59 for CSN and from 1.96 to 2.34 for NAPS vs. -0.59 to -0.50 for IMPROVE. Seasonal
 1190 PM_{2.5}-SO₄ was underpredicted and PM_{2.5}-SS was overpredicted throughout the year for all three speciation networks,
 but PM_{2.5}-EC was overpredicted for the urban-focused CSN and NAPS networks in all seasons but not for the rural-
 focused IMPROVE network (Table S5S). Since Similarly, annual NMB values for PM_{2.5}-TOM ranged from 0.20 to
 0.31 for CSN and from 0.52 to 0.80 for NAPS vs. -0.46 to -0.30 for IMPROVE (Table S5A). And for PM_{2.5}-CM the
 network-dependent biases were even more pronounced: annual NMB values ranged from 1.23 to 1.59 for CSN and
 1195 from 1.96 to 2.34 for NAPS vs. -0.59 to -0.50 for IMPROVE. PM_{2.5}-EC, POM, and CM are all primary pollutants,
~~suggesting that~~ some of these model biases may might be connected to the representation of primary PM_{2.5} emissions.

The systematic biases by network that were identified for some PM_{2.5} chemical components also affect predictions of
 PM_{2.5} composition and total mass. The discussion of Fig. 15 noted that the best agreement was for spring and autumn.
 However, when the same analysis was applied to only CSN measurements and to only IMPROVE measurements, the
 1200 agreement was less good for these two seasons, with the model-RAQDPS-OP023 overpredicting PM_{2.5} total mass for
 CSN for spring and autumn (Fig. S200) and underpredicting PM_{2.5} total mass for IMPROVE (Fig. S201). The findings
 were similar for a regional analysis, where predicted PM_{2.5} composition and total mass were in very good agreement
 with the combined measurements for the WUS and EUS (Fig. S205), but the same regional analysis for CSN-only
 measurements (Fig. S206) and IMPROVE-only measurements (Fig. S207) revealed errors of opposite sign, with
 1205 overpredictions of PM_{2.5} total mass for CSN for the WUS and underpredictions of PM_{2.5} total mass for IMPROVE for
 both the WUS and EUS. The presence of these compensating errors for urban-focused and rural-focused stations again
 points to the benefits of performing a more disaggregated analysis. These network-dependent differences are also
 consistent y also agree with the finding in Sect. 3.2.2 that underprediction of PM_{2.5} total mass by the RAQDPS-OP023
 underprediction appears to be mainly a rural issue. Predicted peak seasonal concentrations for PM_{2.5}-NO₃, NH₄, POM,
 1210 and SS occurred in the winter (Figs. S23, S24, S26, and S30) vs. summer peaks for PM_{2.5}-SO₄, SOM, and TOM (Figs.

S22, S27, and S28). This ~~complementarity~~ seasonal phase shift can help to explain the ~~observed~~ bimodality that was observed in monthly PM_{2.5} total mass (Figs. 8 and S198).

~~Additional~~ close links ~~were~~ also evident between the inorganic PM_{2.5} components and their gas-phase precursors. For example, the monthly mean concentration time series for PM_{2.5}-SO₄ (Fig. S151) was seasonally anticorrelated with ~~and the monthly time series for its gas-phase precursor~~ SO₂ (Fig. S146), ~~which were seasonally anticorrelated~~; that is, the PM_{2.5}-SO₄ time series had an observed and predicted summer maximum and winter minimum and monthly NMB values ~~were~~ underpredicted ~~negative~~, while the SO₂-its precursor, time series had an observed and predicted winter maximum and summer minimum and monthly NMB values ~~were~~ overpredicted ~~positive~~. The monthly mean concentration time series for ~~A similar anticorrelation was evident for~~ PM_{2.5}-NO₃ (Fig. S152) was seasonally anti- ~~correlated with that for~~ and its gas-phase precursor HNO₃ (Fig. S144) ~~(and also PM_{2.5}-SO₄), which were also closely related~~; that is, the PM_{2.5}-NO₃ time series had an observed and predicted summer minimum and winter maximum and was mostly underpredicted while the HNO₃ time series had an observed and predicted winter minimum and summer maximum and was overpredicted. The monthly mean concentration time series for PM_{2.5}-NH₄, the third inorganic component (Fig. S153), was also seasonally anticorrelated with that for its gas-phase precursor NH₃ (Fig. S145) ~~(and also HNO₃)~~; that is, the PM_{2.5}-NH₄ time series had an observed and predicted summer minimum and winter maximum and was mostly overpredicted while the NH₃ time series had an observed and predicted winter minimum and summer maximum and was underpredicted. Lastly, downward time trends for 2013-2016 were also visible in observed monthly surface concentrations of PM_{2.5}-SO₄ and NH₄ (Figs. S151, S153) due to the SO₂ and NO_x emissions decreases that took place over this period.

Formatted: Subscript

Formatted: Subscript

3.3.3 Precipitation chemistry

Precipitation-chemistry measurements are valuable for model evaluation because they are quite different from the air-chemistry measurements considered in the previous sections. One difference is that they quantify a removal process, wet deposition, as opposed to near-surface ambient concentrations determined by dispersion and chemistry. In addition, they represent removal through a column extending from the Earth's surface to cloud top rather than a pure surface-level quantity. They are also an integrated measurement in terms of both gas-particle partitioning and aerosol particle size distribution because they can include contributions from both gas and particle phases and from all aerosol particle sizes. Precipitation-chemistry measurements can thus provide some important insights into removal processes and atmospheric mass budgets for sulfur, oxidized nitrogen, reduced nitrogen, and base cations ~~removal processes and atmospheric mass budgets~~. As described in Sect. 2.3, two large national networks are responsible for North American precipitation-chemistry measurements, CAPMoN in Canada and NADP in the U.S.

Figure 18 shows the RAQDPS-OP023-predicted spatial distributions of annual mean concentration in precipitation over North America of the three major inorganic ions, SO₄⁻, NO₃⁻, and NH₄⁺, for 2013–2016 and 2021/22. Several features are evident. First, the spatial distributions are different for each of these ions, largely in response to the different spatial distributions of their respective precursor emissions (cf. Fig. S1). Annual mean SO₄⁻ concentration in

1245 precipitation tends to be larger over the eastern U.S., whereas annual mean NO_3^- and NH_4^+ concentrations in precipitation are larger over the western and central U.S. Another feature is that predicted SO_4^{2-} and NO_3^- annual mean concentrations in precipitation appear to decrease from 2013 to 2021/22+6, consistent with the 60.37% and 36.48% decreases in North American SO_2 and NO_x anthropogenic emissions, respectively, over this period (Table 1). No time trend is evident for this period, however, for annual mean NH_4^+ concentration in precipitation, which differs from the downward trend for annual mean $\text{PM}_{2.5}\text{-NH}_4$ concentration visible in Table 5 and Fig. 14. Two reasons are that annual NH_3 emissions only decreased slightly (6.7%) from 2013 to 2021/22+6 and both NH_3 and $\text{PM}\text{-NH}_4$ are removed by precipitation scavenging regardless of the exact balance for gas-particle partitioning, whereas annual mean NH_3 VMR displayed a slight upward trend from 2013 to 2021/22+6 (cf. Table 4, Fig. S16). Figure 18 also agrees qualitatively with comparable plots of observed annual mean SO_4^{2-} , NO_3^- , and NH_4^+ concentrations in precipitation for these four years produced by the U.S. NADP network (e.g., National Acid Deposition Program, 2014, 2017), except for the elevated values of annual mean NO_3^- and NH_4^+ concentrations in precipitation predicted over California in 2013. Note too that the corresponding annual wet deposition fields predicted by the RAQDPS-OP023 for 2014–2016 (see Figs. S34–S36) have also been used in a study by Cathcart et al. (2025) to calculate total deposition and acidity and nutrient nitrogen critical-load exceedance fields for Canada.

1260 Table 6 lists all-station annual evaluation statistics for 2013–2016 for RAQDPS-OP023-predicted weekly concentrations in precipitation of SO_4^{2-} , NO_3^- , and NH_4^+ , for weekly precipitation, and for the corresponding predicted weekly wet deposition of these ions. The weekly precipitation scores were already discussed in Sect. 3.1. The reductions in concentrations in precipitation of SO_4^{2-} and NO_3^- from 2013 to 2016 suggested visually by Fig. 18 are confirmed by Table 6. Observed and predicted annual-mean SO_4^{2-} weekly concentration in precipitation for the combined networks decreased from 0.81 to 0.62 $\text{mg}\cdot\text{L}^{-1}$ and from 0.82 to 0.61 $\text{mg}\cdot\text{L}^{-1}$, respectively, over this period, while observed and predicted annual-mean SO_4^{2-} weekly wet deposition decreased from 15.6 to 10.7 $\text{mg}\cdot\text{m}^{-2}\cdot\text{week}^{-1}$ and from 15.9 to 10.1 $\text{mg}\cdot\text{m}^{-2}\cdot\text{week}^{-1}$, respectively. Observed and measured-predicted annual-mean NO_3^- weekly concentration in precipitation and weekly wet deposition also declined from 2013 to 2016, though by smaller percentages, from 0.96 to 0.90 $\text{mg}\cdot\text{L}^{-1}$ and 0.94 to 0.78 $\text{mg}\cdot\text{L}^{-1}$ and from 16.5 to 14.1 $\text{mg}\cdot\text{m}^{-2}\cdot\text{week}^{-1}$ and 16.2 to 11.6 $\text{mg}\cdot\text{m}^{-2}\cdot\text{week}^{-1}$, respectively. By contrast, observed and predicted annual-mean NH_4^+ weekly concentration in precipitation increased slightly while observed and predicted annual-mean NH_4^+ weekly wet deposition decreased slightly.

1275 Table 6 also reveals that model performance can vary considerably by ionic species. For example, all-station annual NMB values for SO_4^{2-} and NO_3^- weekly concentrations in precipitation ranged from -0.01 to 0.14 and from -0.14 to -0.01, respectively, but corresponding all-station annual NMB values for NH_4^+ weekly concentration in precipitation ranged from 0.23 to 0.41, pointing to a considerable and consistent overprediction for this quantity. All-station annual NMB scores for SO_4^{2-} , NO_3^- , and NH_4^+ weekly wet deposition ranged from -0.06 to 0.05, -0.18 to -0.02, and 0.13 to 0.16, respectively, suggesting small biases for SO_4^{2-} wet deposition, a small but consistent underprediction for NO_3^- wet deposition, and a consistent overprediction for NH_4^+ wet deposition. In comparison, Simon et al. (2012) reported

(~~2540%~~, ~~7590%~~) quantile values for NMB scores for accumulated seasonal and annual SO_4^- , NO_3^- , and NH_4^+ wet deposition of (-0.019, 0.2338), (-0.3745, 0.109), and (-0.2133, 0.028), respectively, in a review of North American AQ model performance evaluations. The RAQDPS-OP023 annual NMB scores fit comfortably within these reported ranges ~~despite their much lower level of temporal aggregation (i.e., weekly vs. annual)~~. Zhang et al. (2018c) reported ~~large negative annual mean~~ NMB values for SO_4^- , NO_3^- , and NH_4^+ accumulated annual wet deposition of -0.05, -0.32, and -0.31, respectively, for the 1990–2010 period using the CMAQ model without post-processing adjustments, and Benish et al. (2022) obtained ~~annual-mean~~ NMB values for SO_4^- , NO_3^- , and NH_4^+ accumulated annual wet deposition of -0.12, -0.10, and -0.20 for the 2002–2017 period using a newer version of the CMAQ model ~~and-but~~ also without post-processing adjustments. Note that the negative bias in NO_3^- concentration in precipitation and wet deposition is consistent with the neglect of lightning NO emissions in both ~~models-CMAQ and the RAQDPS-OP023~~ (Zhang et al., 2018c).

Corresponding all-station annual NMAE values from Table 6 for SO_4^- , NO_3^- , and NH_4^+ weekly concentrations in precipitation for 2013–2016 ranged from 0.59 to 0.68, 0.52 to 0.57, and 0.78 to 0.95, respectively, and annual NMAE values for SO_4^- , NO_3^- , and NH_4^+ weekly wet deposition ranged from 0.61 to 0.65, 0.52 to 0.55, and 0.68 to 0.72. The NMAE scores for weekly wet deposition compare favourably with top-quartile NMAE scores for ~~accumulated seasonal and annual monthly~~ SO_4^- , NO_3^- , and NH_4^+ wet deposition of 0.61, 0.51, and 0.57 compiled by Simon et al. (2012) ~~despite their lower level of temporal aggregation~~. All-station annual FAC2 values for weekly concentration in precipitation were slightly higher (better) for NO_3^- (0.68–0.70) than for SO_4^- or NH_4^+ (0.63–0.65; 0.57–0.60), and the same was true for weekly wet deposition (0.62–0.64 vs. 0.53–0.56 and 0.55–0.57). All-station annual R scores for all stations were also slightly higher for NO_3^- weekly concentration in precipitation (0.46–0.52) than for SO_4^- or NH_4^+ weekly concentration in precipitation (0.25–0.41, 0.38–0.47), whereas all-station annual R scores for SO_4^- , NO_3^- , and NH_4^+ weekly wet deposition were comparable (0.49–0.58, 0.46–0.59, 0.47–0.59). By comparison, Zhang et al. (2018c) obtained higher ~~annual-mean~~ R scores for accumulated SO_4^- , NO_3^- , and NH_4^+ annual wet deposition for the 1990–2010 period of 0.92, 0.89, and 0.77, respectively, and Benish et al. (2022) obtained ~~annual-mean~~ R scores for accumulated SO_4^- , NO_3^- , and NH_4^+ annual wet deposition for the 2002–2017 period of 0.788, 0.7788, and 0.6178, but these higher scores may again be explained ~~at least in part~~ by ~~the much~~ greater temporal aggregation ~~and averaging~~. Note also that the values of the statistics in Table 6 were fairly constant across the four years in spite of the large SO_2 and NO_x emission reductions, ~~again~~ suggesting that the year-specific input emissions that were used for the retrospective simulations were representative of each year.

Additional analyses

More evaluation results for predicted SO_4^- , NO_3^- , and NH_4^+ weekly concentrations in precipitation and ~~weekly~~ wet deposition can be found in Sect. S3.3.3. These include tables of separate annual and seasonal scores for the CAPMoN and NADP networks for 2013–2016 as well as regional scores, spatial plots of annual MB, NMB, CRMSE, and R scores at individual stations, spatial plots of predicted seasonal concentration in precipitation and wet deposition fields for 2013–2016 and 2021/22, monthly time series of statistics for weekly concentrations in precipitation and wet

1315 deposition, and monthly density scatterplots. A number of additional insights can be found in these supplemental analyses. For example, the separate annual and seasonal scores for the CAPMoN and NADP networks presented in Tables S6A and S6S revealed ~~some differences that tended to favour~~ that RAQDPS-OP023 scores were better overall for CAPMoN than NADP. For example, annual R scores were consistently higher for CAPMoN than NADP for SO_4^{2-} , NO_3^- , and NH_4^+ weekly concentrations in precipitation and weekly wet deposition. Some regional differences were also evident in many of the spatial distributions of station-specific annual values of MB, NMB, CRMSE, and R. For example, the station-level annual MB scores for SO_4^{2-} weekly concentration in precipitation tended to be positive in eastern Canada and the northeastern U.S. but negative elsewhere (Fig. S109). Annual R values for SO_4^{2-} and NO_3^- weekly wet deposition also tended to be lower in the west and higher in the east (Figs. S128, ~~and~~ S132). It is also clear from Table S6S and Figs. S158–S164 ~~3~~ that seasonal model skill was consistent overall from year to year but sometimes varied markedly between seasons and species. For example, NH_4^+ weekly wet deposition had the largest variations in observed and predicted seasonal mean values of the three major ions, with maximum seasonal values ~~two to three~~ about four times higher than minimum seasonal values (Fig. S164). Scores for SO_4^{2-} weekly concentration in precipitation and weekly wet deposition were worse overall in the winter (Figs. S158, S162) whereas scores for NO_3^- and NH_4^+ weekly concentration in precipitation and weekly wet deposition were worse overall in the summer (Figs. S159–S160, S163–S164). Predicted monthly mean concentrations in precipitation for SO_4^{2-} , NO_3^- , and NH_4^+ all had both negative and positive biases, but the majority of monthly NMB values for SO_4^{2-} and NO_3^- weekly concentrations in precipitation fell in the ± 0.320 range for 2013–2016 (Figs. S158–S159), whereas monthly NMB values for weekly NH_4^+ concentration in precipitation had peak values from 0.70 to 1.70 in July (Fig. S160). Lower monthly NMB values ~~were found~~ for weekly wet deposition were comparable. The predicted seasonal ~~at mean~~ precipitation fields were shown to link ~~but geographically shift~~ seasonal concentration in precipitation fields and the seasonal wet deposition fields but to shift them geographically. Lastly, observed and predicted monthly mean values of SO_4^{2-} weekly concentration in precipitation and SO_4^{2-} weekly wet deposition all declined from 2013 to 2016 (Figs. S158, ~~and~~ S162), providing observational support together with Figs. S146 and S151 for the representativeness of the year-specific decreases in SO_2 annual emissions used for the hindcast annual simulations.

1340 4 Discussion

4.1 Comparison with RAQDPS forecast performance for 2010–2019

The RAQDPS operational AQ forecast system underwent 22 upgrades between 2010 and 2021 (Moran et al., 2026~~5~~). These included eight major upgrades: four that implemented significant changes to the modelling system code and configuration, two that involved major changes to the input emissions files, and two that included changes to both (Table A3). RAQDPS operational performance was routinely monitored over this period using hourly surface measurements of a small number of chemical species, in particular NO_2 , O_3 , and $\text{PM}_{2.5}$, from North American air-chemistry stations that report their measurements in near real time to AirNow or NAPS (Sect. 2.3). In order to assess the impact of this succession of system upgrades on forecast performance, Moran et al. (2021a) used hourly operational forecast outputs and NRT hourly AQ measurements archived at CMC to evaluate 9.5 years of RAQDPS operational

1350 forecasts of hourly surface NO₂, O₃, and PM_{2.5}, starting from RAQDPS-OP001 forecasts at the beginning of 2010 through to July 2019, when the RAQDPS-OP021 became operational (and before 2020 COVID-19 pandemic impacts in 2020: see e.g., Mashayekhi et al., 2021). This analysis aligned with suggestions made by Kelly et al. (2019) by providing as much consistency as possible in the calculation of evaluation statistics, in the model domain and grid resolution, and in the weighting of different time periods.

1355 While some data filtering is performed routinely on the NRT measurements received at CMC before they are used (Sect. 2.3), additional filtering was applied to this 2010–2019 AQ measurement data set (Moran et al., 2021a). More stringent lower and upper cutoff thresholds of 0 and 150 ppbv, 0 and 150 ppbv, and 0 and 200 µg·m⁻³ were imposed on the NO₂, O₃, and PM_{2.5} hourly observations, respectively. This additional filtering removed less than 0.1% of the available hourly measurements but avoided the impacts on the evaluation statistics of some extreme outliers.

1360 Measurement-model pairing was then performed for this 9.5-year period (cf. Sect. 2.4) followed by the calculation of seasonal performance statistics. Seasonal performance statistics for the 2013–2016 annual hindcast runs and 2021/22 forecast runs made with the RAQDPS-OP023 (Table S3S) could then be compared with these earlier results to examine the impact of using the new version of the forecast system along with year-specific emissions for 2013–2016 and projected emissions for 2021/22.

1365 Figure 19 shows decade-long time series of all-station seasonal R scores for hourly NO₂, O₃, and PM_{2.5} abundances for the sequence of operational systems from the RAQDPS-OP001 to the RAQDPS-OP020 that were in use for the 2010–2019 period. The time series of 2010–2019 seasonal R scores for NO₂ and O₃ shown in this figure are broadly comparable: both time series fall in a numerical band from 0.50 to 0.70, both exhibit cyclical seasonal variations, and both exhibit some overall improvement with time. These positive trends in R scores were anticipated since proposed RAQDPS upgrades are only accepted for operational implementation at CMC if they can demonstrate at least equal or better expected forecast skill relative to the existing operational version (Moran et al., 2026). There is also a suggestion of some anticorrelation to the seasonal R scores for NO₂ and O₃, with R scores for NO₂ tending to be highest in the winter and lowest in the summer whereas R scores for O₃ tended to be highest in the summer but lowest in the spring. The 2010–2019 seasonal R scores for PM_{2.5}, on the other hand, are lower than those for NO₂ and O₃, are less cyclical seasonally, and do not show any improvement with time.

1375 Figure 19 also shows seasonal R scores for the five RAQDPS-OP023 annual simulations for 2013–2016 and 2021/22 that are the focus of this paper. The RAQDPS-OP023 seasonal R scores for 2013–2016 were higher for both NO₂ and O₃ but lower for PM_{2.5} compared to the previous operational RAQDPS versions. The RAQDPS-OP023 seasonal scores for 2021/22 forecasts were slightly lower for NO₂, comparable for O₃, and higher for PM_{2.5} compared to the hindcast scores. These differences could be due either to changes to the treatments of atmospheric chemistry in GEM-MACH or to the use of more representative emissions in the RAQDPS-OP023 simulations, but of course neither change was intended to produce poorer PM_{2.5} forecasts. Each panel of Fig. 19 also shows the species-specific values of “acceptable” and “good” benchmarks for R scores recommended by Emery et al. (2017) and Zhai et al. (2024). Seasonal R scores for NO₂ surpassed the more stringent “good” benchmark of 0.60 for later operational versions of the

1385 RAQDPS, seasonal R scores for O₃ for the RAQDPS-OP023 surpassed the “acceptable” threshold of 0.50 but fell
 below the more stringent benchmark of 0.75, ~~but~~ and seasonal R scores for PM_{2.5} did not meet even the less stringent
 “acceptable” threshold of 0.40 for most forecast system versions or time periods.

Seasonal time series plots of four other statistics in the same format as Fig. 19 are shown in Figs. S215 to S219 for
 NO₂, O₃, and PM_{2.5}. It was found that RAQDPS-OP023 seasonal MB and NMB scores for 2013–2016 were better
 1390 than the historical operational scores for NO₂, slightly worse for O₃, and worse for PM_{2.5}, seasonal NMAE scores were
 better for NO₂ and O₃ and neutral for PM_{2.5}, seasonal RMSE scores were better for NO₂ and O₃ and worse for PM_{2.5},
 and seasonal FAC2 scores were better for NO₂, neutral for O₃, and ~~worse~~ better for PM_{2.5}. The RAQDPS-OP023
 seasonal MB and NMB scores for 2021/22 compared to 2013–2016 were worse for NO₂ and PM_{2.5} but slightly better
 for O₃, NMAE scores were slightly better for all three species, RMSE scores were comparable for all three species,
 1395 and FAC2 scores were worse for NO₂ and comparable better for O₃ and slightly worse for PM_{2.5}.

4.2 Impact of biomass burning emissions

As noted in Sect. 2.2, near-real-time BB emissions were included in the 2021/22 RAQDPS-FW023 forecasts but not
 in the 2021/22 RAQDPS-OP023 forecasts or the four annual RAQDPS-OP023 hindcasts considered in this paper.
 Such episodic but often large emissions can have a significant impact on both local and regional air quality (e.g., Jaffe
 1400 et al., 2004; Liu et al., 2015; Rappold et al., 2017; Hand et al., 2024), and discussions in Sect. 3 of a number of figures
 (Figs. 4, 5, 8, and 12) noted a drop in RAQDPS-OP023 skill for predicting PM_{2.5} concentration in the summer, the time
 of year when BB emissions are generally highest (e.g., Munoz-Alpizar et al., 2017; Chen et al., 2019). Table A4
 summarizes annual wildfire statistics for Canada and the U.S. for the 2013–2022 period. Large year-to-year variations
 can be seen for both countries in the number of wildfires and the land area burned each year. At the continental scale,
 1405 2015, 2017, and 2021 stand out as high wildfire years in terms of land area burned whereas 2016, 2019, and 2020 were
 lower wildfire years. The 2021/22 RAQDPS-OP023 forecasts thus corresponded to a high BB emissions year in 2021,
 in fact, a record-breaking year (Jain et al., 2024). Note, however, that years with high levels of land area burned in the
 U.S. (e.g., 2015, 2017, 2018, 2020) may have a greater impact in terms of overall North American population exposure
 to wildfire smoke since many Canadian wildfires occur far from population centres. Note ~~too~~ that summer 2015 was
 1410 identified as an outlier stands out in Fig. S201 the discussion as an outlier of Fig. S201 in Sect. S3.3.2 due to the elevated
 seasonal-mean PM_{2.5}-EC and TOM concentrations that were observed at IMPROVE stations, most of which are located
 in the western U.S. (Fig. S6b).

To assess the impact of the inclusion of BB emissions on forecast scores we can compare the RAQDPS-OP023 and
 RAQDPS-FW023 forecasts for the 12-month 2021/22 period. The only difference between these two forecast system
 1415 versions was the inclusion of BB emissions in the RAQDPS-FW023 runs but not the RAQDPS-OP023 runs. Table 7
 compares seasonal evaluation statistics for hourly NO₂, O₃, and PM_{2.5} forecasts for the two versions. For NO₂ only the
 summer statistics were slightly different (e.g., MB, FAC2). For O₃ there were slight differences in a few scores for the
 winter and spring and larger differences in the summer and autumn, including a reduction in seasonal MB in the

summer of 0.8 ppbv for the RAQDPS-FW023. Differences in O₃ seasonal CRMSE, FAC2, and R scores in the summer and autumn were also small improvements. And for PM_{2.5} there were larger differences in all four seasons, but especially in the summer and autumn. The summer mean PM_{2.5} concentration predicted by the RAQDPS-FW023 was slightly more than double that of the RAQDPS-OP023, which improved the summer NMB score from -0.51 to 0.04. Summer NMAE, FAC2, and R scores were also considerably better for the wildfire version (e.g., R increased from 0.09 to 0.55), although the RMSE and CRMSE values for the wildfire version were worse and the NSD value is now was too high (1.87) vs. too low (0.35). In addition, for the PM_{2.5} benchmarks recommended by Emery et al. (2017) for acceptable performance (NMB=±0.30, NMAE=0.50, R=0.40), seasonal scores for the RAQDPS-OP023 did not meet the thresholds for summer NMB and R and scores or autumn R but the RAQDPS-FW023 scores did meet these thresholds. These large improvements in most many evaluation metrics suggest that BB is emissions are an emissions source for that is important for part of the year that should be considered, but at the same time there is a deterioration in a few scores, suggesting that there is room to improve the estimation of wildfire-BB emissions in the RAQDPS-FW023.

Some additional analyses to understand the impact of BB emissions on 2021/22 RAQDPS-FW023 forecasts are presented in Sect. S4.2. These include plots of spatial distributions of annual and seasonal mean NO₂, O₃, and PM_{2.5} abundance fields and station-specific annual statistics, monthly time series of \bar{O} , median O, \bar{M} , median M, MB, NMB, CRMSE, FAC2, R, and NSD scores, and diurnal time series of five statistics by season and by region. These analyses confirmed that the inclusion of BB emissions improved some summer and autumn, and also annual scores for PM_{2.5} in 2021/22 (e.g., Fig. S227 vs. Fig. 8) along with minor improvements for O₃ scores and no impact for NO₂ scores. Winter and spring scores, on the other hand, were virtually unchanged, which meant that PM_{2.5} mass was underpredicted in these seasons by both system versions for other reasons. Interestingly, annual-mean PM_{2.5} scores also showed significant improvement when BB emissions were included, even though the BB emissions were strongly seasonal (e.g., Fig. S230 vs. Fig. 11). In addition, Fig. S237 showed that the 2021 wildfire season was an outlier even relative to 2015. Monthly time series of predicted median PM_{2.5} suggested that anthropogenic PM_{2.5} emissions may have been too low in the cold-season months (Fig. S234). And regional analyses suggested that wildfire smoke affected all of North America in 2021/22 (Fig. S231 vs. Fig. 12).

4.3 Comparison with other AQ forecast systems

It is also of interest to compare RAQDPS-OP023 and RAQDPS-FW023 forecast performance with that of peer AQ forecast systems operated by other agencies since such peer systems face similar constraints and limitations, including lack of access to year-specific input emissions and to meteorological and/or chemical data assimilation. To perform such a comparison, however, Simon et al. (2012) noted the challenge posed by the use of different measurement networks, evaluation metrics, sampling periods, sampling durations, evaluation metrics, measurement networks, and spatial domains in publications by different forecasting teams.

Formatted: Not Highlight

One such peer AQ forecast system is the U.S. National Air Quality Forecast Capability (NAQFC), which went operational in 2004 followed by many upgrades (see <https://www.emc.ncep.noaa.gov/mmb/qa/AQChangelog.html>; last access: ~~ed~~ 6 Aug-April 2026~~s~~). A number of papers that discuss NAQFC performance evaluations have been published, including Eder et al. (2006, 2009) Saylor and Stein (2012), Chai et al. (2013), Pan et al. (2014), Huang et al. (2017), Lee et al. (2017), Chen et al. (2021), Campbell et al. (2022), and Li et al. (2025). As suggested by Simon et al. (2012), only a limited number of evaluation results for surface PM_{2.5} predictions from these papers, including those summarized in Table A5, ~~can~~ could be used to compare NAQFC and RAQDPS performance over the parallel evolution of these two North American regional operational forecast systems. The overall conclusion based on these limited ~~published~~ comparisons for 2010, 2014, and 2015 is that performance was comparable for the two systems over the past decade (see Sect. S4.3 for details).

An ongoing co-operative North American AQ forecast intercomparison being conducted under the WMO GAFIS initiative (see Sect. S4.2) has allowed direct comparisons of more recent NAQFC and RAQDPS023 quarterly performance ~~to be compared directly~~ for 2021/22 (and subsequent years). The 2022 second-quarter GAFIS report (Manseau et al., 2022) compared monthly MFB (see Table A2 and Sect. S2.5), FAC2, and R scores for daily maximum forecasts of NO₂, O₃, and PM_{2.5} abundances for three North American regional AQ forecast systems, the RAQDPS-OP023, RAQDPS-FW023, and NAQFC, and three global AQ forecast systems for the 12-month 2021/22 forecast period, with a focus on spring 2022. For the monthly ~~mean~~ diurnal time series of daily maximum surface concentrations of NO₂, O₃, and PM_{2.5} presented in this report, there were marked variations evident between the six ~~different~~ AQ forecast systems. There was also considerable variation between the systems in monthly combined performance scores. Although no one system dominated, the NAQFC tended to be the top performer for O₃ forecasts, the RAQDPS-OP023 and RAQDPS-FW023 for NO₂ forecasts, and IFS-CAMS for PM_{2.5} forecasts. ~~T, and the~~ combined performance scores also tended to be highest overall for O₃ forecasts and lowest for PM_{2.5} forecasts. The monthly R scores can also be compared to available benchmarks. Most of the NO₂ R scores for five of the systems (NO₂ forecasts were not available for NAQFC) ~~were above~~ met the acceptable benchmark of 0.50 recommended by Zhai et al. (2024) and some RAQDPS-OP023, RAQDPS-FW023, and IFS-SILAM scores also ~~exceeded~~ met their benchmark goal of 0.60. R scores for O₃ for all six systems ~~exceeded~~ met the acceptable benchmark of 0.50 recommended by Emery et al. (2017) and in a few cases also ~~exceeded~~ met their benchmark goal of 0.75. And for PM_{2.5} R scores none of the systems ~~attained~~ met the acceptable benchmark of 0.60 recommended by Huang et al. (2021), but in July and August 2021, when many wildfires were burning, the lower benchmark of 0.40 recommended by Emery et al. (2017) was ~~reached~~ met by most of the models, including the RAQDPS-FW023 but not the RAQDPS-OP023. Section S4.3 also describes an ongoing evaluation and intercomparison of 11 operational regional AQ forecast models for Europe that is similar to the GAFIS regional intercomparison for North America and ~~compares~~ a few evaluation scores from this European intercomparison are compared with the RAQDPS-OP023 scores.

Formatted: Font: Not Bold

1485 4.4 Forecast system shortcomings, opportunities, and priorities for further development

Many of the evaluation results for RAQDPS-OP023 forecasts and hindcasts versus AQ measurements, previous system versions, and peer forecast systems discussed in previous sections were positive. For example, Figs. 6 and 7 for the 2021/2022 forecasts (and Figs. S140 and S141 for the 2013–2016 hindcasts) show model skill for predicting NO₂ and O₃ surface VMR monthly means at the continental scale as does Fig. 12 for four North American regions. Good agreement for all-station, annual-mean diurnal time series for NO₂ and O₃ is evident in Figs. 9 and 10, in Fig. S168 for four regions, and for seasonal-mean diurnal time series in Figs. S165 and S166. And Fig. 15 shows good model performance in predicting all-station, seasonal-mean PM_{2.5} chemical composition and gravimetric PM_{2.5} total mass. Evaluation results presented in Sect. S3 also suggested that the year-specific 2013–2016 annual emissions that were used for 2013–2016 for the RAQDPS-OP023 retrospective runs broadly represented emissions changes over that period (Table 1) given the year-ordered agreement between measurements and model predictions (e.g., Figs. S144, S146, S151, S158, and S16258 for HNO₃, SO₂, PM_{2.5}-SO₄, SO₄⁼ concentration in precipitation, and SO₄⁼ concentration in precipitation wet deposition, respectively). Results presented in Sect. 4.1 showed some improvements in forecast skill over a 10-year period due to a series of operational RAQDPS upgrades, including increasing seasonal R scores for hourly NO₂ and O₃ forecasts (Fig. 19), decreasing seasonal NMAE scores for hourly O₃ and PM_{2.5} forecasts (Fig. S217), decreasing seasonal RMSE scores for hourly PM_{2.5} forecasts (Fig. S218), and increasing seasonal FAC2 scores for hourly NO₂ and O₃ forecasts (Fig. S219). Relative to suggested benchmark values, seasonal NMB scores for NO₂, O₃, and PM_{2.5} for most RAQDPS operational versions met the acceptable benchmark (Fig. S216) as did seasonal R scores for NO₂ and O₃ (Fig. 19). Lastly, the ongoing GAFIS quarterly evaluation of RAQDPS-OP and RAQDPS-FW forecasts for North America along with those made by four operational AQ forecast peer models described in Sect. 4.3 found that RAQDPS-OP023 and RAQDPS-FW023 performance in 2021/22 was competitive with their peer models for surface NO₂ and O₃ VMRs, though less so for surface PM_{2.5} total mass (for which all of the models performed least well).

1500 4.4.1 PM_{2.5} total mass and chemical composition

It is also evident that many evaluation scores were similar for the five years simulated by the RAQDPS-OP023, and some scores point to systematic errors in the model itself rather than model inputs since the anthropogenic input emissions used were tailored to be year-specific and the similarities in results were present despite interannual variations in meteorology. The most concerning systematic error may be consistent underpredictions of hourly PM_{2.5} surface concentrations. These underpredictions were evident visually in Figs. 1 and 5, in which observed annual and seasonal PM_{2.5} mean values at station locations stood out from the predicted mean PM_{2.5} concentration fields across the continent due to their higher values, and in Table 3 where all-station annual NMB values for hourly PM_{2.5} concentrations were negative for all five years, ranging from -0.09 to -0.06 for 2013–2016 and -0.31 for 2021/22. However, these underpredictions also varied strongly by season and were smallest in winter and largest in summer (e.g., Fig. 8, Table S3S). In addition, Figure Fig. 11 showed a large underprediction of all-station annual-mean diurnal values for hourly PM_{2.5} concentration at all hours but especially in early afternoon, and Fig. S167 showed

Formatted: Subscript

1520 corresponding underpredictions for seasonal-mean diurnal values, with the largest differences in the early afternoon
1525 and the summer.

Some other PM_{2.5} evaluation results, however, tell a more nuanced story. First, the results just summarized are largely
for aggregated all-station aggregated statistics. When monthly statistics were calculated separately for urban stations
only and for rural stations only, as shown in Figs. S213 and S214, a key difference was that hourly PM_{2.5}
1525 underpredictions for 2013–2016 were limited to rural stations in all months and to urban stations in the summer. For
most of the year, however, hourly PM_{2.5} mass was overpredicted at urban stations. RAQDPS-OP023 Model predictions
also showed better agreement with daily gravimetric PM_{2.5} total mass measurements for 2013–2016 than with hourly
continuous PM_{2.5} measurements for those years (cf. Fig. S198 vs. Fig. S142). Interestingly, monthly scores for the
1530 daily gravimetric PM_{2.5} total mass measurements were similar to those for urban hourly PM_{2.5} total mass measurements
(cf. Fig. S198 vs. Fig. S142), which is consistent with the gravimetric PM_{2.5} total mass measurements being urban-
focused (Demerjian, 2000). Negative biases also tended to be more common and larger at western stations than eastern
stations (e.g., Fig. S45, S46). Results from the evaluation of PM_{2.5} chemical composition and PM_{2.5} reconstructed mass
for 2013–2016 add further complications. Two PM_{2.5} chemical components (EC, SS) were found to be consistently
overpredicted in all months (Figs. S154, S157), one component (SO₄) was consistently underpredicted in all months
1535 (Fig. S151), and another component (CM) had large overpredictions for most months (Fig. S156). As a consequence,
predicted annual mean PM_{2.5} composition was incorrect on a rank-ordered basis since annual mean PM_{2.5}-CM was
predicted to be the second-largest PM_{2.5} component after annual mean PM_{2.5}-TOM but was observed to be the fourth-
largest annual mean PM_{2.5} component after PM_{2.5}-TOM, SO₄, and NO₃ (Tables 5 and S5A). Despite these errors in
predicting PM_{2.5} composition, however, predictions of PM_{2.5} reconstructed mass were surprisingly good because of
1540 partial cancellation of overpredictions and underpredictions of the mass of individual chemical components. In fact,
Fig. 15 showed that observed seasonal reconstructed PM_{2.5} dry mass for the combined CSN, IMPROVE, and NAPS
PM_{2.5} speciation networks for 2013–2016 was lower than predicted seasonal PM_{2.5} dry mass for three of the four seasons
in all years, summer being the exception. For the corresponding analysis based only on CSN measurements, however,
observed seasonal reconstructed PM_{2.5} dry mass was lower than predicted seasonal PM_{2.5} dry mass for 15 out of 16
1545 seasons (summer 2015, a high wildfire period, was the exception), with the largest model overpredictions occurring in
the winter (Fig. S200). But for the same analysis based only on IMPROVE measurements, observed seasonal
reconstructed PM_{2.5} mass was higher than predicted seasonal PM_{2.5} mass for all 16 seasons, with the largest model
underpredictions occurring in the summer (Fig. S201). Since the CSN network consists largely of urban stations while
the IMPROVE network consists largely of rural stations, these differences are consistent with Figs. S213 and S214.

1550 Taken together the above findings offer five clues to possible improvements of the RAQDPS-OP023 hourly PM_{2.5} total
mass predictions:

- (i) model underpredictions were largest for the summer months and are consistent across multiple years;
- (ii) underpredictions were larger in western North America than eastern North America;

Formatted: Space Before: 0 pt

(iii) ~~rural stations underpredictions~~ were strongly associated with ~~underpredictions rural stations~~ while urban stations were ~~oftensometimes~~ associated with overpredictions;

(iv) predictions of some PM_{2.5} chemical components had systematic biases, both negative and positive; and

(v) underpredictions were greater for the combined ~~continuous~~-hourly ~~continuous~~ PM_{2.5} measurement networks than the combined daily gravimetric PM_{2.5} measurement networks.

The RAQDPS-OP023 ~~maximum summertime negative biases for PM_{2.5} total mass and in the summer and in~~ western North America ~~bias~~, which are both consistent with the timing and location of the majority of wildfires in North America (e.g., Holden et al., 2011; Mao et al., 2011; Hand et al., 2013; Schichtel et al., 2017), strongly suggest the importance of including wildfire emissions. The comparison of RAQDPS-OP023 and RAQDPS-FW023 scores for 2021/22 discussed in Sect. 4.2 strongly supports this conclusion. However, Figs. S245 and S246 showed that while mean PM_{2.5} underpredictions were much improved in the summer months at both urban and rural stations ~~for the RAQDPS-FW023~~, this was not true for the rest of the year, especially at rural stations, so that other improvements to hourly PM_{2.5} total mass predictions are also needed.

Formatted: Subscript

It is also clear that multiple actions will be required to address the shortcomings identified for predictions of the multiple chemical components that make up PM_{2.5}. For example, the overprediction of monthly mean PM_{2.5} total mass in urban areas vs. underprediction in rural areas suggests that the spatial allocation of anthropogenic primary PM_{2.5} emissions might need to be modified to re-allocate some of these emissions from urban to rural areas. This change might also help to address persistent PM_{2.5}-EC overpredictions (Fig. S154), whose emissions vary directly with population (e.g., Fig. 14). Another approach to reduce urban PM_{2.5} overpredictions might be to add an urban heat island mixing parameterization (e.g., Ren et al., 2020) or a SGS on-road mobile mixing parameterization (Makar et al., 2021). Figures 12 and S231 showed that PM_{2.5} total mass was underpredicted in spring 2022 in the eastern U.S., where biogenic emissions are high (e.g., Fig. S21), and Fig. S207 showed that PM_{2.5}-TOM was underpredicted at IMPROVE measurement sites in the eastern U.S. from 2013 to 2016. These results suggest that biogenic SOA levels might be underpredicted there, so the parameterization of biogenic SOA should be reviewed to see whether its contribution to PM_{2.5}-TOM in rural areas might be increased (e.g., Schichtel et al., 2017; Zhang et al., 2018a). Process representations related to PM_{2.5}-SO₄ production and PM_{2.5}-CM emissions should also be reviewed to see whether the contributions of these processes in rural areas could be increased (Fig. S201), ~~and~~ the contribution of PM_{2.5}-CM emissions in urban areas reduced, and the poor monthly representation of PM_{2.5}-CM concentration evident in Fig. S156 addressed). One possible way to increase rural PM_{2.5}-CM levels would be to add a parameterization for wind-blown dust emissions from natural sources, which is not part of the RAQDPS-OP023 system, as another source of PM_{2.5} emissions (e.g., Park et al., 2010; Appel et al., 2013; Foroutan et al., 2017). Another avenue to investigate given the overpredictions of PM_{2.5}-CM in the winter is to review the meteorological modulation scheme that was used by the RAQDPS-OP023 to reduce fugitive dust emissions when the ground was predicted to be wet or snow-covered (Moran et al., 2026). In addition, the PM_{2.5}-SS component, ~~which~~ should be included in the calculation of predicted PM_{2.5} total mass. This component was used in the calculation of predicted PM_{2.5} total mass in Fig. 15, where it made a non-negligible contribution, but it was not included in the disseminated RAQDPS-OP023 operational forecasts of PM_{2.5} concentration

1590 due to the extreme PM_{2.5}-SS overpredictions that were encountered in the earliest RAQDPS versions. This omission should be addressed, but at the same time an effort should be made to reduce the remaining PM_{2.5}-SS overprediction (e.g., Table 5, Figs. S105, S157, ~~S105~~, S186) while keeping in mind the higher uncertainties of these scores due to the use of a measured proxy species to estimate PM_{2.5}-SS mass (see Sect. S2.4).

The RAQDPS-OP023 predictions of hourly PM_{2.5} total mass also only considered PM_{2.5} dry mass. The better agreement of predicted PM_{2.5} total mass with gravimetric PM_{2.5} total mass measurements, which are analyzed under low-humidity laboratory conditions and only contain particle-bound water, than with non-FRM continuous PM_{2.5} total mass measurements, which are made regardless of humidity levels and include both ~~include~~ semi-volatile and particle-bound water, suggests that predicted hourly PM_{2.5} total mass should include an aerosol water component (e.g., Frank, 2006; Malm et al., 2011; Nguyen et al., 2016; Pye et al., 2017; Widziewicz-Rzońca and Tytła, 2020). The gravimetric PM_{2.5} filter analysis can also result~~s~~ in the loss of some PM_{2.5}-NO₃ and NH₄ as well as some aerosol water due to volatilization (e.g., Frank, 2006; Malm et al., 2011; Chow et al., 2015; Nguyen et al., 2016; Hand et al., 2019). In addition, predicted PM_{2.5}-NO₃ is biased low when compared to laboratory-analyzed speciation measurements (e.g., Table S5S-mr, Fig. S152). The representation of inorganic heterogeneous chemistry used by the RAQDPS-OP023 (Moran et al., 2026~~5~~) should be examined critically. For example, one process missing from the RAQDPS-OP023 inorganic heterogeneous chemistry parameterization was an explicit treatment of the role of base cations (~~e.g.~~, Miller et al., 2024).

4.4.2 Ozone

Turning to gas-phase species, ~~o~~One shortcoming revealed by the evaluation of O₃ forecasts was the underprediction of the well-known Northern Hemisphere spring O₃ peak (e.g., Penkett and Brice, 1986; Monks, 2000; Liudchik et al., 2015). All-station spring NMB values for O₃ surface VMR were the lowest of the four seasons for 2013–2016 and ranged from -0.16 to -0.20 (Table S3S). The largest negative all-station monthly NMB values for O₃ occurred in April and May in 2013–2016 (Fig. S141), ~~and~~ ~~Other~~ Fig. S166 provides another examples of negative O₃ bias in spring and early summer months. Other analyses found larger O₃ underpredictions at western stations are evident in (e.g., Table S7 ~~and~~ ~~in~~ Figs. ~~3~~, 12, and S42, ~~and~~ S166). Different explanations for ~~the~~ ~~se~~ systematic springtime and western underprediction~~s~~ are possible, but one obvious candidate for investigation is the model's treatment of O₃ chemical lateral boundary conditions (e.g., Pendlebury et al., 2018; Moran et al., 2026~~5~~), where O₃ levels at the western boundary in the spring and summer may be too low. Two more aspects of the O₃ predictions that could be improved are also worth noting. First, annual mean O₃ surface VMRs showed a latitudinal step jump over the southeastern U.S. for all five years (Fig. 13). This artefact was likely caused by the parameterization of O₃ dry deposition used by the RAQDPS-OP023, which considered five coarse “seasons” that were defined based only on broad latitudinal bands with no dependence on longitude or elevation (e.g., Zhang et al., 2002; Makar et al., 2018; Moran et al., 2026~~5~~). And second, Fig. S42 showed that many coastal stations along the U.S. Gulf of Mexico and Florida peninsula had positive annual NMB values for 2013–2016. These O₃ overpredictions at coastal stations are consistent with the ~~model's~~ ~~lack~~ in the

1625 RAQDPS-OP023 of any treatment of marine halogen chemistry, which can reduce surface O₃ concentrations (e.g., Sarwar et al., 2015; Li et al., 2019).

4.4.3 PM_{2.5} gas-phase precursors

The evaluation of predictions of other gas-phase species besides NO₂ and O₃ also pointed to shortcomings in modelling some PM_{2.5} precursors. For example, all-station, annual-mean SO₂, HNO₃, and ISOP VMRs were consistently overpredicted and annual-mean-NH₃ VMRs were consistently underpredicted for 2013–2016 (Table 4). All-station seasonal-mean SO₂ VMRs were also overpredicted for all 16 seasons in 2013–2016 (Table S4S), which was consistent with the underprediction of all-station, seasonal-mean ~~mean~~ PM_{2.5}-SO₄ air concentrations for the same 16 seasons (Table S5S). Figure S146 showed the largest monthly SO₂ NMB values to be associated with the winter and summer seasons. Table S8 showed that the highest annual-mean regional SO₂ VMRs were predicted to occur in eastern Canada whereas measurements put the highest annual-mean regional SO₂ VMRs in either the eastern U.S. or western Canada.

1635 The majority of measurement stations with annual SO₂ overpredictions were located in eastern North America or Alberta, whereas many stations in the western U.S. exhibited underpredictions (Figs. S61, S62). Two SO₂ removal processes were found to be missing from the RAQDPS-OP023: the soil-wetness and cuticle-wetness gas-phase dry deposition pathways (Moran et al., 20265). Adding treatments for these two pathways is an obvious first step to reduce SO₂ overpredictions.

1640 In addition, the RAQDPS dry deposition scheme was examined in detail as part of the AQMEII-4 deposition intercomparison study (Clifton et al., 2023; Hogrefe et al., 2025; Kioutsioukis et al., 2025), and the results from this study may lead to further improvements to the RAQDPS scheme. Note that other gas-phase species such as HNO₃ and NH₃, which use SO₂ as an archetypal species for modelling dry deposition (Zhang et al., 2002), would also be impacted by ~~have reduced levels due to~~ this change: note that monthly mean HNO₃ VMR was also consistently overpredicted by the RAQDPS-OP023 for all months (Fig. S144) although monthly mean NH₃ VMR was not-actually underpredicted (Fig. S145). Reduced HNO₃ levels, however, would reduce NH₃ removal to the particle phase. In addition, the facts that monthly mean SO₂ VMR was consistently overpredicted while monthly mean PM_{2.5}-SO₄ air concentration was consistently underpredicted (Fig. S151) suggests that predicted SO₂-to-SO₄ conversion was too low.

1645 The two chemical pathways for SO₂-to-SO₄ conversion considered by the RAQDPS-OP023 were gas-phase oxidation and aqueous-phase oxidation. It is shown in Fig. S158 that monthly NMB values for weekly SO₄²⁻ concentration in precipitation for 2013–2016 were positive for most of the year. This result makes it more likely that the RAQDPS-OP023 representation of gas-phase oxidation of SO₂ might ~~ay~~ be the main reason for the year-round underprediction of PM_{2.5}-SO₄ air concentration.

1655 All-station, seasonal-mean NH₃ VMR was underpredicted for all seasons and months in 2013–2016, with the largest seasonal NMB values occurring in the winter (Table S4S; Fig. S145). In addition, Puchalski et al. (2011) found the Radiello passive samplers used by the AMoN network, which provided most NH₃ measurements, to be biased low, thus suggesting an even larger model underprediction. This consistent underprediction for NH₃ VMR occurred at the same time as overpredictions for most of the year efor (i) PM_{2.5}-NH₄ air concentration (Fig. S153), (ii) NH₄⁺ concentration in precipitation (Fig. S160), and (iii) NH₄⁺ wet deposition (Fig. S164). Table S8 showed that the highest

Formatted: Subscript

Formatted: Not Superscript/ Subscript

Formatted: Subscript

annual-mean NH_3 VMRs were predicted by the RAQDPS-OP023 to occur in eastern Canada, whereas the western U.S. had the highest observed annual-mean VMRs. ~~Figure S145 shows time series of monthly mean NH_3 VMRs and related evaluation statistics for 2013–2016, for which monthly NMB values were negative for all months and years but were largest in the winter.~~ The accuracy of emissions is always a potential factor to explain either model over- or underpredictions, and the large negative NMB values for NH_3 VMR occurring ~~in the west and~~ in the winter ~~and in the west could might~~ point to an underestimate of ~~western and~~ wintertime ~~and western~~ NH_3 emissions (e.g., Momeni et al., 2025). The level of autumn NH_3 emissions could also be underestimated (Fig. S145). In addition, Figs. S160 and S164 show peak overpredictions of monthly NH_4^+ wet concentration and wet deposition in the summer at the same time as monthly ambient NH_3 was underpredicted (Fig. S145) but ambient $\text{PM}_{2.5}\text{-NH}_4$ was overpredicted (Fig. S153). This ~~could might~~ mean that too much NH_3 gas was being removed in the RAQDPS-OP023 model by wet deposition in the summer when inorganic aerosol thermodynamics favours ambient NH_3 over $\text{PM}_{2.5}\text{-NH}_4$ and ambient HNO_3 over $\text{PM}_{2.5}\text{-NO}_3$ (e.g., Ansari and Pandis, 1998).

Improvements to the prediction of HNO_3 and $\text{PM}_{2.5}\text{-NO}_3$ could also improve the prediction of $\text{PM}_{2.5}\text{-NH}_4$. For example, monthly NMB scores for $\text{PM}_{2.5}\text{-NH}_4$ peak in September and October (Fig. S153) when monthly NMB scores for HNO_3 also peak (Fig. S144), ~~while whereas~~ monthly $\text{PM}_{2.5}\text{-NO}_3$ was underpredicted in all months except September and October (Fig. S152), and monthly NO_3^- wet concentration ~~in precipitation~~ was also overpredicted in September and October (Fig. S159). HNO_3 precursors NO_2 and NO were overpredicted in almost all months (Figs. S140 and S143), so reducing their levels by ~~decreases to NO_x emissions~~ (if justifiable) ~~decreasing NO_x emissions~~ would decrease HNO_3 levels. Increases to available NH_3 levels in the cold season through temporal reallocation of NH_3 emissions would result in increased $\text{PM}_{2.5}\text{-NO}_3$ levels and decreased HNO_3 levels in those months. And implementation of the missing dry deposition pathways for SO_2 to wet surfaces noted above ~~would~~ also increase HNO_3 dry deposition. It is clear, though, from this discussion how intertwined the sulfur, oxidized nitrogen, and reduced nitrogen budgets are via emissions, chemistry, gas-phase partitioning, and wet and dry removal.

Lastly, seasonal-mean ISOP was overpredicted for all 16 seasons in the 2013–2016 period (Table S4S). Annual overpredictions also occurred at all available PAMS measurement stations (Figs. S77, S78). Figure S150 showed time series of monthly ISOP prediction errors, which included very high NMB scores, poor FAC2 values, and near-zero R scores in the cold season. Although the ISOP measurements considered here were obtained from a small number of U.S. stations, an earlier study by Stroud et al. (2008) that compared Canadian ISOP measurements against predictions by the AURAMS ~~chemical transport~~ model, which used the same gas-phase chemistry mechanism and a similar treatment of biogenic emissions as the RAQDPS-OP023, also found ISOP overpredictions, especially in eastern Canada. When considered together these findings suggest that further examination of the RAQDPS-OP023 biogenic emissions scheme (Moran et al., 2026) is warranted for both magnitude and timing, including ~~the level of isoprene emissions as well as other biogenic emitted species such as monoterpenes and sesquiterpenes and also the spatiotemporal specification of vegetation phenology.~~

This section has discussed possible improvements to the RAQDPS-OP023 as suggested by an assessment and analysis of the full set of evaluation results from Sects. 3 and S3. Note that it has not been possible, however, to consider all aspects of the model. For example, due to limitations on the availability of measurement data, performance scores were examined for only one meteorological quantity, precipitation, even though, as noted in Sect. 3.1, other meteorological factors such as horizontal transport and vertical mixing are also very important in AQ modelling and forecasting. The same comment applies to the vertical distributions of pollutants, which are also of interest when assessing model performance but for which relatively few studies have been published (e.g., Solazzo et al., 2013; Astitha et al., 2018) given the scarcity of available measurements in the vertical. While acknowledging these limitations, it is still possible to extend the model performance assessment through inference. For example, it was noted in the discussion of Fig. 17 in Sect. 3.3.2 that the times of day when the maxima of primary pollutants occur is determined by the balance between surface emissions and vertical stability and mixing. Figures 9, S165, S168, S228 S238, and S241 show all-station annual-mean, seasonal-mean, and annual-mean regional diurnal time series for NO₂ VMR. In all of these figures, the timing of the twice-daily maxima in NO₂ VMR is well represented by the model. This suggests that both the diurnal variations in emissions and in vertical stability and mixing have been captured well by the RAQDPS-OP023. As a second example, it was noted in Sect. 2.1 that the injection of surface emissions into the lowest layer of the atmosphere is handled differently by the RAQDPS-OP023 forecasts for 2021/22 versus the hindcasts for 2013–2016, leaving open the possibility that unrealistically high surface pollutant abundances might have been predicted in the hindcasts for primary pollutants under conditions of strong near-surface vertical stability and low wind speeds. However, examination of the five years of mid-season monthly density scatterplots for NO₂ in Fig. S169 show little difference in the January scatterplots for the highest NO₂ monthly values between January 2022 and the other four Januarys. This comparison thus provides at least an indication that unrealistically high NO₂ surface VMR values were very infrequent even if they did occur.

5 Summary and conclusions

This paper presents results from a comprehensive, five-year performance evaluation and analysis of both prospective and retrospective annual simulations made with version 023 of the ECCC Regional Air Quality Deterministic Prediction System (RAQDPS023), an operational online chemical weather forecast system for North America. A companion paper by Moran et al. (2026~~5~~) provides a comprehensive and detailed description of this forecast system. The performance evaluation described in this paper consists of three parts. In the first part, near-real-time (NRT) hourly measurements of three pollutant species, NO₂, O₃, and PM_{2.5} total mass, were used to perform an operational evaluation of the first year of RAQDPS023 forecasts from July 2021 to June 2022 made by the RAQDPS-OP023, the system version without biomass burning (BB) emissions. The Canadian Air Quality Health Index is based on these three species, so they are considered to be the key forecast species out of the dozens that were predicted by the RAQDPS-OP023. The anthropogenic input emission files used for these 2021/22 forecasts were based on a projected 2020 Canadian national emission inventory and projected 2023 U.S. and Mexican national emission inventories (i.e., emission inventories forecasted from retrospective base-year inventories). The performance of the RAQDPS-FW023,

a second version of the ECCC operational AQ forecast system that is a duplicate of the RAQDPS-OP023 except for the addition of NRT ~~biomass burning (BB)~~ emissions, was also evaluated for 2021/22 using the same measurement data set.

The 2021/22 NRT measurement data set spanned much of North America and included measurements from roughly 200 surface sites in Canada and 1100 sites in the U.S., although only one or two of the three pollutants were measured at some sites. Before being used for the evaluation, the AQ measurements underwent a two-step station-level screening process at ECCC. The first step was to apply validity checks to discard negative concentrations and above-threshold concentration values flagged as suspicious or invalid. Each valid measurement (~~or scaled or combination of measurements for some PM_{2.5} chemical components~~) was then paired with a forecast value, after which the second screening step, period-specific completeness checking, was performed to ensure that at least a minimum number of valid hourly measurements were available at a site for a station for the evaluation period being considered to ensure temporal representativeness. ~~No calculation was performed. If~~ there were not enough valid measurements for the period, then none of the measurements for that station were included in the statistical calculations for that period.

Annual, seasonal, monthly, and hour-of-day values of 10 statistical metrics were then calculated for both individual measurement networks and combined networks, for both the entire continent and four continental quadrants, and for urban sites only and rural sites only. In addition to summary tables, some of these statistical scores were presented visually in multiple ways, including site-specific “dot” statistics maps, monthly and diurnal time series, and density scatterplots.

In the second part of the performance evaluation, an expanded and more detailed analysis was performed on four annual hindcasts for 2013–2016 made with the RAQDPS-OP024, which was ~~(algorithmically equivalent to the RAQDPS-OP023 but run on a newer computer system (see companion paper by Moran et al., 2026)).~~ The anthropogenic input emission files used for each of these four annual simulations were year-specific since they were generated for each year based on multi-year retrospective data sets of Canadian, U.S., and Mexican annual emission inventories. The evaluation of retrospective simulations makes it possible to access a much larger set of AQ measurement data for North America, including more AQ measurement networks (AMoN, CAPMoN, CASTNET, CSN, IMPROVE, NADP, NATTS, PAMS), more chemical species (23 vs. 3), and more measurement sites (roughly 2000 vs. 1300). These historical data sets have also undergone quality assurance and quality control checks by the individual networks before being released publicly. The consideration of multiple simulation years reduces the confounding influence of interannual meteorological variability, which helps with the identification of systematic prediction errors. However, differences between measurement network infrastructure and procedures, in particular, sampling methodology and duration but also sampling frequency and instrument type, mean that pre-processing of both measurements and model predictions is often required before measured values and model predictions can be combined or compared across networks. Most importantly, after station-level screening for validity and completeness, the measurements from some networks had to be averaged or accumulated in time to match the longest sampling duration employed by any network for that same species in order to calculate consistent all-station (i.e., multiple-network or combined) statistics. For

example, the U.S. CASTNET and NADP networks collect weekly samples and the U.S. AMoN network collects biweekly samples. ~~In a few cases~~For the same reason, predicted hourly model-RAQDPS-OP023 species values ~~also frequently~~ had to be averaged or summed before being paired with measurements.

Of the three key AQHI forecast species, evaluation scores for O₃ hourly forecasts made by the RAQDPS-OP023 were generally the highest for all five years, followed by NO₂ scores and then PM_{2.5} scores. The finding that PM_{2.5} total mass was the most difficult AQHI pollutant to predict was not surprising given its inherent complexity as a hybrid, primary-secondary multi-pollutant that spans a wide size range and has numerous sources. Another important finding was that monthly mean hourly PM_{2.5} total mass predicted by the RAQDPS-OP023 was biased low in all months in 2021/22 and in most months, especially in the summer, in 2013–2016. Relative to the NMB, NMAE, and R “acceptability” benchmarks recommended by Zhai et al. (2024) for NO₂ VMR predictions, all-station seasonal RAQDPS-OP023 predictions met the NMB benchmark for 19 out of 20 seasons for these five years, met the NMAE benchmark for the five winter seasons, and met the R benchmark for all 20 seasons. Similarly, for the NMB, NMAE, and R acceptability benchmarks recommended by Emery et al. (2017) for O₃ VMR predictions, all-station seasonal RAQDPS-OP023 predictions met the NMB benchmark for 15 seasons (but none of the springs), met the NMAE benchmark for only one season, but met the R benchmark for all 20 seasons. And for the NMB, NMAE, and R acceptability benchmarks recommended by Emery et al. (2017) for PM_{2.5} concentration predictions, all-station seasonal RAQDPS-OP023 predictions met the NMB benchmark for 16 seasons (but not four summers), did not meet the NMAE benchmark for any season, but met the R benchmark for all 20 seasons. The ongoing WMO GAFIS multi-model comparison of operational AQ forecast systems for North America also found RAQDPS-OP023 forecasts to be competitive with four peer forecast systems for NO₂ and O₃ for all months in 2021/22 and for PM_{2.5} total mass for cold-season months.

Biomass burning is an important seasonal source of emissions of both primary PM_{2.5} mass and some of its gas-phase precursors. A comparison of RAQDPS-FW023 and RAQDPS-OP023 performance for 2021/22 found much improved PM_{2.5} evaluation scores for the RAQDPS-FW023 for the summer months, when BB emissions peak. It was also shown that the inclusion of BB emissions that occur mainly in the summer and early autumn affected annual evaluation statistics significantly. This comparison has quantified the impact of BB emissions on AQ forecasts for one year and has provided strong evidence for the importance of including BB emissions, which mainly affect PM_{2.5} levels in the summer and, to a lesser degree, autumn. One further insight came from separate evaluations with hourly PM_{2.5} measurements that had been divided into urban and rural subsets, which was that once BB emissions were included, remaining model underpredictions of hourly PM_{2.5} concentration were found to occur mainly in rural areas from October to June for both system versions, whereas model overpredictions of PM_{2.5} concentration were sometimes a second issue in urban areas. Other explanations are thus still needed for hourly PM_{2.5} underpredictions outside of the wildfire season, especially in rural areas and in the eastern U.S.

The evaluation of PM_{2.5} predictions for the 2013–2016 annual hindcasts was expanded by considering two additional types of PM_{2.5} measurements available from multiple networks, namely (i) daily gravimetric PM_{2.5} total mass

measurements from the U.S. PM_{2.5} mass monitoring network and (ii) daily PM_{2.5} chemical composition measurements from the CSN, IMPROVE, and NAPS networks. These additional PM_{2.5} data sets ~~augmented-included measurements~~ from nearly as many stations as the hourly PM_{2.5} total mass data sets but employed very different measurement technologies with different error characteristics. By comparing and contrasting evaluation results for these multiple networks, ~~and provided~~ insights could be drawn into causes of the hourly PM_{2.5} mass underpredictions. One finding was that RAQDPS-OP0234 predictions of daily gravimetric PM_{2.5} total mass were less negatively biased than those for hourly PM_{2.5} mass, which immediately draws attention to instrument and analysis differences between the two types of measurements. Unlike hourly continuous PM_{2.5} total mass measurements, the daily gravimetric PM_{2.5} total mass measurements are known to have negative artefacts due to the volatilization of semi-volatile species such as ammonium, nitrate, and particle water. This difference suggests that hourly continuous PM_{2.5} measurements might be higher than gravimetric measurements if those measurements were taken at the same time and location, thus resulting in a larger negative bias for the former. Monthly evaluation scores for the daily gravimetric PM_{2.5} total mass measurements were also closer to those for the CSN and NAPS networks than the IMPROVE network, which is consistent with the first three networks being urban-focused whereas the IMPROVE network is rural-focused. A second finding was that daily PM_{2.5} mass reconstruction results based on observed daily PM_{2.5} speciation measurements agreed well both with observed daily gravimetric PM_{2.5} total mass measurements for 2013–2016 and with RAQDPS-OP0234 predictions of daily gravimetric PM_{2.5} total mass, which was again was somewhat surprising in view-light of the consistent model underpredictions of hourly PM_{2.5} total mass. However, PM_{2.5} mass reconstruction values did not include aerosol water and the RAQDPS-OP0234 calculation of hourly PM_{2.5} total mass, however, did not include either aerosol water or SS components, but comparisons with observed gravimetric PM_{2.5} total mass, which would still include a particle-bound water component, suggested that both PM_{2.5} chemical components should be included in the model calculation of PM_{2.5} total mass. And-Moreover, while RAQDPS-OP0234 predictions of all-station PM_{2.5} chemical composition were reasonably good, it was also shown that the good agreement between observed and predicted daily gravimetric PM_{2.5} total mass was partly due to compensating RAQDPS-OP0234 model errors in the prediction of individual PM_{2.5} chemical components. In particular, because the model was found to overpredict PM_{2.5}-EC and SS but underpredict SO₄ in all seasons and to overpredict PM_{2.5}-TOM and CM at urban stations but underpredict these components at rural stations. Lastly, both observed and predicted seasonal PM_{2.5} residual mass (the difference between gravimetric mass and reconstructed mass) were found to be largest in the summer while annual PM_{2.5} residual mass was largest in eastern North America. Some possible explanations include incorrect partitioning spatial allocation of primary PM_{2.5} emissions between urban and rural areas and underpredictions of ammonium nitrate, crustal material, and biogenic SOA in the summer.

In the third part of the evaluation, trends in seasonal performance were shown for the first decade of operational forecasts by the online GEM-MACH-based version of the RAQDPS from 2010 to 2019. Overall skill in predicting hourly NO₂ and O₃ VMRs improved modestly over this period due to a series of modelling system upgrades, including code improvements and updated input emissions files (see companion paper by Moran et al., 20265). Predictions of hourly PM_{2.5} total mass, on the other hand, improved initially but then declined after 2017. These seasonal forecast

scores for earlier operational RAQDPS versions were then compared to seasonal scores for the RAQDPS-~~OP0233~~ hindcast simulations for 2013–2016 and 2021/22 forecasts. RAQDPS-~~OP0233~~ seasonal scores were better overall for NO₂ and O₃ but showed little improvement for PM_{2.5}.

Meteorology and climate can also affect ~~model-RAQDPS~~ performance through the direct influence of some meteorological variables, such as wind speed, PBL height, temperature, precipitation, solar radiation, and cloud cover, on pollutant abundances and removal, and indirectly through related factors such as vegetation phenology, snow cover, and emissions affected by meteorology. As a consequence, there were seasonal or diurnal cycles in objective scores for many pollutants that were as large or larger than year-to-year fluctuations or trends in model performance. These temporal variations in model performance can provide further clues and guidance to identify those components of the modelling system where further improvements may be needed. Examples include maximum underprediction of surface O₃ VMR in the spring, peak-maximum underprediction of NH₃ VMR in winter, and consistent underpredictions of PM_{2.5}-SO₄ for all seasons. Some model errors are also correlated in time for chemically coupled species, such as those for SO₂ and PM_{2.5}-SO₄, for HNO₃ and PM_{2.5}-NO₃, and for NH₃ and PM_{2.5}-NH₄, and may be in phase or out of phase.

One confounding factor faced by this study was the changing chemical environment in North America caused by significant changes in regional and national emissions that have occurred over the past two decades, including the four-year period from 2013 to 2016 and the six-year period from 2016 to 2021. For example, the impact of large monotonic reductions in Canadian and U.S. SO₂ annual emissions of 16% and 50%, respectively, from 2013 to 2016 can be seen in both observed and predicted monthly time series of SO₂ VMR, PM_{2.5}-SO₄ concentration, and SO₄⁻ concentration in precipitation and wet deposition. This agreement in temporal trends between measurements and ~~model RAQDPS-OP023~~ predictions affirms the representativeness of the retrospective, multi-year emission inventory data sets used ~~for~~ in this study for 2013–2016 and hence represents a positive result from a dynamic evaluation perspective. However, having successfully represented these emissions changes in the 2013–2016 ~~RAQDPS-OP023model~~ simulations, monthly and seasonal scores were found to vary in a similar manner from year to year, which points to systematic errors in the ~~RAQDPS-OP023model~~ itself (although 2016 seemed to be an outlier for some species). In addition, these results clearly show the value of using year-specific emissions, although this is not possible in the case of AQ forecast models because current emissions cannot be known beforehand.

This study has demonstrated the value of a comprehensive, quasi-diagnostic model performance evaluation. Consideration of a wide range of pollutant species allows some pollutant mass budgets to be examined and consistency to be checked for coupled pollutant species. Different statistical analyses can also provide different information. For example, spatial plots of ~~site-level~~ station statistics can show regional clustering of similar station scores and regional differences in station scores, including compensating ~~site-level~~ errors between regions or between urban and rural stations that can be hidden ~~by~~ in and improve network-level aggregated statistics. Density scatterplots can show different levels of scatter between species or seasons at the station level and reveal low measurement precision by making quantization of observed values visible (e.g., NO and NO₂). Time series of monthly or hourly mean values are more aggregated than the scatterplots but can help to understand temporal variations in performance and, when collated,

Formatted: Subscript

mass budgets. Other sStratified analyses (e.g., by individual network, season, monthly, hour of day, region, or urban/rural) have also revealed model behaviour, including compensating errors, that was not visible in highly aggregated (e.g., all-station, annual) “headline” statistics. This comprehensive, quasi-diagnostic model performance evaluation has also provided a baseline set of scores against which future system versions can be compared.

Results from the performance evaluation described in this paper have thus pointed to aspects of the RAQDPS-OP023 that warrant further investigation and improvement. First, the anthropogenic input emissions files and the parameterizations of natural emissions used by the forecast system should be one important focus, especially as anthropogenic emissions continue to change. In addition to strong evidence to support the inclusion of BB emissions, other results point to the likely overallocation of PM_{2.5} primary emissions to urban areas and underallocation to rural areas, overallocation of NH₃ emissions to summer and underallocation to winter, overallocation of fugitive dust emissions to winter, excessive sea-salt emissions in all seasons, and several missing natural emissions sources, including wind-blown dust from natural surfaces and lightning NO emissions. Evaluation results for ISOP VMR also showed large positive biases, arguing for the biogenic emissions scheme to be revisited. Second, O₃ forecasts might be improved by (i) revising O₃ western lateral boundary conditions for the spring and summer and (ii) introducing a parameterization of halogen chemistry impacts near oceans on O₃ near oceans. Third, the RAQDPS-OP023 was missing two gas-phase dry deposition processes for SO₂, and the addition of these processes should decrease SO₂ and HNO₃ levels, which were both overpredicted. Seasonal surface properties in the gas-phase dry deposition scheme also need to have a more detailed representation of seasonal variations and to include dependence on longitude and elevation, which was lacking in the RAQDPS-OP023. Fourth, precipitation-chemistry measurements suggested that too much NH₃ gas was being removed by wet deposition. Fifth, the RAQDPS-OP023 was found to underpredict PM_{2.5}-SO₄ and overpredict PM_{2.5}-EC and PM_{2.5}-SS concentrations in all seasons, and the treatments of the lifecycles of each of these components will need to be examined. Particulate organic matter, especially PM_{2.5}-SOM from biogenic emissions, may be underpredicted in the summer, which will require examination of the representation of biogenic emissions and of SOA formation. PM_{2.5}-NH₄ and PM_{2.5}-NO₃ may also be underpredicted in the summer, which will require the representation of inorganic heterogeneous thermodynamics to be assessed, including the addition of an explicit treatment of base cations, a known gap in the RAQDPS-OP023. Lastly, the calculation of hourly PM_{2.5} total mass in the RAQDPS by summation of PM_{2.5} chemical components should include sea salt and both volatile and particle-bound aerosol water.

As a final comment it should be noted that the RAQDPS-OP025, which was introduced operationally at ECCC in June 2024, did implement some of the changes recommended above (see companion paper by Moran et al., 2026). One very significant change was to merge the two operational system versions, the RAQDPS-OP024 and RAQDPS-FW024, into a single system version that included NRT biomass burning emissions. This particular change had the multiple advantages of improving forecast scores, simplifying maintenance of the operational AQ forecast system, and reducing computer usage.

Appendix

Table A1. List of acronyms, ~~and~~ abbreviations, and symbols.

<u>ADOM</u>	<u>Acid Deposition and Oxidant Model (Canada)</u>
<u>ADOM-2</u>	<u>Acid Deposition and Oxidant Model gas-phase chemical mechanism version 2</u>
<u>AirNow</u>	<u>Aerometric Information Retrieval Now (U.S.)</u>
<u>ALD2</u>	<u>acetaldehyde and higher aldehydes (ADOM-2 lumped VOC species)</u>
<u>AMoN</u>	<u>Ammonia Monitoring Network (U.S.)</u>
<u>APEI</u>	<u>Air Pollutant Emissions Inventory (Canada)</u>
<u>AQ</u>	<u>air quality</u>
<u>AQHI</u>	<u>Air Quality Health Index (Canada)</u>
<u>AQS</u>	<u>Air Quality System (U.S.)</u>
<u>BB</u>	<u>biomass burning</u>
<u>BDL</u>	<u>below detection limit</u>
<u>BEIS</u>	<u>Biogenic Emission Inventory System (U.S.)</u>
<u>CAMS</u>	<u>Copernicus Atmosphere Monitoring Service (EU)</u>
<u>CAPMoN</u>	<u>Canadian Acid Precipitation Monitoring Network</u>
<u>CASTNET</u>	<u>Clean Air Status and Trends Network (U.S.)</u>
<u>CEDS</u>	<u>Community Emissions Data System</u>
<u>CFFEPS</u>	<u>Canadian Forest Fire Emissions Prediction System</u>
<u>CFR</u>	<u>Code of Federal Regulations (U.S.)</u>
<u>CM</u>	<u>crustal material</u>
<u>CMC</u>	<u>Canadian Meteorological Centre</u>
<u>CRES</u>	<u>cresols and phenols (ADOM-2 lumped VOC species)</u>
<u>CRMSE</u>	<u>centered root mean square error</u>
<u>CSN</u>	<u>Chemical Speciation Network (U.S.)</u>
<u>CV</u>	<u>coefficient of variation (or relative standard deviation)</u>
<u>CVM</u>	<u>coefficient of variation (model)</u>
<u>CVO</u>	<u>coefficient of variation (observations)</u>
<u>EC</u>	<u>elemental carbon</u>
<u>ECA</u>	<u>eastern Canada</u>
<u>ECCC</u>	<u>Environment and Climate Change Canada</u>
<u>ECMWF</u>	<u>European Centre for Medium-range Weather Forecasts</u>
<u>EEA</u>	<u>European Environment Agency</u>
<u>EI</u>	<u>emission inventory</u>
<u>EMEP</u>	<u>European Monitoring and Evaluation Programme</u>
<u>EOTH</u>	<u>total non-reactive or low-reactivity VOC species (ADOM-2 lumped VOC species)</u>
<u>EPA</u>	<u>Environmental Protection Agency (U.S.)</u>
<u>EQUATES</u>	<u>EPA's air QUALity TimE Series</u>
<u>EST</u>	<u>Eastern Standard Time</u>
<u>ETHE</u>	<u>ethene and some isoprene oxidation products (ADOM-2 lumped VOC species)</u>
<u>EUS</u>	<u>eastern U.S.</u>
<u>FAC2</u>	<u>factor-of-two metric</u>
<u>FB</u>	<u>fractional bias</u>

Formatted Table

<u>FE</u>	<u>fractional error</u>
<u>FEM</u>	<u>Federal Equivalent Method (U.S.)</u>
<u>FRM</u>	<u>Federal Reference Method (U.S.)</u>
<u>FW</u>	<u>FireWork</u>
<u>GAFIS</u>	<u>Global Air quality Forecasting and Information System (WMO)</u>
<u>GAW</u>	<u>Global Atmospheric Watch (WMO)</u>
<u>GEM</u>	<u>Global Environmental Multiscale (model) (ECCC)</u>
<u>GEM-MACH</u>	<u>Global Environmental Multiscale-Modelling Atmospheric CHemistry (model) (ECCC)</u>
<u>GEMS</u>	<u>Global and regional Earth-system Monitoring using Satellite and in-situ data (EU)</u>
<u>GEOS-CF</u>	<u>Goddard Earth Observing System - Composition Forecasting (NASA)</u>
<u>GIS</u>	<u>geographic information system</u>
<u>HETV</u>	<u>HETerogeneous Vectorized scheme</u>
<u>IAU</u>	<u>incremental analysis update</u>
<u>IAY</u>	<u>Instantaneous secondary organic Aerosol Yield</u>
<u>IFS-CAMS</u>	<u>Integrated Forecasting System – Copernicus Atmosphere Monitoring Service (ECMWF)</u>
<u>IFS-SILAM</u>	<u>Integrated Forecasting System – SILAM (ECMWF/Finnish Meteorological Institute)</u>
<u>IOA</u>	<u>index of agreement</u>
<u>IMPROVE</u>	<u>Interagency Monitoring of Protected Visual Environments (U.S.)</u>
<u>ISOP</u>	<u>isoprene</u>
<u>LBC</u>	<u>lateral boundary condition</u>
<u>LT</u>	<u>local time</u>
<u>MAE</u>	<u>mean absolute error</u>
<u>MB</u>	<u>mean bias</u>
<u>MDA8</u>	<u>maximum daily 8-hr average</u>
<u>MDL</u>	<u>minimum detection limit</u>
<u>MFB</u>	<u>mean fractional bias</u>
<u>MFE</u>	<u>mean fractional error</u>
<u>MMR</u>	<u>mass mixing ratio</u>
<u>MOVES</u>	<u>MOtor Vehicle Emission Simulator (U.S.)</u>
<u>N</u>	<u>number of measurement-model pairs (i.e., sample size)</u>
<u>NAAQS</u>	<u>National Ambient Air Quality Standards (U.S.)</u>
<u>NACC</u>	<u>NOAA-EPA Atmosphere-Chemistry Coupler</u>
<u>NADP</u>	<u>National Atmospheric Deposition Program (U.S.)</u>
<u>NAPS</u>	<u>National Air Pollution Surveillance system (Canada)</u>
<u>NAQFC</u>	<u>National Air Quality Forecast Capability (U.S.)</u>
<u>NASA</u>	<u>National Aeronautics and Space Administration (U.S.)</u>
<u>NAtChem</u>	<u>National Atmospheric Chemistry database (Canada)</u>
<u>NATTS</u>	<u>National Air Toxics Trends Sites (U.S.)</u>
<u>NEI</u>	<u>National Emission Inventory (U.S.)</u>
<u>NH4</u>	<u>particle ammonium</u>
<u>NMAE</u>	<u>normalized MAE</u>
<u>NMB</u>	<u>normalized mean bias</u>
<u>NME</u>	<u>normalized mean error (assumed equivalent to NMAE)</u>
<u>NMSE</u>	<u>normalized mean square error</u>

Formatted: French (Canada)

<u>NO3</u>	<u>particle nitrate</u>
<u>NOAA</u>	<u>National Oceanic and Atmospheric Administration (U.S.)</u>
<u>NPRI</u>	<u>National Pollutant Release Inventory (Canada)</u>
<u>NRT</u>	<u>near real time</u>
<u>NSD</u>	<u>normalized standard deviation</u>
<u>NTN</u>	<u>National Trends Network (U.S. NADP)</u>
<u>NWP</u>	<u>numerical weather prediction</u>
<u>OC</u>	<u>organic carbon</u>
<u>OM</u>	<u>organic matter</u>
<u>PAMS</u>	<u>Photochemical Assessment Monitoring Stations (U.S.)</u>
<u>PBL</u>	<u>planetary boundary layer</u>
<u>PCL</u>	<u>Precipitation Coverage Length</u>
<u>PM</u>	<u>particulate matter</u>
<u>PM_{2.5}</u>	<u>particulate matter with aerodynamic diameter smaller than 2.5 µm</u>
<u>PM_{2.5}-noSS</u>	<u>PM_{2.5} without sea-salt component</u>
<u>POM</u>	<u>primary organic matter</u>
<u>PR</u>	<u>precipitation</u>
<u>QA/QC</u>	<u>quality assurance/quality control</u>
<u>R</u>	<u>Pearson correlation coefficient</u>
<u>RAQDPS</u>	<u>Regional Air Quality Deterministic Prediction System (ECCC)</u>
<u>RAQDPS-FW</u>	<u>RAQDPS-FireWork (with BB emissions)</u>
<u>RAQDPS-OP</u>	<u>RAQDPS-Operational (standard, no BB emissions)</u>
<u>RDPS</u>	<u>Regional Deterministic Prediction System (ECCC)</u>
<u>RH</u>	<u>relative humidity</u>
<u>RMSE</u>	<u>root mean square error</u>
<u>SCC</u>	<u>Source Classification Code</u>
<u>SDM</u>	<u>standard deviation of model predictions</u>
<u>SDO</u>	<u>standard deviation of observations</u>
<u>SEMARNAT</u>	<u>Secretariat of Environment and Natural Resources (Mexico)</u>
<u>SGS</u>	<u>subgrid-scale</u>
<u>SILAM</u>	<u>System for Integrated modelLling of Atmospheric composition (Finnish Meteorological Institute)</u>
<u>S/L</u>	<u>state/local</u>
<u>SMOKE</u>	<u>Sparse Matrix Operator Kernel Emissions (modeling system)</u>
<u>SO4</u>	<u>particle sulfate</u>
<u>SOA</u>	<u>secondary organic aerosol</u>
<u>SOM</u>	<u>secondary organic matter</u>
<u>SS</u>	<u>sea salt</u>
<u>STP</u>	<u>standard temperature and pressure</u>
<u>TEOM</u>	<u>tapered element oscillating microbalance</u>
<u>TF</u>	<u>transportable fraction</u>
<u>TOC</u>	<u>total organic carbon</u>
<u>TOM</u>	<u>total organic matter</u>
<u>TP</u>	<u>total precipitation</u>
<u>UTC</u>	<u>Coordinated Universal Time</u>

	<u>VMR</u>	volume mixing ratio
	<u>VOC</u>	volatile organic compound
	<u>WCA</u>	western Canada
	<u>WMO</u>	World Meteorological Organization
	<u>WRF</u>	Weather Research and Forecasting NWP model (U.S.)
	<u>WUS</u>	western U.S.
1905	ADOM	Acid Deposition and Oxidant Model (Canada)
	AirNow	Aerometric Information Retrieval Now (U.S.)
	ALD2	acetaldehyde and higher aldehydes (ADOM 2 lumped VOC species)
	AMoN	Ammonia Monitoring Network (U.S.)
	APEI	Air Pollutant Emissions Inventory (Canada)
1910	AQ	air quality
	AQHI	Air Quality Health Index (Canada)
	AQS	Air Quality System (U.S.)
	BB	biomass burning
	BDL	below detection limit
1915	BEIS	Biogenic Emission Inventory System (U.S.)
	CAMS	Copernicus Atmosphere Monitoring Service (EU)
	CAPMoN	Canadian Acid Precipitation Monitoring Network
	CASTNET	Clean Air Status and Trends Network (U.S.)
	CEDS	Community Emissions Data System
1920	CFFEPS	Canadian Forest Fire Emissions Prediction System
	CFR	Code of Federal Regulations (U.S.)
	CM	crystal material
	CMC	Canadian Meteorological Centre
	CRS	cresols and phenols (ADOM 2 lumped VOC species)
1925	CRMSE	centered root mean square error
	CSN	Chemical Speciation Network (U.S.)
	CV	coefficient of variation (or relative standard deviation)
	EC	elemental carbon
	ECA	eastern Canada
1930	ECCC	Environment and Climate Change Canada
	ECMWF	European Centre for Medium-range Weather Forecasts
	EEA	European Environment Agency
	EI	emission inventory
	EMEP	European Monitoring and Evaluation Programme
1935	EPA	Environmental Protection Agency (U.S.)
	EQUATES	EPA's Air QUALity Time Series
	EST	Eastern Standard Time
	ETHE	ethene and some isoprene oxidation products (ADOM 2 lumped VOC species)
	EUS	eastern U.S.
1940	FAC2	factor of two metric
	FB	fractional bias
	FE	fractional error

	FEM	Federal Equivalent Method (U.S.)
	FRM	Federal Reference Method (U.S.)
1945	FW	FireWork
	GAFIS	Global Air quality Forecasting and Information System (WMO)
	GAW	Global Atmospheric Watch (WMO)
	GEM	Global Environmental Multiscale (model) (ECCC)
	GEM MACH	Global Environmental Multiscale Modelling Atmospheric Chemistry (model) (ECCC)
1950	GEMS	Global and regional Earth system Monitoring using Satellite and in situ data (EU)
	GEOS CF	Goddard Earth Observing System Composition Forecasting (NASA)
	GIS	geographic information system
	HETV	HETerogeneous Vectorized scheme
	IAU	incremental analysis update
1955	IAY	Instantaneous secondary organic Aerosol Yield
	IFS CAMS	Integrated Forecasting System Copernicus Atmosphere Monitoring Service (ECMWF)
	IFS SILAM	Integrated Forecasting System SILAM (ECMWF/Finnish Meteorological Institute)
	IOA	index of agreement
	IMPROVE	Interagency Monitoring of Protected Visual Environments (U.S.)
1960	ISOP	isoprene
	LBC	lateral boundary condition
	LT	local time
	MAE	mean absolute error
	MB	mean bias
1965	MDA8	maximum daily 8 hr average
	MDL	minimum detection limit
	MFB	mean fractional bias
	MFE	mean fractional error
	MMR	mass mixing ratio
1970	MOVES	MOtor Vehicle Emission Simulator (U.S.)
	NAAQS	National Ambient Air Quality Standards (U.S.)
	NACC	NOAA EPA Atmosphere Chemistry Coupler
	NADP	National Atmospheric Deposition Program (U.S.)
	NAPS	National Air Pollution Surveillance system (Canada)
1975	NAQFC	National Air Quality Forecast Capability (U.S.)
	NASA	National Aeronautics and Space Administration (U.S.)
	NAChem	National Atmospheric Chemistry database (Canada)
	NATTS	National Air Toxics Trends Sites (U.S.)
	NEI	National Emission Inventory (U.S.)
1980	NH4	partiele ammonium
	NMAE	normalized MAE
	NMB	normalized mean bias
	NME	normalized mean absolute error
	NMSE	normalized mean square error
1985	NO3	partiele nitrate
	NOAA	National Oceanic and Atmospheric Administration (U.S.)

	NPRI	National Pollutant Release Inventory (Canada)
	NRT	near real time
	NSD	normalized standard deviation
1990	NTN	National Trends Network (U.S. NADP)
	NWP	numerical weather prediction
	OC	organic carbon
	OM	organic matter
	PAMS	Photochemical Assessment Monitoring Stations (U.S.)
1995	PBL	planetary boundary layer
	PCL	Precipitation Coverage Length
	PM	particulate matter
	PM _{2.5}	particulate matter with aerodynamic diameter smaller than 2.5 µm
	POM	primary organic matter
2000	PR	precipitation
	QA/QC	quality assurance/quality control
	RAQDPS	Regional Air Quality Deterministic Prediction System (ECCC)
	RAQDPS FW	RAQDPS FireWork
	RDPS	Regional Deterministic Prediction System (ECCC)
2005	RH	relative humidity
	RMSE	root mean square error
	SCC	Source Classification Code
	SDM	standard deviation of model predictions
	SDO	standard deviation of observations
2010	SEMARNAT	Secretariat of Environment and Natural Resources (Mexico)
	SGS	subgrid scale
	SILAM	System for Integrated modelLling of Atmospheric composition (Finnish Meteorological Institute)
	S/L	state/local
	SMOKE	Sparse Matrix Operator Kernel Emissions (modeling system)
2015	SO ₄	partiele sulfate
	SOA	secondary organic aerosol
	SOM	secondary organic matter
	SS	sea salt
	STP	standard temperature and pressure
2020	TEOM	tapered element oscillating microbalance
	TF	transportable fraction
	TOC	total organic carbon
	TOM	total organic matter
	TP	total precipitation
2025	UTC	Coordinated Universal Time
	VMR	volume mixing ratio
	VOC	volatile organic compound
	WCA	western Canada
	WMO	World Meteorological Organization
2030	WRF	Weather Research and Forecasting NWP model (U.S.)

~~WUS~~ western U.S.

~~Non-classifié~~ | ~~Unclassified~~

Table A2. Statistical metrics used in this study for model performance evaluation plus coefficient of variation (or relative standard deviation). MFB and MFE have been used in some related studies (e.g., Manseau et al., 2022)

<u>Metric Name</u>	<u>Abbreviation</u>	<u>Definition</u>
<u>Observed mean</u>	\bar{O}	$\frac{1}{N} \sum_1^N O_i$
<u>Model mean</u>	\bar{M}	$\frac{1}{N} \sum_1^N M_i$
<u>Mean bias</u>	<u>MB</u>	$\frac{1}{N} \sum_1^N (M_i - O_i)$
<u>Root mean square error</u>	<u>RMSE</u>	$\left(\frac{1}{N} \sum_1^N (M_i - O_i)^2 \right)^{1/2}$
<u>Normalized mean bias</u>	<u>NMB</u>	$\frac{\sum_1^N (M_i - O_i)}{\sum_1^N O_i}$
<u>Normalized mean absolute error</u>	<u>NMAE</u>	$\frac{\sum_1^N M_i - O_i }{\sum_1^N O_i }$
<u>Pearson correlation coefficient</u>	<u>R</u>	$\frac{\sum [(M_i - \bar{M}) \times (O_i - \bar{O})]}{\sqrt{\sum (M_i - \bar{M})^2 \times \sum (O_i - \bar{O})^2}}$
<u>Centred RMSE</u>	<u>CRMSE</u>	$\left(\frac{1}{N} \sum_1^N [(M_i - \bar{M}) - (O_i - \bar{O})]^2 \right)^{1/2}$
<u>Standard deviation (observations)</u>	σ_O (or SDO)	$\left(\frac{1}{N} \sum_1^N (O_i - \bar{O})^2 \right)^{1/2}$

Formatted: Font: Bold

Formatted: Left

Formatted: Centered

Formatted: Left

Formatted: Left

Formatted: Left

Formatted: Left

Formatted: Left

Formatted: Left

Formatted: Left

Formatted: Left

Formatted: Left

Formatted: Left

Standard deviation (model)	σ_M (or SDM)	$\left(\frac{1}{N} \sum_1^N (M_i - \bar{M})^2\right)^{1/2}$
Normalized standard deviation	NSD	σ_M / σ_O
Coefficient of variation (observations)	CVO	σ_O / \bar{O}
Coefficient of variation (model)	CVM	σ_M / \bar{M}
Mean fractional bias	MFB	$\frac{2}{N} \sum_1^N \left(\frac{M_i - O_i}{M_i + O_i}\right)$
Mean fractional error	MFE	$\frac{2}{N} \sum_1^N \left \frac{M_i - O_i}{M_i + O_i}\right $

- Formatted: Left
- Formatted: Left
- Formatted: Centered
- Formatted: Left
- Formatted: Centered
- Formatted: Left
- Formatted: Centered
- Formatted: Left

2035

Metric Name	Abbreviation	Definition
-------------	--------------	------------

Observed mean	\bar{O}	$\frac{1}{N} \sum_1^N O_i$
Model mean	\bar{M}	$\frac{1}{N} \sum_1^N M_i$
Mean bias	MB	$\frac{1}{N} \sum_1^N (M_i - O_i)$
Root mean square error	RMSE	$\left(\frac{1}{N} \sum_1^N (M_i - O_i)^2\right)^{1/2}$
Normalized mean bias	NMB	$\frac{\sum_1^N (M_i - O_i)}{\sum_1^N O_i}$
Normalized mean absolute error	NME	$\frac{\sum_1^N M_i - O_i }{\sum_1^N O_i }$
Pearson correlation coefficient	R	$\frac{\sum_1^N (M_i - \bar{M}) \times (O_i - \bar{O})}{\sqrt{\sum_1^N (M_i - \bar{M})^2 \times \sum_1^N (O_i - \bar{O})^2}}$
Centred RMSE	CRMSE	$\left(\frac{1}{N} \sum_1^N [(M_i - \bar{M}) - (O_i - \bar{O})]^2\right)^{1/2}$
Standard deviation (observations)	σ_O (or SDO)	$\left(\frac{1}{N} \sum_1^N (O_i - \bar{O})^2\right)^{1/2}$

2040

2045

Standard deviation (model) — σ_M (or SDM) — $\left(\frac{1}{N} \sum_{i=1}^N (M_i - \bar{M})^2 \right)^{1/2}$

Normalized standard deviation — NSD — σ_M / σ_O

Coefficient of variation (observations) — CVO — σ_O / \bar{O}

2050 Coefficient of variation (model) — CVM — σ_M / \bar{M}

Mean fractional bias — MFB — $\frac{2}{N} \sum_{i=1}^N \frac{(M_i - O_i)}{(M_i + O_i)}$

Mean fractional error — MFE — $\frac{2}{N} \sum_{i=1}^N \frac{|M_i - O_i|}{(M_i + O_i)}$

2055 Table A3. Major upgrades to the operational RAQDPS from 2009-2021. See Moran et al. (20265) for more details.

Version	Release Date	Short Description
001	Nov. 2009	First version (Emission Inventories: 2006 CA, 2005 US, 1999 MX)
004	Oct. 2011	New emissions (EIs: 2006 CA, projected 2012 US, 1999 MX)
007	Oct. 2012	New model code, new grid (15 km → 10 km, 58 → 80 levels)
009	Feb. 2013	New model code with 3 bug fixes, including one to near-surface vertical diffusion
013	Jun. 2015	New emissions (EIs: 2010 CA, 2011 US, 1999 MX)
016	Sep. 2016	New model code, new vertical discretization (non-staggered → staggered)
020	Sep. 2018	New model code, new emissions (EIs: 2013 CA, projected 2017 US, 2008 MX)
021	Jul. 2019	New model code, new vertical discretization (80 → 84 levels), longer forecast (2→3 days)
023	Nov. 2021	New model code, new emissions (EIs: projected 2020 CA, projected 2023 US & 2023 MX)

Table A4. Summary of Canadian and U.S. national annual wildfire statistics for the 2013–2022 period. Data sources: Canadian Interagency Forest Fire Centre (2023); NOAA National Centers for Environmental Information (2023).

Year	Number of Fires			Hectares Burned		
	Canada	U.S.	Total	Canada	U.S.	Total
2013	6,246	46,615	52,861	4,203,867	1,743,054	5,946,921
2014	5,126	63,345	68,471	4,563,847	1,451,836	6,015,683
2015	7,068	61,922	68,990	3,903,277	4,097,506	8,000,783
2016	5,173	65,575	70,748	1,532,440	2,204,130	3,736,570
2017	5,611	66,131	71,742	3,371,825	3,958,259	7,330,084
2018	7,068	55,911	62,979	2,272,269	3,473,262	5,745,531
2019	3,933	49,786	53,719	1,787,793	1,873,699	3,661,492
2020	3,916	58,258	62,174	227,389	4,158,019	4,385,408
2021	6,596	58,733	65,329	4,307,520	2,889,342	7,196,862
2022	5,726	66,255	71,981	1,656,504	3,049,067	4,705,571

2060 Table A5. Comparison of selected NAQFC domain-average monthly statistics for daily mean surface $PM_{2.5}$ predictions ($\mu\text{g}\cdot\text{m}^{-3}$) for 2014 and 2015 (from Lee et al., 2017) with domain-average seasonal statistics for RAQDPS010 forecasts for hourly mean surface $PM_{2.5}$ predictions ($\mu\text{g}\cdot\text{m}^{-3}$) for spring (MAM) and summer (JJA) 2014 and RAQDPS011 forecasts for winter (DJF) 2015 (from Moran et al., 2021a).

Period	System	O	M	MB	NMB	RMSE	R
May 2014	NAQFC	7.76	6.20	-1.56	-0.20	4.46	0.32
Spring 2014	RAQDPS010			-0.88	-0.12	8.02	0.37
July 2014	NAQFC	9.93	6.62	-2.71	-0.28	5.36	0.23
Summer 2014	RAQDPS010			0.64	0.07	11.21	0.29
January 2015	NAQFC	9.83	11.16	1.33	0.13	6.46	0.38
Winter 2015	RAQDPS011			-1.04	-0.12	10.15	0.38

2065 Code and data availability

Version 5.1 of the GEM numerical weather prediction model code used by the RAQDPS023 is free software which can be redistributed and/or modified under the terms of version 2.1 of the GNU Lesser General Public License as published by the Free Software Foundation. The GEM source code has been developed by the Meteorological Research Division of ECCC. This code is available for download from <https://zenodo.org/records/17782580> (Environment and Climate Change Canada/ECCC, 2025b).

MACH, the atmospheric chemistry library for the GEM model (©2007–2021, Air Quality Research Division and National Prediction Operations Division, Environment and Climate Change Canada), is free software that can be redistributed and/or modified under the terms of the GNU Lesser General Public License as published by the Free

Software Foundation – either version 2.1 of the license or any later version. The GEM-MACH version 3.1.0.0 code used by the RAQDPS023 can be downloaded from website <https://doi.org/10.5281/zenodo.15330612> (Savic-Jovicic et al., 2025). Related documentation is also available on that website, including information about key input and configuration files and copies of several relevant reports. The GEM-MACH v3.1.1.2 source code for the RAQDPS024, an equivalent version to the RAQDPS023 that went into operation after a migration to a new ECCC high-performance computer system in June 2022, is available at <https://zenodo.org/records/13952893> (GEM-MACH development team, 2022).

Formatted: Font: 11 pt

Formatted: Font: (Default) Times New Roman, English (United Kingdom)

The CFFEPS version 4.1 code that was used by the RAQDPS-FW023 and RAQDPS-FW024 is free software that can be redistributed and/or modified under the terms of the GNU Lesser General Public License, either version 2.1 or any later version, as published by the Free Software Foundation. It is available to download from website <https://doi.org/10.5281/zenodo.15305591> (Anderson and Chen, 2021).

Data sources for the AQ measurement data sets used in this study are listed in Table S2a of the Supplement. Multiple sets of files containing (i) the “raw” measurements that were used in this study, (ii) intermediate measurement files after necessary unit conversions and proxy calculations, (iii) filtered measurement files after application of validity and temporal completeness checks, and (iv) final, evaluation-ready, paired model-measurement files after temporal aggregation for data pooling and filtering for reconstructed mass completeness are available from <https://doi.org/10.5281/zenodo.16944371> (Lupu and Moran, 2025). This data repository also contains a complete set of the output files of evaluation scores that were the basis for all of the evaluation-related tables and figures presented in this paper.

A package of seasonal and annual model-predicted gridded surface concentration fields and dry, wet, and total acidic deposition fields for the 2013-2016 simulations is available from the website <https://doi.org/10.5281/zenodo.16970403> (Moran and Savic-Jovicic, 2025). Some of the archived model hourly output fields used to create this package were also used by Cathcart et al. (2025) and Robichaud et al. (2025, 2026) in their recent papers.

All other data sets used in this work are available upon request from the authors. Please contact one of the corresponding authors to make a request.

Supplement

The supplement related to this article is available on-line at <https://doi.org/10.5281/zenodo.19489036> (Moran and Lupu, 2026).

Formatted: Font: 11 pt

Formatted: Line spacing: 1.5 lines

Field Code Changed

Formatted: Font: 11 pt

Author contributions

MDM was the science lead for the development of the online RAQDPS from the RAQDPS001 up to the RAQDPS023 and was the co-supervisor for all operational deliveries from 2009 to 2021. He conceived the objectives and scope of

2105 this study, oversaw the evaluations of the RAQDPS023, and prepared the initial and final versions of this paper. AL assisted with the 2013–2016 simulations, obtained all AQ measurement data sets, developed all measurement data processing and evaluation scripts, and generated all evaluation tables and data-related figures for the 2013–2016 and 2021/22 annual simulations, VSJ developed and maintained RAQDPS code and scripts, performed the 2013–2016 annual simulations, and prepared model-related figures and analyses. JZ performed the 2010–2019 operational 2110 evaluation, and JZ, QZ, EIB, and RM generated the 2013–2016 and 2021/22 anthropogenic emissions files and performed the analyses to construct Tables 1 and S1 and Figure S1. CAS led the migration from the RAQDPS023 to the RAQDPS024 on the new CMC supercomputers in June 2022 and the development of the RAQDPS025, which became operational in June 2024. SM has been the co-supervisor for all operational deliveries of the RAQDPS with the assistance of VSJ, JC, KM, RMA, and DK. JC led the development and delivery of the RAQDPS-FW023 and all 2115 CFFEPS versions with the assistance of KM and RMA. PMM oversaw operational evaluation of North American NRT AQ forecasts at ECCC for GAFIS. Lastly, AL, VSJ, JZ, RM, CAS, JC, QZ, EIB, SM, and RMA reviewed the manuscript.

Competing interests

The authors declare that they have no conflicts of interest.

Acknowledgements

2120 ~~The authors~~We would like to thank Ayodeji Akingunola, David Anselmo, Didier Davignon, Annie Duhamel, Samuel Gilbert, Hugo Landry, Jessica Miville, David Niemi, Radenko Pavlovic, Si-Jun Peng, Jacinthe Racine, and Mourad Sassi of ECCC for their contributions to this project. We appreciate the generosity of Kristen Foley, Alison Eyth, and their colleagues at the U.S. EPA and General Dynamics Information Technology for providing early access to the 2125 EQUATES emissions data set (Foley et al., 2023). Access to a host of AQ measurement data sets was key to this study (see Table S2a), and we thank (i) ECCC for the use of daily filter pack and precipitation–chemistry observations from the CAPMoN network, (ii) ECCC and the provincial, territorial, and regional government NAPS partners for the use of their NAPS network ambient AQ observations, (iii) the U.S. NADP network for the use of observations from the AMoN and NTN networks, (iv) the U.S. EPA for use of observations from the CASTNET and CSN networks and the 2130 AQS, (v) the U.S. EPA, the U.S. National Park Service, and other federal, state, and tribal partners for use of observations from the IMPROVE network, and (vi) the U.S. EPA and its state and local, tribal, federal, and Canadian and Mexican partners (<https://www.airnow.gov/partners/>, last access: 6 April 2026) for the use of near-real-time observations from the AirNow metanetwork. AL thanks Kulbir Banwait, Amanda Cole, Amy Hou, and Bill Sukloff of the ECCC CAPMoN and NAtChem groups for insightful discussions about various AQ measurement datasets. We 2135 also appreciate the provision of operational AQ forecasts by NOAA, NASA, ECMWF, and the Finnish Meteorological Institute to ECCC in NRT under the WMO GAFIS initiative. MDM would also like to thank Rosa Wu for her continuing support of this paper over multiple years. ~~Lastly, w~~We note too that we have chosen to use colour-vision-

Formatted: Font: 11 pt

Formatted: Font: 11 pt

deficiency-friendly, perceptually-uniform colour maps designed by Crameri et al. (2020) for some figures in this paper.

2140 Lastly, the authors would like to thank two anonymous reviewers for their constructive comments that helped to improve the manuscript and the topic editor, Emmanouil Flaounas, for overseeing the review of two lengthy manuscripts.

2145 References

- Ames, R. B. and Malm, W. C.: Comparison of sulfate and nitrate particle mass concentrations measured by IMPROVE and the CDN, *Atmos. Environ.*, 35, 905–916, [https://doi.org/10.1016/S1352-2310\(00\)00369-1](https://doi.org/10.1016/S1352-2310(00)00369-1), 2001.
- Anderson, K. and Chen, J.: Canadian Fire Emissions Prediction System (CFFEPS) v4.1, [Environment and Climate Change Canada, Zenodo \[software\]](https://doi.org/10.5281/zenodo.153055912579382), <https://doi.org/10.5281/zenodo.153055912579382>, 2021.
- 2150 Ansari, A. S. and Pandis, S. N.: Response of inorganic PM to precursor concentrations, *Environ. Sci. Technol.*, 32, 2706–2714, <https://doi.org/10.1021/es971130j>, 1998.
- Appel, K. W., Bhawe, P. V., Gilliland, A. B., Sarwar, G., and Roselle, S. J.: Evaluation of the Community Multiscale Air Quality (CMAQ) model version 4.5: Sensitivities impacting model performance; Part II—particulate matter, *Atmos. Environ.*, 42, 6057–6066, <https://doi.org/10.1016/j.atmosenv.2008.03.036>, 2008.
- 2155 Appel, K. W., Foley, K. M., Bash, J. O., Pinder, R. W., Dennis, R. L., Allen, D. J., and Pickering, K.: A multi-resolution assessment of the Community Multiscale Air Quality (CMAQ) model v4.7 wet deposition estimates for 2002–2006, *Geosci. Model Dev.*, 4, 357–371, <https://doi.org/10.5194/gmd-4-357-2011>, 2011.
- Appel, K. W., Pouliot, G. A., Simon, H., Sarwar, G., Pye, H. O. T., Napelenok, S. L., Akhtar, F., and Roselle, S. J.: Evaluation of dust and trace metal estimates from the Community Multiscale Air Quality (CMAQ) model version 5.0, *Geosci. Model Dev.*, 6, 883–899, <https://doi.org/10.5194/gmd-6-883-2013>, 2013.
- 2160 Appel, K. W., Napelenok, S. L., Foley, K. M., Pye, H. O. T., Hogrefe, C., Luecken, D. J., Bash, J. O., Roselle, S. J., Pleim, J. E., Foroutan, H., Hutzell, W. T., Pouliot, G. A., Sarwar, G., Fahey, K. M., Gantt, B., Gilliam, R. C., Heath, N. K., Kang, D., Mathur, R., Schwede, D. B., Spero, T. L., Wong, D. C., and Young, J. O.: Description and evaluation of the Community Multiscale Air Quality (CMAQ) modeling system version 5.1, *Geosci. Model Dev.*, 10, 1703–1732, <https://doi.org/10.5194/gmd-10-1703-2017>, 2017.
- 2165 Appel, K. W., Bash, J. O., Fahey, K. M., Foley, K. M., Gilliam, R. C., Hogrefe, C., Hutzell, W. T., Kang, D., Mathur, R., Murphy, B. N., Napelenok, S. L., Nolte, C. G., Pleim, J. E., Pouliot, G. A., Pye, H. O. T., Ran, L., Roselle, S. J., Sarwar, G., Schwede, D. B., Sidi, F. I., Spero, T. L., and Wong, D. C.: The Community Multiscale Air Quality (CMAQ) model versions 5.3 and 5.3.1: system updates and evaluation, *Geosci. Model Dev.*, 14, 2867–2897, <https://doi.org/10.5194/gmd-14-2867-2021>, 2021.
- 2170 Astitha, M., Kioutsoukakis, I., Fisseha, G. A., Bianconi, R., Bieser, J., Christensen, J. H., Cooper, O. R., Galmarini, S., Hogrefe, C., Im, U., Johnson, B., Liu, P., Nopmongkol, U., Petropavlovskikh, I., Solazzo, E., Tarasick, D. W., and Yarwood, G.: Seasonal ozone vertical profiles over North America using the AQMEII3 group of air quality models: model inter-comparison and stratospheric intrusions, *Atmospheric Chem. Phys.*, 18, 13925–13945, <https://doi.org/10.5194/acp-18-13925-2018>, 2018.
- 2175 Bachmann, J. D.: Tackling multi-pollutant particles, *EM Air Waste Manag. Assoc. Mag. Environ. Manag.*, 6–9, https://www.researchgate.net/publication/268280224_Tackling_Multi-pollutant_Particles (last access: 6 April 2026), 2013.
- Bencala, K. E. and Seinfeld, J. H.: An air quality model performance assessment package, *Atmospheric Environ.* 1967, 13, 1181–1185, [https://doi.org/10.1016/0004-6981\(79\)90043-X](https://doi.org/10.1016/0004-6981(79)90043-X), 1979.
- 2180 Benish, S. E., Bash, J. O., Foley, K. M., Appel, K. W., Hogrefe, C., Gilliam, R., and Pouliot, G.: Long-term regional trends of nitrogen and sulfur deposition in the United States from 2002 to 2017, *Atmospheric Chem. Phys.*, 22, 12749–12767, <https://doi.org/10.5194/acp-22-12749-2022>, 2022.
- Bermejo, R. and Conde, J.: A conservative quasi-monotone semi-Lagrangian scheme, *Mon. Weather Rev.*, 130, 423–430, [https://doi.org/10.1175/1520-0493\(2002\)130<0423:ACQMSL>2.0.CO;2](https://doi.org/10.1175/1520-0493(2002)130<0423:ACQMSL>2.0.CO;2), 2002.
- Biswas, J., Hogrefe, C., Rao, S. T., Hao, W., and Sista, G.: Evaluating the performance of regional-scale photochemical modeling systems. Part III—Precursor predictions, *Atmos. Environ.*, 35, 6129–6149, [https://doi.org/10.1016/S1352-2310\(01\)00401-0](https://doi.org/10.1016/S1352-2310(01)00401-0), 2001.
- 2185 Bloom, S. C., Takacs, L. L., da Silva, A. M., and Ledvina, D.: Data assimilation using incremental analysis updates, *Mon. Weather Rev.*, 124, 1256–1271, [https://doi.org/10.1175/1520-0493\(1996\)124<1256:DAUIAU>2.0.CO;2](https://doi.org/10.1175/1520-0493(1996)124<1256:DAUIAU>2.0.CO;2), 1996.
- Borrego, C., Monteiro, A., Ferreira, J., Miranda, A. I., Costa, A. M., Carvalho, A. C., and Lopes, M.: Procedures for estimation of modelling uncertainty in air quality assessment, *Environ. Int.*, 34, 613–620, <https://doi.org/10.1016/j.envint.2007.12.005>, 2008.
- 2190 Brasseur, G. P. and Kumar, R.: Chemical weather and chemical climate, *AGU Adv.*, 2, e2021AV000399, <https://doi.org/10.1029/2021AV000399>, 2021.
- Cai, C., Hogrefe, C., Katsafados, P., Kallos, G., Beauharnois, M., Schwab, J. J., Ren, X., Brune, W. H., Zhou, X., He, Y., and Demerjian, K. L.: Performance evaluation of an air quality forecast modeling system for a summer and winter season – Photochemical oxidants and their precursors, *Atmos. Environ.*, 42, 8585–8599, <https://doi.org/10.1016/j.atmosenv.2008.08.029>, 2008.

- 2195 Campbell, P. C., Tang, Y., Lee, P., Baker, B., Tong, D., Saylor, R., Stein, A., Huang, J., Huang, H.-C., Strobach, E., McQueen, J., Pan, L., Stajner, I., Sims, J., Tirado-Delgado, J., Jung, Y., Yang, F., Spero, T. L., and Gilliam, R. C.: Development and evaluation of an advanced National Air Quality Forecasting Capability using the NOAA Global Forecast System version 16, *Geosci. Model Dev.*, 15, 3281–3313, <https://doi.org/10.5194/gmd-15-3281-2022>, 2022.
- 2200 Canadian Interagency Forest Fire Centre: Canada Report 2022, 15 pp., <https://ciffc.ca/publications/canada-reports/> (last access: 6 April 2026) <https://doi.org/10.5194/bg-22-535-2025>, 2023.
- Caron, J.-F., Milewski, T., Buehner, M., Fillion, L., Reszka, M., Macpherson, S., and St-James, J.: Implementation of deterministic weather forecasting systems based on ensemble–variational data assimilation at Environment Canada. Part II: The regional system, *Mon. Weather Rev.*, 143, 2560–2580, <https://doi.org/10.1175/MWR-D-14-00353.1>, 2015.
- 2205 Cathcart, H., Aherne, J., Moran, M. D., Savic-Jovicic, V., Makar, P. A., and Cole, A.: Estimates of critical loads and exceedances of acidity and nutrient nitrogen for mineral soils in Canada for 2014–2016 average annual sulfur and nitrogen atmospheric deposition, *Biogeosciences*, 22, 535–554, <https://doi.org/10.5194/bg-22-535-2025>, 2025.
- Chai, T., Kim, H.-C., Lee, P., Tong, D., Pan, L., Tang, Y., Huang, J., McQueen, J., Tsidulko, M., and Stajner, I.: Evaluation of the United States National Air Quality Forecast Capability experimental real-time predictions in 2010 using Air Quality System ozone and NO₂ measurements, *Geosci. Model Dev.*, 6, 1831–1850, <https://doi.org/10.5194/gmd-6-1831-2013>, 2013.
- 2210 Chan, E. A. W., Gantt, B., and McDow, S.: The reduction of summer sulfate and switch from summertime to wintertime PM_{2.5} concentration maxima in the United States, *Atmos. Environ.*, 175, 25–32, <https://doi.org/10.1016/j.atmosenv.2017.11.055>, 2018.
- Chang, J. C. and Hanna, S. R.: Air quality model performance evaluation, *Meteorol. Atmospheric Phys.*, 87, <https://doi.org/10.1007/s00703-003-0070-7>, 2004.
- 2215 Chen, J. and Menelaou, K.: Regional Air Quality Deterministic Prediction System with near-real-time wildfire emissions (RAQDPSFW): Upgrade to version 023, Technical note, November, Canadian Centre for Meteorological and Environmental Prediction, Montreal, 31 pp., https://collaboration.cmc.ec.gc.ca/cmc/CMOI/product_guide/docs/tech_notes/technote_raqdpsfw_e.pdf (last access: 6 April 2026), 2021.
- 2220 Chen, J., Anderson, K., Pavlovic, R., Moran, M. D., Englefield, P., Thompson, D. K., Munoz-Alpizar, R., and Landry, H.: The FireWork v2.0 air quality forecast system with biomass burning emissions from the Canadian Forest Fire Emissions Prediction System v2.03, *Geosci. Model Dev.*, 12, 3283–3310, <https://doi.org/10.5194/gmd-12-3283-2019>, 2019.
- Chen, X., Zhang, Y., Wang, K., Tong, D., Lee, P., Tang, Y., Huang, J., Campbell, P. C., McQueen, J., Pye, H. O. T., Murphy, B. N., and Kang, D.: Evaluation of the offline-coupled GFSv15–FV3–CMAQv5.0.2 in support of the next-generation National Air Quality Forecast Capability over the contiguous United States, *Geosci. Model Dev.*, 14, 3969–3993, <https://doi.org/10.5194/gmd-14-3969-2021>, 2021.
- 2225 Chow, J. C.: Measurement methods to determine compliance with ambient air quality standards for suspended particles, *J. Air Waste Manag. Assoc.*, 45, 320–382, <https://doi.org/10.1080/10473289.1995.10467369>, 1995.
- Chow, J. C., Lowenthal, D. H., Chen, L.-W. A., Wang, X., and Watson, J. G.: Mass reconstruction methods for PM_{2.5}: a review, *Air Qual. Atmosphere Health*, 8, 243–263, <https://doi.org/10.1007/s11869-015-0338-3>, 2015.
- 2230 Chuang, M.-T., Zhang, Y., and Kang, D.: Application of WRF/Chem-MADRID for real-time air quality forecasting over the southeastern United States, *Atmos. Environ.*, 45, 6241–6250, <https://doi.org/10.1016/j.atmosenv.2011.06.071>, 2011.
- 2235 Clifton, O. E., Schwede, D., Hogrefe, C., Bash, J. O., Bland, S., Cheung, P., Coyle, M., Emberson, L., Flemming, J., Fredj, E., Galmarini, S., Ganzeveld, L., Gazetas, O., Goded, I., Holmes, C. D., Horváth, L., Huijnen, V., Li, Q., Makar, P. A., Mammarella, I., Manca, G., Munger, J. W., Pérez-Camanyo, J. L., Pleim, J., Ran, L., San Jose, R., Silva, S. J., Staebler, R., Sun, S., Tai, A. P. K., Tas, E., Vesala, T., Weidinger, T., Wu, Z., and Zhang, L.: A single-point modeling approach for the intercomparison and evaluation of ozone dry deposition across chemical transport models (Activity 2 of AQMEII4), *Atmospheric Chem. Phys.*, 23, 9911–9961, <https://doi.org/10.5194/acp-23-9911-2023>, 2023.
- 2240 CMC-RAQDPS-023: The Regional Air Quality Deterministic Prediction System (RAQDPS) version 023 and the Regional Air Quality Deterministic Prediction System with Near-Real-Time Wildfire Emissions (RAQDPSFW) version 023 of the Meteorological Service of Canada (MSC): Technical Specifications Document, November, Canadian Centre for Meteorological and Environmental Prediction, Montreal, 19 pp., https://collaboration.cmc.ec.gc.ca/cmc/cmoei/product_guide/docs/tech_specifications/tech_specifications_RAQDPS_023_e.pdf (last access: 6 April 2026), 2021.
- 2245 CMC-RAQDPS-025: The Regional Air Quality Deterministic Prediction System (RAQDPS): Upgrade from version 024 to version 025, June, Canadian Centre for Meteorological and Environmental Prediction, Montreal, 89 pp.,

https://collaboration.emc.ec.gc.ca/emc/cmoe/product_guide/docs/tech_notes/technote_raqdps-v25_e.pdf (last access: 6 April 2026), 2024.

2250 CMC-RDPS-8.0.0: The Regional Deterministic Prediction System (RDPS) version 8.0.0 of the Meteorological Service of Canada (MSC): Technical specifications document, December, Canadian Centre for Meteorological and Environmental Prediction, Montreal, 10 pp., https://collaboration.emc.ec.gc.ca/emc/cmoe/product_guide/docs/tech_specifications/tech_specifications_RDPS_8.0.0_e.pdf (last access: 6 April 2026), 2021.

2255 Colette, A., Andersson, C., Manders, A., Mar, K., Mircea, M., Pay, M.-T., Raffort, V., Tsyro, S., Cuvelier, C., Adani, M., Bessagnet, B., Bergström, R., Briganti, G., Butler, T., Cappelletti, A., Couvidat, F., D'Isidoro, M., Doumbia, T., Fagerli, H., Granier, C., Heyes, C., Klimont, Z., Ojha, N., Otero, N., Schaap, M., Sindelarova, K., Stegehuis, A. I., Roustan, Y., Vautard, R., Van Meijgaard, E., Vivanco, M. G., and Wind, P.: EURODELTA-Trends, a multi-model experiment of air quality hindcast in Europe over 1990–2010, *Geosci. Model Dev.*, 10, 3255–3276, <https://doi.org/10.5194/gmd-10-3255-2017>, 2017.

2260 [Colette, A., Collin, G., Besson, F., Blot, E., Guidard, V., Meleux, F., Royer, A., Petiot, V., Miller, C., Fermond, O., Jeant, A., Adani, M., Arteta, J., Benedictow, A., Bergström, R., Bowdalo, D., Brandt, J., Briganti, G., Carvalho, A. C., Christensen, J. H., Couvidat, F., D'Elia, I., D'Isidoro, M., Denier Van Der Gon, H., Descombes, G., Di Tomaso, E., Douros, J., Escrivano, J., Eskes, H., Fagerli, H., Fatahi, Y., Flemming, J., Friese, E., Frohn, L., Gauss, M., Geels, C., Guarnieri, G., Guevara, M., Guion, A., Guth, J., Hänninen, R., Hansen, K., Im, U., Janssen, R., Jeoffrion, M., Joly, M., Jones, L., Jorba, O., Kadantsev, E., Kahnert, M., Kaminski, J. W., Kouznetsov, R., Kranenburg, R., Kuenen, J., Lange, A. C., Langner, J., Lannuque, V., Macchia, F., Manders, A., Mircea, M., Nyiri, A., Olid, M., Pérez García-Pando, C., Palamarchuk, Y., Piersanti, A., Raux, B., Razinger, M., Robertson, L., Segers, A., Schaap, M., Siljamo, P., Simpson, D., Sofiev, M., Stangel, A., Struzewska, J., Tena, C., Timmermans, R., Tsjerdekis, T., Tsyro, S., Tyuryakov, S., Ung, A., Uppstu, A., Valdebenito, A., Van Velthoven, P., Vitali, L., Ye, Z., Peuch, V.-H., and Rouil, L.: Copernicus Atmosphere Monitoring Service – Regional Air Quality Production System v1.0, *Geosci. Model Dev.*, 18, 6835–6883, <https://doi.org/10.5194/gmd-18-6835-2025>, 2025.](#)

2270 Cramer, F., Shephard, G. E., and Heron, P. J.: The misuse of colour in science communication, *Nat. Commun.*, 11, 5444, <https://doi.org/10.1038/s41467-020-19160-7>, 2020.

Dabek-Zlotorzynska, E., Dann, T. F., Kalyani Martinelango, P., Celso, V., Brook, J. R., Mathieu, D., Ding, L., and Austin, C. C.: Canadian National Air Pollution Surveillance (NAPS) PM_{2.5} speciation program: Methodology and PM_{2.5} chemical composition for the years 2003–2008, *Atmos. Environ.*, 45, 673–686, <https://doi.org/10.1016/j.atmosenv.2010.10.024>, 2011.

2275 Demerjian, K.: A review of national monitoring networks in North America, *Atmos. Environ.*, 34, 1861–1884, [https://doi.org/10.1016/S1352-2310\(99\)00452-5](https://doi.org/10.1016/S1352-2310(99)00452-5), 2000.

Dennis, R., Fox, T., Fuentes, M., Gilliland, A., Hanna, S., Hogrefe, C., Irwin, J., Rao, S. T., Scheffe, R., Schere, K., Steyn, D., and Venkatram, A.: A framework for evaluating regional-scale numerical photochemical modeling systems, *Environ. Fluid Mech.*, 10, 471–489, <https://doi.org/10.1007/s10652-009-9163-2>, 2010.

2280 Dennis, R. L. and Downton, M. W.: Evaluation of urban photochemical models for regulatory use, *Atmospheric Environ.* 1967, 18, 2055–2069, [https://doi.org/10.1016/0004-6981\(84\)90192-6](https://doi.org/10.1016/0004-6981(84)90192-6), 1984.

Dennis, R. L., McHenry, J. N., Barchet, W. R., Binkowski, F. S., and Byun, D. W.: Correcting RADM's sulfate underprediction: Discovery and correction of model errors and testing the corrections through comparisons against field data, *Atmospheric Environ. Part Gen. Top.*, 27, 975–997, [https://doi.org/10.1016/0960-1686\(93\)90012-N](https://doi.org/10.1016/0960-1686(93)90012-N), 1993.

2285 Derwent, R., Fraser, A., Abbot, J., Jenkin, M., Willis, P., and Murrells, T.: Evaluating the Performance of Air Quality Models, Department for Environment Food and Rural Affairs, United Kingdom, https://uk-air.defra.gov.uk/assets/documents/reports/cat05/1006241607_100608_MIP_Final_Version.pdf (last access 6 April 2026), 2010.

[Dickerson, R. R., Anderson, D. C., and Ren, X.: On the use of data from commercial NOx analyzers for air pollution studies, *Atmos. Environ.*, 214, 116873, <https://doi.org/10.1016/j.atmosenv.2019.116873>, 2019.](#)

2290 Dickson, R. J. and Oliver, W. R.: Emissions models for regional air quality studies, *Environ. Sci. Technol.*, 25, 1533–1535, <https://doi.org/10.1021/es00021a003>, 1991.

2295 Dunlea, E. J., Herndon, S. C., Nelson, D. D., Volkamer, R. M., San Martini, F., Sheehy, P. M., Zahniser, M. S., Shorter, J. H., Wormhoudt, J. C., Lamb, B. K., Allwine, E. J., Gaffney, J. S., Marley, N. A., Grutter, M., Marquez, C., Blanco, S., Cardenas, B., Retama, A., Ramos Villegas, C. R., Kolb, C. E., Molina, L. T., and Molina, M. J.: Evaluation of nitrogen dioxide chemiluminescence monitors in a polluted urban environment, *Atmospheric Chem. Phys.*, 7, 2691–2704, <https://doi.org/10.5194/acp-7-2691-2007>, 2007.

Dye, T. S., Chan, A. C., Anderson, C. B., D.E.B. Strohm, Wayland, R. A., and White, J. E.: From raw air quality data to the nightly news: an overview of how EPA's AirNow program operates, Sixth Conference on Atmospheric Chemistry, 12-14 January, Seattle,

- Washington, American Meteorological Society, <https://ams.confex.com/ams/pdfpapers/72477.pdf> (last access: 6 April 2026), 2004.
- 2300 ECCC: 1990–2016 Air Pollutant Emission Inventory Report, Environment and Climate Change Canada, Gatineau, Quebec, 92 pp., https://publications.gc.ca/collections/collection_2018/eccc/En81-26-2016-eng.pdf (last access: 6 April 2026), 2018.
- [ECCC: Canada's Air Pollutant Emissions Inventory Report 1990–2023, Environment and Climate Change Canada, Gatineau, Quebec, 72 pp., https://publications.gc.ca/collections/collection_2025/eccc/En81-30-2023-eng.pdf](https://publications.gc.ca/collections/collection_2025/eccc/En81-30-2023-eng.pdf) (last access: 6 April 2026), 2025a.
- 2305 [ECCC: Version 5.1 package for the Global Environmental Multiscale \(GEM\) model \(ECCC-ASTD-MRD/gem: 5.1.0\), Environment and Climate Change Canada, Zenodo \[software\], https://doi.org/10.5281/zenodo.17782580, 2025b.](https://doi.org/10.5281/zenodo.17782580)
- Eder, B., Kang, D., Mathur, R., Yu, S., and Schere, K.: An operational evaluation of the Eta–CMAQ air quality forecast model, *Atmos. Environ.*, 40, 4894–4905, <https://doi.org/10.1016/j.atmosenv.2005.12.062>, 2006.
- 2310 Eder, B., Kang, D., Mathur, R., Pleim, J., Yu, S., Otte, T., and Pouliot, G.: A performance evaluation of the National Air Quality Forecast Capability for the summer of 2007, *Atmos. Environ.*, 43, 2312–2320, <https://doi.org/10.1016/j.atmosenv.2009.01.033>, 2009.
- Eder, B., Kang, D., Rao, S. T., Mathur, R., Yu, S., Otte, T., Schere, K., Wayland, R., Jackson, S., Davidson, P., McQueen, J., and Bridgers, G.: Using National Air Quality Forecast Guidance to develop local Air Quality Index forecasts, *Bull. Am. Meteorol. Soc.*, 91, 313–326, <https://doi.org/10.1175/2009BAMS2734.1>, 2010.
- 2315 Emery, C., Liu, Z., Russell, A. G., Odman, M. T., Yarwood, G., and Kumar, N.: Recommendations on statistics and benchmarks to assess photochemical model performance, *J. Air Waste Manag. Assoc.*, 67, 582–598, <https://doi.org/10.1080/10962247.2016.1265027>, 2017.
- Entekhabi, D., Reichle, R. H., Koster, R. D., and Crow, W. T.: Performance metrics for soil moisture retrievals and application requirements, *J. Hydrometeorol.*, 11, 832–840, <https://doi.org/10.1175/2010JHM1223.1>, 2010.
- 2320 ~~[Environment and Climate Change Canada: Version 5.1 package for the Global Environmental Multiscale \(GEM\) model \(ECCC-ASTD-MRD/gem: 5.1.0\), Zenodo \[software\], https://doi.org/10.5281/zenodo.17782580, 2025.](https://doi.org/10.5281/zenodo.17782580)~~
- Feng, J., Chan, E., and Vet, R.: Air quality in the eastern United States and eastern Canada for 1990–2015: 25 years of change in response to emission reductions of SO₂ and NO_x in the region, *Atmospheric Chem. Phys.*, 20, 3107–3134, <https://doi.org/10.5194/acp-20-3107-2020>, 2020.
- 2325 Feng, J., Cole, A., Wetherbee, G. A., and Banwait, K.: Inter-comparison of measurements of inorganic chemical components in precipitation from NADP and CAPMoN at collocated sites in the USA and Canada during 1986–2019, *Environ. Monit. Assess.*, 195, 1333, <https://doi.org/10.1007/s10661-023-11771-z>, 2023.
- Fillion, L., Mitchell, H. L., Ritchie, H., and Staniforth, A.: The impact of a digital filter finalization technique in a global data assimilation system, *Tellus A*, 47, 304–323, <https://doi.org/10.1034/j.1600-0870.1995.t01-2-00002.x>, 1995.
- 2330 Fillion, L., Tanguay, M., Lapalme, E., Denis, B., Desgagné, M., Lee, V., Ek, N., Liu, Z., Lajoie, M., Caron, J.-F., and Pagé, C.: The Canadian Regional Data Assimilation and Forecasting System, *Weather Forecast.*, 25, 1645–1669, <https://doi.org/10.1175/2010WAF2222401.1>, 2010.
- Foley, K. M., Hogrefe, C., Pouliot, G., Possiel, N., Roselle, S. J., Simon, H., and Timin, B.: Dynamic evaluation of CMAQ part I: Separating the effects of changing emissions and changing meteorology on ozone levels between 2002 and 2005 in the eastern US, *Atmos. Environ.*, 103, 247–255, <https://doi.org/10.1016/j.atmosenv.2014.12.038>, 2015.
- 2335 Foley, K. M., Pouliot, G. A., Eyth, A., Aldridge, M. F., Allen, C., Appel, K. W., Bash, J. O., Beardsley, M., Beidler, J., Choi, D., Farkas, C., Gilliam, R. C., Godfrey, J., Henderson, B. H., Hogrefe, C., Koplitz, S. N., Mason, R., Mathur, R., Misenis, C., Possiel, N., Pye, H. O. T., Reynolds, L., Roark, M., Roberts, S., Schwede, D. B., Seltzer, K. M., Sonntag, D., Talgo, K., Toro, C., Vukovich, J., Xing, J., and Adams, E.: 2002–2017 anthropogenic emissions data for air quality modeling over the United States, *Data Brief*, 47, 109022, 33 pp., <https://doi.org/10.1016/j.dib.2023.109022>, 2023.
- 2340 Foroutan, H., Young, J., Napelenok, S., Ran, L., Appel, K. W., Gilliam, R. C., and Pleim, J. E.: Development and evaluation of a physics-based windblown dust emission scheme implemented in the CMAQ modeling system, *J. Adv. Model. Earth Syst.*, 9, 585–608, <https://doi.org/10.1002/2016MS000823>, 2017.
- 2345 Frank, N. H.: Retained nitrate, hydrated sulfates, and carbonaceous mass in Federal Reference Method fine particulate matter for six eastern U.S. cities, *J. Air Waste Manag. Assoc.*, 56, 500–511, <https://doi.org/10.1080/10473289.2006.10464517>, 2006.
- Fruin, S., Urman, R., Lurmann, F., McConnell, R., Gauderman, J., Rappaport, E., Franklin, M., Gilliland, F. D., Shafer, M., Gorski, P., and Avol, E.: Spatial variation in particulate matter components over a large urban area, *Atmos. Environ.*, 83, 211–219, <https://doi.org/10.1016/j.atmosenv.2013.10.063>, 2014.

- Galmarini, S., Bonnardot, F., Jones, A., Potemski, S., Robertson, L., and Martet, M.: Multi-model vs. EPS-based ensemble atmospheric dispersion simulations: A quantitative assessment on the ETEX-I tracer experiment case, *Atmos. Environ.*, 44, 3558–3567, <https://doi.org/10.1016/j.atmosenv.2010.06.003>, 2010.
- Galmarini, S., Makar, P., Clifton, O. E., Hogrefe, C., Bash, J. O., Bellasio, R., Bianconi, R., Bieser, J., Butler, T., Ducker, J., Flemming, J., Hodzic, A., Holmes, C. D., Kioutsioukis, I., Kranenburg, R., Lupascu, A., Perez-Camanyo, J. L., Pleim, J., Ryu, Y.-H., San Jose, R., Schwede, D., Silva, S., and Wolke, R.: Technical note: AQMEII4 Activity 1: evaluation of wet and dry deposition schemes as an integral part of regional-scale air quality models, *Atmospheric Chem. Phys.*, 21, 15663–15697, <https://doi.org/10.5194/acp-21-15663-2021>, 2021.
- Gan, C. M., Binkowski, F., Pleim, J., Xing, J., Wong, D., Mathur, R., and Gilliam, R.: Assessment of the aerosol optics component of the coupled WRF–CMAQ model using CARES field campaign data and a single column model, *Atmos. Environ.*, 115, 670–682, <https://doi.org/10.1016/j.atmosenv.2014.11.028>, 2015.
- Gantt, B.: 10 Years (2011–2020) of the NCore Network: FEMs vs FRMs, 2022 National Ambient Air Monitoring Conference, Aug. 22–25, Pittsburgh, Pennsylvania, https://www.epa.gov/system/files/documents/2022-10/Gantt_Brett_Wed1030.pdf (last access: 6 April 2026), 2022.
- Gaudel, A., Cooper, O. R., Ancellet, G., Barret, B., Boynard, A., Burrows, J. P., Clerbaux, C., Coheur, P.-F., Cuesta, J., Cuevas, E., Doniki, S., Dufour, G., Ebojic, F., Foret, G., Garcia, O., Granados-Muñoz, M. J., Hannigan, J. W., Hase, F., Hassler, B., Huang, G., Hurtmans, D., Jaffe, D., Jones, N., Kalabokas, P., Kerridge, B., Kulawik, S., Latter, B., Leblanc, T., Le Flochmoën, E., Lin, W., Liu, J., Liu, X., Mahieu, E., McClure-Begley, A., Neu, J. L., Osman, M., Palm, M., Petetin, H., Petropavlovskikh, I., Querel, R., Rappoe, N., Rozanov, A., Schultz, M. G., Schwab, J., Siddans, R., Smale, D., Steinbacher, M., Tanimoto, H., Tarasick, D. W., Thouret, V., Thompson, A. M., Trickl, T., Weatherhead, E., Wespes, C., Worden, H. M., Vigouroux, C., Xu, X., Zeng, G., and Ziemke, J.: Tropospheric Ozone Assessment Report: Present-day distribution and trends of tropospheric ozone relevant to climate and global atmospheric chemistry model evaluation, *Elem. Sci. Anthr.*, 6, 39, <https://doi.org/10.1525/elementa.291>, 2018.
- GEM-MACH development team: GEM-MACHv3.1.1.2, Zenodo [code], <https://doi.org/10.5281/zenodo.13952893>, 2022.
- Gilliam, R. C., Hogrefe, C., Godowitch, J. M., Napelenok, S., Mathur, R., and Rao, S. T.: Impact of inherent meteorology uncertainty on air quality model predictions, *J. Geophys. Res. Atmospheres*, 120, <https://doi.org/10.1002/2015JD023674>, 2015.
- Gilliam, R. C., Herwehe, J. A., Bullock, O. R., Pleim, J. E., Ran, L., Campbell, P. C., and Foroutan, H.: Establishing the suitability of the Model for Prediction Across Scales for global retrospective air quality modeling, *J. Geophys. Res. Atmospheres*, 126, e2020JD033588, <https://doi.org/10.1029/2020JD033588>, 2021.
- Gilliland, A. B., Hogrefe, C., Pinder, R. W., Godowitch, J. M., Foley, K. L., and Rao, S. T.: Dynamic evaluation of regional air quality models: Assessing changes in O₃ stemming from changes in emissions and meteorology, *Atmos. Environ.*, 42, 5110–5123, <https://doi.org/10.1016/j.atmosenv.2008.02.018>, 2008.
- Godowitch, J. M., Pouliot, G. A., and Trivikrama Rao, S.: Assessing multi-year changes in modeled and observed urban NO_x concentrations from a dynamic model evaluation perspective, *Atmos. Environ.*, 44, 2894–2901, <https://doi.org/10.1016/j.atmosenv.2010.04.040>, 2010.
- Godowitch, J. M., Gilliam, R. C., and Rao, S. T.: Diagnostic evaluation of ozone production and horizontal transport in a regional photochemical air quality modeling system, *Atmos. Environ.*, 45, 3977–3987, <https://doi.org/10.1016/j.atmosenv.2011.04.062>, 2011.
- Hand, J. L., Schichtel, B. A., Pitchford, M., Malm, W. C., and Frank, N. H.: Seasonal composition of remote and urban fine particulate matter in the United States, *J. Geophys. Res. Atmospheres*, 117, 22 pp., <https://doi.org/10.1029/2011JD017122>, 2012.
- Hand, J. L., Schichtel, B. A., Malm, W. C., and Frank, N. H.: Spatial and temporal trends in PM_{2.5} organic and elemental carbon across the United States, *Adv. Meteorol.*, 2013, 1–13, <https://doi.org/10.1155/2013/367674>, 2013.
- Hand, J. L., Prenni, A. J., Schichtel, B. A., Malm, W. C., and Chow, J. C.: Trends in remote PM_{2.5} residual mass across the United States: Implications for aerosol mass reconstruction in the IMPROVE network, *Atmos. Environ.*, 203, 141–152, <https://doi.org/10.1016/j.atmosenv.2019.01.049>, 2019.
- Hand, J. L., Prenni, A. J., and Schichtel, B. A.: Trends in seasonal mean speciated aerosol composition in remote areas of the United States from 2000 through 2021, *J. Geophys. Res. Atmospheres*, 129, e2023JD039902, <https://doi.org/10.1029/2023JD039902>, 2024.
- Hanna, S. R., Russell, A. G., Wilkinson, J. G., Vukovich, J., and Hansen, D. A.: Monte Carlo estimation of uncertainties in BEIS3 emission outputs and their effects on uncertainties in chemical transport model predictions, *J. Geophys. Res.*, 110, D01302, 15 pp., <https://doi.org/10.1029/2004JD004986>, 2005.
- Hoesly, R. M., Smith, S. J., Feng, L., Klimont, Z., Janssens-Maenhout, G., Pitkanen, T., Seibert, J. J., Vu, L., Andres, R. J., Bolt, R. M., Bond, T. C., Dawidowski, L., Kholod, N., Kurokawa, J., Li, M., Liu, L., Lu, Z., Moura, M. C. P., O'Rourke, P. R., and

- Zhang, Q.: Historical (1750–2014) anthropogenic emissions of reactive gases and aerosols from the Community Emissions Data System (CEDS), *Geosci. Model Dev.*, 11, 369–408, <https://doi.org/10.5194/gmd-11-369-2018>, 2018.
- Hogrefe, C., Rao, S. T., Kasibhatla, P., Hao, W., Sistla, G., Mathur, R., and McHenry, J.: Evaluating the performance of regional-scale photochemical modeling systems: Part II—ozone predictions, *Atmos. Environ.*, 35, 4175–4188, [https://doi.org/10.1016/S1352-2310\(01\)00183-2](https://doi.org/10.1016/S1352-2310(01)00183-2), 2001a.
- Hogrefe, C., Rao, S. T., Kasibhatla, P., Kallos, G., Tremback, C. J., Hao, W., Olerud, D., Xiu, A., McHenry, J., and Alapaty, K.: Evaluating the performance of regional-scale photochemical modeling systems: Part I—meteorological predictions, *Atmos. Environ.*, 35, 4159–4174, [https://doi.org/10.1016/S1352-2310\(01\)00182-0](https://doi.org/10.1016/S1352-2310(01)00182-0), 2001b.
- Hogrefe, C., Pouliot, G., Wong, D., Torian, A., Roselle, S., Pleim, J., and Mathur, R.: Annual application and evaluation of the online coupled WRF–CMAQ system over North America under AQMEII phase 2, *Atmos. Environ.*, 115, 683–694, <https://doi.org/10.1016/j.atmosenv.2014.12.034>, 2015.
- Hogrefe, C., Galmarini, S., Makar, P. A., Kioutsioukis, I., Clifton, O. E., Alyuz, U., Bash, J. O., Bellasio, R., Bianconi, R., Butler, T., Cheung, P., Hodzic, A., Kranenburg, R., Lupascu, A., Momoh, K., Perez-Camanyo, J. L., Pleim, J. E., Ryu, Y.-H., San Jose, R., Schaap, M., Schwede, D. B., and Sokhi, R.: A diagnostic intercomparison of modeled ozone dry deposition over North America and Europe using AQMEII4 regional-scale simulations, *Atmospheric Chem. Phys.*, 25, 12629–12656, <https://doi.org/10.5194/acp-25-12629-2025>, 2025.
- Holden, A. S., Sullivan, A. P., Munchak, L. A., Kreidenweis, S. M., Schichtel, B. A., Malm, W. C., and Collett, J. L.: Determining contributions of biomass burning and other sources to fine particle contemporary carbon in the western United States, *Atmos. Environ.*, 45, 1986–1993, <https://doi.org/10.1016/j.atmosenv.2011.01.021>, 2011.
- Houyoux, M. R., Vukovich, J. M., Coats, C. J., Wheeler, N. J. M., and Kasibhatla, P. S.: Emission inventory development and processing for the Seasonal Model for Regional Air Quality (SMRAQ) project, *J. Geophys. Res. Atmospheres*, 105, 9079–9090, <https://doi.org/10.1029/1999JD900975>, 2000.
- Huang, J., McQueen, J., Wilczak, J., Djalalova, I., Stajner, I., Shafran, P., Allured, D., Lee, P., Pan, L., Tong, D., Huang, H.-C., DiMego, G., Upadhyay, S., and Delle Monache, L.: Improving NOAA NAQFC PM_{2.5} predictions with a bias correction approach, *Weather Forecast.*, 32, 407–421, <https://doi.org/10.1175/WAF-D-16-0118.1>, 2017.
- Huang, L., Zhu, Y., Zhai, H., Xue, S., Zhu, T., Shao, Y., Liu, Z., Emery, C., Yarwood, G., Wang, Y., Fu, J., Zhang, K., and Li, L.: Recommendations on benchmarks for numerical air quality model applications in China – Part I: PM_{2.5} and chemical species, *Atmospheric Chem. Phys.*, 21, 2725–2743, <https://doi.org/10.5194/acp-21-2725-2021>, 2021.
- Hystad, P., Setton, E., Cervantes, A., Poplawski, K., Deschenes, S., Brauer, M., Van Donkelaar, A., Lamsal, L., Martin, R., Jerrett, M., and Demers, P.: Creating national air pollution models for population exposure assessment in Canada, *Environ. Health Perspect.*, 119, 1123–1129, <https://doi.org/10.1289/ehp.1002976>, 2011.
- Im, U., Bianconi, R., Solazzo, E., Kioutsioukis, I., Badia, A., Balzarini, A., Baró, R., Bellasio, R., Brunner, D., Chemel, C., Curci, G., Flemming, J., Forkel, R., Giordano, L., Jiménez-Guerrero, P., Hirtl, M., Hodzic, A., Honzak, L., Jorba, O., Knote, C., Kuenen, J. J. P., Makar, P. A., Manders-Groot, A., Neal, L., Pérez, J. L., Pirovano, G., Pouliot, G., San Jose, R., Savage, N., Schroder, W., Sokhi, R. S., Syrakov, D., Torian, A., Tuccella, P., Werhahn, J., Wolke, R., Yahya, K., Zabkar, R., Zhang, Y., Zhang, J., Hogrefe, C., and Galmarini, S.: Evaluation of operational on-line-coupled regional air quality models over Europe and North America in the context of AQMEII phase 2. Part I: Ozone, *Atmos. Environ.*, 115, 404–420, <https://doi.org/10.1016/j.atmosenv.2014.09.042>, 2015a.
- Im, U., Bianconi, R., Solazzo, E., Kioutsioukis, I., Badia, A., Balzarini, A., Baró, R., Bellasio, R., Brunner, D., Chemel, C., Curci, G., Denier Van Der Gon, H., Flemming, J., Forkel, R., Giordano, L., Jiménez-Guerrero, P., Hirtl, M., Hodzic, A., Honzak, L., Jorba, O., Knote, C., Makar, P. A., Manders-Groot, A., Neal, L., Pérez, J. L., Pirovano, G., Pouliot, G., San Jose, R., Savage, N., Schroder, W., Sokhi, R. S., Syrakov, D., Torian, A., Tuccella, P., Wang, K., Werhahn, J., Wolke, R., Zabkar, R., Zhang, Y., Zhang, J., Hogrefe, C., and Galmarini, S.: Evaluation of operational online-coupled regional air quality models over Europe and North America in the context of AQMEII phase 2. Part II: Particulate matter, *Atmos. Environ.*, 115, 421–441, <https://doi.org/10.1016/j.atmosenv.2014.08.072>, 2015b.
- Jaffe, D., Bertschi, I., Jaegle, L., Novelli, P., Reid, J. S., Tanimoto, H., Vingarzan, R., and Westphal, D. L.: Long-range transport of Siberian biomass burning emissions and impact on surface ozone in western North America, *Geophys. Res. Lett.*, 31, L16106, 4 pp., <https://doi.org/10.1029/2004GL020093>, 2004.
- Jain, P., Sharma, A. R., Acuna, D. C., Abatzoglou, J. T., and Flannigan, M.: Record-breaking fire weather in North America in 2021 was initiated by the Pacific northwest heat dome, *Commun. Earth Environ.*, 5, 202, <https://doi.org/10.1038/s43247-024-01346-2>, 2024.

- Jerrett, M., Arain, A., Kanaroglou, P., Beckerman, B., Potoglou, D., Sahsuvaroglu, T., Morrison, J., and Giovis, C.: A review and evaluation of intraurban air pollution exposure models, *J. Expo. Sci. Environ. Epidemiol.*, 15, 185–204, <https://doi.org/10.1038/sj.jea.7500388>, 2005.
- 2455 [Kajino, M., Deushi, M., Sekiyama, T. T., Oshima, N., Yumimoto, K., Tanaka, T. Y., Ching, J., Hashimoto, A., Yamamoto, T., Ikegami, M., Kamada, A., Miyashita, M., Inomata, Y., Shima, S., Adachi, K., Zaizen, Y., Igarashi, Y., Ueda, H., Maki, T., and Mikami, M.: NHM-Chem, the Japan Meteorological Agency's regional meteorology – chemistry model \(v1.0\): model description and aerosol representations, <https://doi.org/10.5194/gmd-2018-128>, 21 June 2018.](#)
- 2460 Kelly, J. T., Koplitz, S. N., Baker, K. R., Holder, A. L., Pye, H. O. T., Murphy, B. N., Bash, J. O., Henderson, B. H., Possiel, N. C., Simon, H., Eyth, A. M., Jang, C., Phillips, S., and Timin, B.: Assessing PM_{2.5} model performance for the conterminous U.S. with comparison to model performance statistics from 2007–2015, *Atmos. Environ.*, 214, 116872, <https://doi.org/10.1016/j.atmosenv.2019.116872>, 2019.
- 2465 [Kioutsioukis, I., Hogrefe, C., Makar, P. A., Alyuz, U., Bash, J. O., Bellasio, R., Bianconi, R., Butler, T., Clifton, O. E., Cheung, P., Hodzic, A., Kranenburg, R., Lupascu, A., Momoh, K., Perez-Camaño, J. L., Pleim, J., Ryu, Y.-H., San Jose, R., Schwede, D., Sokhi, R., and Galmarini, S.: Operational, diagnostic, and probabilistic evaluation of AQMEII-4 regional-scale ozone dry deposition: time to harmonize our LULC masks, *Atmospheric Chem. Phys.*, 25, 12923–12953, <https://doi.org/10.5194/acp-25-12923-2025>, 2025.](#)
- 2470 Knote, C., Tuccella, P., Curci, G., Emmons, L., Orlando, J. J., Madronich, S., Baró, R., Jiménez-Guerrero, P., Luecken, D., Hogrefe, C., Forkel, R., Werhahn, J., Hirtl, M., Pérez, J. L., San José, R., Giordano, L., Brunner, D., Yahya, K., and Zhang, Y.: Influence of the choice of gas-phase mechanism on predictions of key gaseous pollutants during the AQMEII phase-2 intercomparison, *Atmos. Environ.*, 115, 553–568, <https://doi.org/10.1016/j.atmosenv.2014.11.066>, 2015.
- Koo, B., Kumar, N., Knipping, E., Nopmongcol, U., Sakulyanontvittaya, T., Odman, M. T., Russell, A. G., and Yarwood, G.: Chemical transport model consistency in simulating regulatory outcomes and the relationship to model performance, *Atmos. Environ.*, 116, 159–171, <https://doi.org/10.1016/j.atmosenv.2015.06.036>, 2015.
- 2475 Kukkonen, J., Olsson, T., Schultz, D. M., Baklanov, A., Klein, T., Miranda, A. I., Monteiro, A., Hirtl, M., Tarvainen, V., Boy, M., Peuch, V.-H., Poupkou, A., Kioutsioukis, I., Finardi, S., Sofiev, M., Sokhi, R., Lehtinen, K. E. J., Karatzas, K., San José, R., Astitha, M., Kallos, G., Schaap, M., Reimer, E., Jakobs, H., and Eben, K.: A review of operational, regional-scale, chemical weather forecasting models in Europe, *Atmospheric Chem. Phys.*, 12, 1–87, <https://doi.org/10.5194/acp-12-1-2012>, 2012.
- 2480 Lamsal, L. N., Duncan, B. N., Yoshida, Y., Krotkov, N. A., Pickering, K. E., Streets, D. G., and Lu, Z.: U.S. NO₂ trends (2005–2013): EPA Air Quality System (AQS) data versus improved observations from the Ozone Monitoring Instrument (OMI), *Atmos. Environ.*, 110, 130–143, <https://doi.org/10.1016/j.atmosenv.2015.03.055>, 2015.
- Lavery, T. F., Rogers, C. M., Baumgardner, R., and Mishoe, K. P.: Intercomparison of Clean Air Status and Trends Network nitrate and nitric acid measurements with data from other monitoring programs, *J. Air Waste Manag. Assoc.*, 59, 214–226, <https://doi.org/10.3155/1047-3289.59.2.214>, 2009.
- 2485 Lee, H. J., Chatfield, R. B., and Bell, M. L.: Spatial analysis of concentrations of multiple air pollutants using NASA DISCOVER-AQ aircraft measurements: Implications for exposure assessment, *Environ. Res.*, 160, 487–498, <https://doi.org/10.1016/j.envres.2017.10.017>, 2018.
- 2490 Lee, P., McQueen, J., Stajner, I., Huang, J., Pan, L., Tong, D., Kim, H., Tang, Y., Kondragunta, S., Ruminski, M., Lu, S., Rogers, E., Saylor, R., Shafran, P., Huang, H.-C., Gorline, J., Upadhayay, S., and Artz, R.: NAQFC developmental forecast guidance for fine particulate matter (PM_{2.5}), *Weather Forecast.*, 32, 343–360, <https://doi.org/10.1175/WAF-D-15-0163.1>, 2017.
- Li, Q., Borge, R., Sarwar, G., de la Paz, D., Gantt, B., Domingo, J., Cuevas, C. A., and Saiz-Lopez, A.: Impact of halogen chemistry on summertime air quality in coastal and continental Europe: application of the CMAQ model and implications for regulation, *Atmospheric Chem. Phys.*, 19, 15321–15337, <https://doi.org/10.5194/acp-19-15321-2019>, 2019.
- 2495 Li, W., Tang, B., Campbell, P. C., Tang, Y., Baker, B., Moon, Z., Tong, D., Huang, J., Wang, K., Stajner, I., and Montuoro, R.: Updates and evaluation of NOAA's online-coupled air quality model version 7 (AQMV7) within the Unified Forecast System, *Geosci. Model Dev.*, 18, 1635–1660, <https://doi.org/10.5194/gmd-18-1635-2025>, 2025.
- Liu, J. C., Pereira, G., Uhl, S. A., Bravo, M. A., and Bell, M. L.: A systematic review of the physical health impacts from non-occupational exposure to wildfire smoke, *Environ. Res.*, 136, 120–132, <https://doi.org/10.1016/j.envres.2014.10.015>, 2015.
- 2500 Liudchik, A., Pakatashkin, V., Umreika, S., and Girgzdieni, R.: Role of ozone deposition in the occurrence of the spring maximum, *Atmosphere-Ocean*, 53, 42–49, <https://doi.org/10.1080/07055900.2013.853284>, 2015.
- Lupu, A. and Moran, M. D.: Operational GEM-MACH model evaluation against air quality surface observation networks across Canada and the United States for 2013–16 and 2021/22, Zenodo [dataset], <https://doi.org/10.5281/zenodo.16944371>, 2025.

Formatted: Subscript

- 2505 Ma, S., Tong, D., Lamsal, L., Wang, J., Zhang, X., Tang, Y., Saylor, R., Chai, T., Lee, P., Campbell, P., Baker, B., Kondragunta, S., Judd, L., Berkoff, T. A., Janz, S. J., and Stajner, I.: Improving predictability of high-ozone episodes through dynamic boundary conditions, emission refresh and chemical data assimilation during the Long Island Sound Tropospheric Ozone Study (LISTOS) field campaign, *Atmospheric Chem. Phys.*, 21, 16531–16553, <https://doi.org/10.5194/acp-21-16531-2021>, 2021.
- Makar, P. A., Nissen, R., Teakles, A., Zhang, J., Zheng, Q., Moran, M. D., Yau, H., and diCenzo, C.: Turbulent transport, emissions and the role of compensating errors in chemical transport models, *Geosci. Model Dev.*, 7, 1001–1024, <https://doi.org/10.5194/gmd-7-1001-2014>, 2014.
- 2510 Makar, P. A., Akingunola, A., Aherne, J., Cole, A. S., Aklilu, Y., Zhang, J., Wong, I., Hayden, K., Li, S.-M., Kirk, J., Scott, K., Moran, M. D., Robichaud, A., Cathcart, H., Baratzedah, P., Pabla, B., Cheung, P., Zheng, Q., and Jeffries, D. S.: Estimates of exceedances of critical loads for acidifying deposition in Alberta and Saskatchewan, *Atmospheric Chem. Phys.*, 18, 9897–9927, <https://doi.org/10.5194/acp-18-9897-2018>, 2018.
- Makar, P. A., Stroud, C., Akingunola, A., Zhang, J., Ren, S., Cheung, P., and Zheng, Q.: Vehicle-induced turbulence and atmospheric pollution, *Atmospheric Chem. Phys.*, 21, 12291–12316, <https://doi.org/10.5194/acp-21-12291-2021>, 2021.
- [Mallet, V. and Sportisse, B.: Ensemble-based air quality forecasts: A multimodel approach applied to ozone, *J. Geophys. Res. Atmospheres*, 111, 2005JD006675, <https://doi.org/10.1029/2005JD006675>, 2006.](https://doi.org/10.1029/2005JD006675)
- 2520 Malm, W. C., Schichtel, B. A., Pitchford, M. L., Ashbaugh, L. L., and Eldred, R. A.: Spatial and monthly trends in speciated fine particle concentration in the United States, *J. Geophys. Res. Atmospheres*, 109, D03306, 22 pp., <https://doi.org/10.1029/2003JD003739>, 2004.
- Malm, W. C., Schichtel, B. A., and Pitchford, M. L.: Uncertainties in PM_{2.5} gravimetric and speciation measurements and what we can learn from them, *J. Air Waste Manag. Assoc.*, 61, 1131–1149, <https://doi.org/10.1080/10473289.2011.603998>, 2011.
- Manseau, P. M., Peng, S. J., Stroud, C., Savic-Jovicic, V., and Lupu, A.: AQ Multi Model Verification for North America: 2022/04 - 2022/06, Environment and Climate Change Canada, July, 11 pp., https://hpfx.collab.science.gc.ca/~svfs000/na-aq-mm-fe/reports/2022/na-aq-mm-fe_reports_2022_Q2.pdf (last access: 6 April 2026), 2022.
- 2525 Mao, Y. H., Li, Q. B., Zhang, L., Chen, Y., Randerson, J. T., Chen, D., and Liou, K. N.: Biomass burning contribution to black carbon in the western United States mountain ranges, *Atmospheric Chem. Phys.*, 11, 11253–11266, <https://doi.org/10.5194/acp-11-11253-2011>, 2011.
- 2530 Marécal, V., Peuch, V.-H., Andersson, C., Andersson, S., Arteta, J., Beekmann, M., Benedictow, A., Bergström, R., Bessagnet, B., Cansado, A., Chéroux, F., Colette, A., Coman, A., Curier, R. L., Denier Van Der Gon, H. A. C., Drouin, A., Elbern, H., Emili, E., Engelen, R. J., Eskes, H. J., Foret, G., Friese, E., Gauss, M., Giannaros, C., Guth, J., Joly, M., Jaumouillé, E., Josse, B., Kadyrov, N., Kaiser, J. W., Krajsek, K., Kuenen, J., Kumar, U., Liora, N., Lopez, E., Malherbe, L., Martinez, I., Melas, D., Meleux, F., Menut, L., Moinat, P., Morales, T., Parmentier, J., Piacentini, A., Plu, M., Poupkou, A., Queguiner, S., Robertson, L., Rouil, L., Schaap, M., Segers, A., Sofiev, M., Tarasson, L., Thomas, M., Timmermans, R., Valdebenito, Á., Van Velthoven, P., Van Versendaal, R., Vira, J., and Ung, A.: A regional air quality forecasting system over Europe: the MACC-II daily ensemble production, *Geosci. Model Dev.*, 8, 2777–2813, <https://doi.org/10.5194/gmd-8-2777-2015>, 2015.
- 2535 Mashayekhi, R., Pavlovic, R., Racine, J., Moran, M. D., Manseau, P. M., Duhamel, A., Katal, A., Miville, J., Niemi, D., Peng, S. J., Sassi, M., Griffin, D., and McLinden, C. A.: Isolating the impact of COVID-19 lockdown measures on urban air quality in Canada, *Air Qual. Atmosphere Health*, 14, 1549–1570, <https://doi.org/10.1007/s11869-021-01039-1>, 2021.
- 2540 Mathur, R., Yu, S., Kang, D., and Schere, K. L.: Assessment of the wintertime performance of developmental particulate matter forecasts with the Eta-Community Multiscale Air Quality modeling system, *J. Geophys. Res. Atmospheres*, 113, 2007JD008580, <https://doi.org/10.1029/2007JD008580>, 2008.
- 2545 Matthias, V., Arndt, J. A., Aulinger, A., Bieser, J., Denier Van Der Gon, H., Kranenburg, R., Kuenen, J., Neumann, D., Pouliot, G., and Quante, M.: Modeling emissions for three-dimensional atmospheric chemistry transport models, *J. Air Waste Manag. Assoc.*, 68, 763–800, <https://doi.org/10.1080/10962247.2018.1424057>, 2018.
- McKeen, S., Wilczak, J., Grell, G., Djalalova, I., Peckham, S., Hsie, E. -Y., Gong, W., Bouchet, V., Menard, S., Moffet, R., McHenry, J., McQueen, J., Tang, Y., Carmichael, G. R., Pagowski, M., Chan, A., Dye, T., Frost, G., Lee, P., and Mathur, R.: Assessment of an ensemble of seven real-time ozone forecasts over eastern North America during the summer of 2004, *J. Geophys. Res. Atmospheres*, 110, 2005JD005858, <https://doi.org/10.1029/2005JD005858>, 2005.
- 2550 McKeen, S., Chung, S. H., Wilczak, J., Grell, G., Djalalova, I., Peckham, S., Gong, W., Bouchet, V., Moffet, R., Tang, Y., Carmichael, G. R., Mathur, R., and Yu, S.: Evaluation of several PM_{2.5} forecast models using data collected during the ICARTT/NEAQS 2004 field study, *J. Geophys. Res. Atmospheres*, 112, 2006JD007608, <https://doi.org/10.1029/2006JD007608>, 2007.

- 2555 McKeen, S., Grell, G., Peckham, S., Wilczak, J., Djalalova, I., Hsie, E. -Y., Frost, G., Peischl, J., Schwarz, J., Spackman, R., Holloway, J., De Gouw, J., Warneke, C., Gong, W., Bouchet, V., Gaudreault, S., Racine, J., McHenry, J., McQueen, J., Lee, P., Tang, Y., Carmichael, G. R., and Mathur, R.: An evaluation of real-time air quality forecasts and their urban emissions over eastern Texas during the summer of 2006 Second Texas Air Quality Study field study, *J. Geophys. Res. Atmospheres*, 114, 2008JD011697, <https://doi.org/10.1029/2008JD011697>, 2009.
- 2560 McNair, L. A., Harley, R. A., and Russell, A. G.: Spatial inhomogeneity in pollutant concentrations, and their implications for air quality model evaluation, *Atmos. Environ.*, 30, 4291–4301, [https://doi.org/10.1016/1352-2310\(96\)00098-2](https://doi.org/10.1016/1352-2310(96)00098-2), 1996.
- McNider, R. T. and Pour-Biazar, A.: Meteorological modeling relevant to mesoscale and regional air quality applications: a review, *J. Air Waste Manag. Assoc.*, 70, 2–43, <https://doi.org/10.1080/10962247.2019.1694602>, 2020.
- 2565 McTaggart-Cowan, R., Vaillancourt, P. A., Zadra, A., Chamberland, S., Charron, M., Corvec, S., Milbrandt, J. A., Paquin-Ricard, D., Patoine, A., Roch, M., Separovic, L., and Yang, J.: Modernization of atmospheric physics parameterization in Canadian NWP, *J. Adv. Model. Earth Syst.*, 11, 3593–3635, <https://doi.org/10.1029/2019MS001781>, 2019.
- Meng, Z., Dabdub, D., and Seinfeld, J. H.: Chemical coupling between atmospheric ozone and particulate matter, *Science*, 277, 116–119, <https://doi.org/10.1126/science.277.5322.116>, 1997.
- 2570 Miller, S. J., Makar, P. A., and Lee, C. J.: HETerogeneous vectorized or Parallel (HETPv1.0): an updated inorganic heterogeneous chemistry solver for the metastable-state $\text{NH}_4^+ - \text{Na}^+ - \text{Ca}^{2+} - \text{K}^+ - \text{Mg}^{2+} - \text{SO}_4^{2-} - \text{NO}_3^- - \text{Cl}^- - \text{H}_2\text{O}$ system based on ISORROPIA II, *Geosci. Model Dev.*, 17, 2197–2219, <https://doi.org/10.5194/gmd-17-2197-2024>, 2024.
- Momeni, M., Kashfi Yeganeh, A., Zanganeh Kia, H., Ghahremanloo, M., Mousavinezhad, S., De Guzman, H. J., Shephard, M. W., Jacobson, M. Z., and Choi, Y.: Using multi-satellite observations to constrain ammonia emissions and unlock their potential over open water, *Sci. Rep.*, 15, <https://doi.org/10.1038/s41598-025-09933-9>, 2025.
- 2575 Monks, P. S.: A review of the observations and origins of the spring ozone maximum, *Atmos. Environ.*, 34, 3545–3561, [https://doi.org/10.1016/S1352-2310\(00\)00129-1](https://doi.org/10.1016/S1352-2310(00)00129-1), 2000.
- [Moran, M.D. and Lupu, A.: Supplementary material for paper "Operational chemical weather forecasting with the ECCC online Regional Air Quality Deterministic Prediction System version 023 \(RAQDPS023\) - Part 2: Multi-year prospective and retrospective performance evaluation" by Moran et al. \(2026\). Zenodo \[journal article\]. https://doi.org/10.5281/zenodo.19489036.2026.](#)
- 2580 Moran, M. D. and Savic-Jovcic, V.: RAQDPS023 Predicted 2013-2016 and 2021/22 Seasonal and Annual Dry, Wet, and Total Acidic Deposition Fields and Related Concentration Fields for North America, Zenodo [dataset], <https://doi.org/10.5281/zenodo.16970403>, 2026.
- 2585 Moran, M., Zhang, J., Pavlovic, R., Savic-Jovcic, V., Ménard, S., Landry, H., Zheng, Q., Lupu, A., Gilbert, S., Peng, S. J., and Manseau, P. M.: Evolution of the performance of the Canadian operational Regional Air Quality Deterministic Prediction System from 2010 to 2019, in: *Air Pollution Modeling and its Application XXVII*, edited by: Mensink, C. and Matthias, V., Springer Berlin Heidelberg, Berlin, Heidelberg, 157–166, https://doi.org/10.1007/978-3-662-63760-9_24, 2021a.
- 2590 Moran, M. D., Ménard, S., and Kormic, D.: Regional Air Quality Deterministic Prediction System (RAQDPS): Upgrade from version 022 to version 023, Technical note, December, Canadian Centre for Meteorological and Environmental Prediction, Montreal, 48 pp., https://collaboration.cmc.ec.gc.ca/cmc/cmoin/product_guide/docs/lib/technote_raqdps023_20211130_e.pdf (last access: 6 April 2026), 2021b.
- 2595 Moran, M. D., Savic-Jovcic, V., Stroud, C. A., Ménard, S., Gong, W., Zhang, J., Zheng, Q., Chen, J., Akingunola, A., Lupu, A., Menelaou, K., and Munoz-Alpizar, R.: Operational chemical weather forecasting with the ECCC online Regional Air Quality Deterministic Prediction System version 023 (RAQDPS023) - Part 1: System description, *Geosci. Model Dev.* (under review/accepted), <https://doi.org/10.5194/egusphere-2025-4323> [the link will be implemented upon publication], 2026.
- 2595 Nappo, C. J., Caneill, J. Y., Furman, R. W., Gifford, F. W., Kaimal, J. C., Kramer, M. L., Lockhart, T. J., Pendergast, M. M., Pielke, R. A., Randerson, D., Shreffler, J. H., and Wyngaard, J. C.: The workshop on the representativeness of meteorological observations, June 1981, Boulder, Colo., *Bull. Amer. Meteor. Soc.*, 63, 761–764, 1982.
- 2600 National Atmospheric Deposition Program: National Atmospheric Deposition Program 2013 Annual Summary, Illinois State Water Survey, University of Illinois at Urbana-Champaign, Illinois, 28 pp., <https://nadp.slh.wisc.edu/wp-content/uploads/2021/05/2013as.pdf> (last access: 6 April 2026), 2014.
- National Atmospheric Deposition Program: National Atmospheric Deposition Program 2016 Annual Summary, Illinois State Water Survey, University of Illinois at Urbana-Champaign, Illinois, 28 pp., <https://nadp.slh.wisc.edu/wp-content/uploads/2021/05/2016as.pdf> (last access: 6 April 2026), 2017.
- 2605 Nguyen, T. K. V., Zhang, Q., Jimenez, J. L., Pike, M., and Carlton, A. G.: Liquid water: ubiquitous contributor to aerosol mass, *Environ. Sci. Technol. Lett.*, 3, 257–263, <https://doi.org/10.1021/acs.estlett.6b00167>, 2016.

- NOAA National Centers for Environmental Information: Monthly Wildfires Report for Annual 2022, WWW Document, <https://www.ncei.noaa.gov/access/monitoring/monthly-report/fire/202213> (last access: 6 April 2026), 2023.
- 2610 Noble, C. A., Vanderpool, R. W., Peters, T. M., McElroy, F. F., Gemmill, D. B., and Wiener, R. W.: Federal reference and equivalent methods for measuring fine particulate matter, *Aerosol Sci. Technol.*, 34, 457–464, <https://doi.org/10.1080/02786820121582>, 2001.
- Pagowski, M., Grell, G. A., McKeen, S. A., Peckham, S. E., and Devenyi, D.: Three-dimensional variational data assimilation of ozone and fine particulate matter observations: some results using the Weather Research and Forecasting—Chemistry model and Grid-Point Statistical Interpolation, *Q. J. R. Meteorol. Soc.*, 136, 2013–2024, <https://doi.org/10.1002/qj.700>, 2010.
- 2615 Pan, L., Tong, D., Lee, P., Kim, H.-C., and Chai, T.: Assessment of NO_x and O₃ forecasting performances in the U.S. National Air Quality Forecasting Capability before and after the 2012 major emissions updates, *Atmos. Environ.*, 95, 610–619, <https://doi.org/10.1016/j.atmosenv.2014.06.020>, 2014.
- Park, S. H., Gong, S. L., Gong, W., Makar, P. A., Moran, M. D., Zhang, J., and Stroud, C. A.: Relative impact of windblown dust versus anthropogenic fugitive dust in PM_{2.5} on air quality in North America, *J. Geophys. Res. Atmospheres*, 115, 2009JD013144, <https://doi.org/10.1029/2009JD013144>, 2010.
- 2620 Parrish, D. D. and Fehsenfeld, F. C.: Methods for gas-phase measurements of ozone, ozone precursors and aerosol precursors, *Atmos. Environ.*, 34, 1921–1957, [https://doi.org/10.1016/S1352-2310\(99\)00454-9](https://doi.org/10.1016/S1352-2310(99)00454-9), 2000.
- Pavlovic, R., Chen, J., Anderson, K., Moran, M. D., Beaulieu, P.-A., Davignon, D., and Cousineau, S.: The FireWork air quality forecast system with near-real-time biomass burning emissions: Recent developments and evaluation of performance for the 2015 North American wildfire season, *J. Air Waste Manag. Assoc.*, 66, 819–841, <https://doi.org/10.1080/10962247.2016.1158214>, 2016.
- 2625 Pendlebury, D., Gravel, S., Moran, M. D., and Lupu, A.: Impact of chemical lateral boundary conditions in a regional air quality forecast model on surface ozone predictions during stratospheric intrusions, *Atmos. Environ.*, 174, 148–170, <https://doi.org/10.1016/j.atmosenv.2017.10.052>, 2018.
- 2630 Penkett, S. A. and Brice, K. A.: The spring maximum in photo-oxidants in the Northern Hemisphere troposphere, *Nature*, 319, 655–657, <https://doi.org/10.1038/319655a0>, 1986.
- Puchalski, M. A., Sather, M. E., Walker, J. T., Lehmann, C. M. B., Gay, D. A., Mathew, J., and Robarge, W. P.: Passive ammonia monitoring in the United States: Comparing three different sampling devices, *J. Environ. Monit.*, 13, 3156, <https://doi.org/10.1039/c1em10553a>, 2011.
- 2635 Pun, B. K., Seigneur, C., Bailey, E. M., Gautney, L. L., Douglas, S. G., Haney, J. L., and Kumar, N.: Response of atmospheric particulate matter to changes in precursor emissions: A comparison of three air quality models, *Environ. Sci. Technol.*, 42, 831–837, <https://doi.org/10.1021/es702333d>, 2008.
- Pye, H. O. T., Murphy, B. N., Xu, L., Ng, N. L., Carlton, A. G., Guo, H., Weber, R., Vasilakos, P., Appel, K. W., Budisulistiorini, S. H., Surratt, J. D., Nenes, A., Hu, W., Jimenez, J. L., Isaacman-VanWertz, G., Misztal, P. K., and Goldstein, A. H.: On the implications of aerosol liquid water and phase separation for organic aerosol mass, *Atmospheric Chem. Phys.*, 17, 343–369, <https://doi.org/10.5194/acp-17-343-2017>, 2017.
- 2640 Rappold, A. G., Reyes, J., Pouliot, G., Cascio, W. E., and Diaz-Sanchez, D.: Community vulnerability to health impacts of wildland fire smoke exposure, *Environ. Sci. Technol.*, 51, 6674–6682, <https://doi.org/10.1021/acs.est.6b06200>, 2017.
- 2645 Ren, S., Stroud, C., Belair, S., Leroyer, S., Munoz-Alpizar, R., Moran, M., Zhang, J., Akingunola, A., and Makar, P.: Impact of urbanization on the predictions of urban meteorology and air pollutants over four major North American cities, *Atmosphere*, 11, 969, <https://doi.org/10.3390/atmos11090969>, 2020.
- Robichaud, A. and Ménard, R.: Multi-year objective analyses of warm season ground-level ozone and PM_{2.5} over North America using real-time observations and Canadian operational air quality models, *Atmospheric Chem. Phys.*, 14, 1769–1800, <https://doi.org/10.5194/acp-14-1769-2014>, 2014.
- 2650 Robichaud, A., Ménard, R., Zaitseva, Y., and Anselmo, D.: Multi-pollutant surface objective analyses and mapping of air quality health index over North America, *Air Qual. Atmosphere Health*, 9, 743–759, <https://doi.org/10.1007/s11869-015-0385-9>, 2016.
- [Robichaud, A., Cole, A., Cheng, I., Cathcart, H., Feng, J., and Hou, A.: Data fusion of modelled and-measured deposition in the U.S. and Canada, Part I: description of methodology and validation of wet deposition of sulfur and nitrogen. *Atmos. Environ.*, 121074, <https://doi.org/10.1016/j.atmosenv.2025.121074>, 2025.](https://doi.org/10.1016/j.atmosenv.2025.121074)
- [Robichaud, A., Cole, A., Cheng, I., Cathcart, H., Feng, J., Hou, A., Griffin, D., and Shephard, M. W.: Data fusion of modelled and measured deposition in the US and Canada, part II: Dry deposition of sulfur, nitrogen and ozone. *Atmos. Environ.*, 364, 121656, <https://doi.org/10.1016/j.atmosenv.2025.121656>, 2026.](https://doi.org/10.1016/j.atmosenv.2025.121656)

- Sakaguchi, K., Zeng, X., and Brunke, M. A.: The hindcast skill of the CMIP ensembles for the surface air temperature trend, *J. Geophys. Res. Atmospheres*, 117, 2012JD017765, <https://doi.org/10.1029/2012JD017765>, 2012.
- 2660 Sarwar, G., Gantt, B., Schwede, D., Foley, K., Mathur, R., and Saiz-Lopez, A.: Impact of enhanced ozone deposition and halogen chemistry on tropospheric ozone over the Northern Hemisphere, *Environ. Sci. Technol.*, 49, 9203–9211, <https://doi.org/10.1021/acs.est.5b01657>, 2015.
- Savage, N. H., Agnew, P., Davis, L. S., Ordóñez, C., Thorpe, R., Johnson, C. E., O'Connor, F. M., and Dalvi, M.: Air quality modelling using the Met Office Unified Model (AQUM OS24-26): model description and initial evaluation, *Geosci. Model Dev.*, 6, 353–372, <https://doi.org/10.5194/gmd-6-353-2013>, 2013.
- 2665 Savic-Jovicic, V., Moran, M. D., and GEM-MACH Development Team: Global Environmental Multiscale model–Modelling Atmospheric CHemistry (GEM-MACH) version 3.1.0.0, Zenodo [software] [dataset], <https://doi.org/10.5281/zenodo.15330612>, 2025.
- Saylor, R. D. and Stein, A. F.: Identifying the causes of differences in ozone production from the CB05 and CBMIV chemical mechanisms, *Geosci. Model Dev.*, 5, 257–268, <https://doi.org/10.5194/gmd-5-257-2012>, 2012.
- 2670 Schichtel, B. A., Hand, J. L., Barna, M. G., Gebhart, K. A., Copeland, S., Vimont, J., and Malm, W. C.: Origin of fine particulate carbon in the rural United States, *Environ. Sci. Technol.*, 51, 9846–9855, <https://doi.org/10.1021/acs.est.7b00645>, 2017.
- Schutgens, N. A. J., Gryspeerdt, E., Weigum, N., Tsyro, S., Goto, D., Schulz, M., and Stier, P.: Will a perfect model agree with perfect observations? The impact of spatial sampling, *Atmospheric Chem. Phys.*, 16, 6335–6353, <https://doi.org/10.5194/acp-16-6335-2016>, 2016.
- 2675 Schwede, D., Zhang, L., Vet, R., and Lear, G.: An intercomparison of the deposition models used in the CASTNET and CAPMoN networks, *Atmos. Environ.*, 45, 1337–1346, <https://doi.org/10.1016/j.atmosenv.2010.11.050>, 2011.
- Seigneur, C. and Moran, M. D.: Chemical transport models, in: Particulate Matter Science for Policy Makers: A NARSTO Assessment, ISBN 0-521-84287-5, Cambridge University Press, Cambridge, 283–323, 2004.
- 2680 [Semeniuk, K., Dastoor, A., and Lupu, A.: Implementation of the MOSAIC aerosol module \(v1.0\) in the Canadian air quality model GEM-MACH \(v3.1\), *Geosci. Model Dev.*, 18, 6479–6515, <https://doi.org/10.5194/gmd-18-6479-2025>, 2025.](https://doi.org/10.5194/gmd-18-6479-2025)
- Sillman, S.: The relation between ozone, NO_x and hydrocarbons in urban and polluted rural environments, *Atmos. Environ.*, 33, 1821–1845, [https://doi.org/10.1016/S1352-2310\(98\)00345-8](https://doi.org/10.1016/S1352-2310(98)00345-8), 1999.
- Simon, H., Baker, K. R., and Phillips, S.: Compilation and interpretation of photochemical model performance statistics published between 2006 and 2012, *Atmos. Environ.*, 61, 124–139, <https://doi.org/10.1016/j.atmosenv.2012.07.012>, 2012.
- 2685 Sirois, A., Vet, R., and Lamb, D.: A comparison of the precipitation chemistry measurements obtained by the CAPMoN and NADP/NTN networks, *Environ. Monit. Assess.*, 62, 273–303, <https://doi.org/10.1023/A:1006272609744>, 2000.
- Smyth, S. C., Jiang, W., Roth, H., Moran, M. D., Makar, P. A., Yang, F., Bouchet, V. S., and Landry, H.: A comparative performance evaluation of the AURAMS and CMAQ air-quality modelling systems, *Atmos. Environ.*, 43, 1059–1070, <https://doi.org/10.1016/j.atmosenv.2008.11.027>, 2009.
- 2690 Solazzo, E., Bianconi, R., Vautard, R., Appel, K. W., Moran, M. D., Hogrefe, C., Bessagnet, B., Brandt, J., Christensen, J. H., Chemel, C., Coll, I., Denier Van Der Gon, H., Ferreira, J., Forkel, R., Francis, X. V., Grell, G., Grossi, P., Hansen, A. B., Jeričević, A., Kraljević, L., Miranda, A. I., Nopmongcol, U., Pirovano, G., Prank, M., Riccio, A., Sartelet, K. N., Schaap, M., Silver, J. D., Sokhi, R. S., Vira, J., Werhahn, J., Wolke, R., Yarwood, G., Zhang, J., Rao, S. T., and Galmarini, S.: Model evaluation and ensemble modelling of surface-level ozone in Europe and North America in the context of AQMEII, *Atmos. Environ.*, 53, 60–74, <https://doi.org/10.1016/j.atmosenv.2012.01.003>, 2012a.
- 2695 Solazzo, E., Bianconi, R., Pirovano, G., Matthias, V., Vautard, R., Moran, M. D., Wyatt Appel, K., Bessagnet, B., Brandt, J., Christensen, J. H., Chemel, C., Coll, I., Ferreira, J., Forkel, R., Francis, X. V., Grell, G., Grossi, P., Hansen, A. B., Miranda, A. I., Nopmongcol, U., Prank, M., Sartelet, K. N., Schaap, M., Silver, J. D., Sokhi, R. S., Vira, J., Werhahn, J., Wolke, R., Yarwood, G., Zhang, J., Rao, S. T., and Galmarini, S.: Operational model evaluation for particulate matter in Europe and North America in the context of AQMEII, *Atmos. Environ.*, 53, 75–92, <https://doi.org/10.1016/j.atmosenv.2012.02.045>, 2012b.
- 2700 [Solazzo, E., Bianconi, R., Pirovano, G., Moran, M. D., Vautard, R., Hogrefe, C., Appel, K. W., Matthias, V., Grossi, P., Bessagnet, B., Brandt, J., Chemel, C., Christensen, J. H., Forkel, R., Francis, X. V., Hansen, A. B., McKeen, S., Nopmongcol, U., Prank, M., Sartelet, K. N., Segers, A., Silver, J. D., Yarwood, G., Werhahn, J., Zhang, J., Rao, S. T., and Galmarini, S.: Evaluating the capability of regional-scale air quality models to capture the vertical distribution of pollutants, *Geosci. Model Dev.*, 6, 791–818, <https://doi.org/10.5194/gmd-6-791-2013>, 2013.](https://doi.org/10.5194/gmd-6-791-2013)
- 2705

- Solomon, P. A., Crumpler, D., Flanagan, J. B., Jayanty, R. K. M., Rickman, E. E., and McDade, C. E.: U.S. national PM_{2.5} chemical speciation monitoring networks—CSN and IMPROVE: Description of networks, *J. Air Waste Manag. Assoc.*, 64, 1410–1438, <https://doi.org/10.1080/10962247.2014.956904>, 2014.
- 2710 Spicer, C. W., Buxton, B. E., Holdren, M. W., Smith, D. L., Kelly, T. J., Rust, S. W., Pate, A. D., Sverdrup, G. M., and Chuang, J. C.: Variability of hazardous air pollutants in an urban area, *Atmos. Environ.*, 30, 3443–3456, [https://doi.org/10.1016/1352-2310\(95\)00200-6](https://doi.org/10.1016/1352-2310(95)00200-6), 1996.
- Stanski, H. R., Wilson, L. J., and Burrows, W. R.: Survey of Common Verification Methods in Meteorology, World Weather Watch Technical Report No. 8, World Meteorological Organization, Geneva, 81 pp., https://www.cawcr.gov.au/projects/verification/Stanski_et_al/Stanski_et_al.html (last access: 6 April 2026), 1989.
- 2715 Steyn, D. G. and Galmarini, S.: Evaluating the predictive and explanatory value of atmospheric numerical models: Between relativism and objectivism, *Open Atmospheric Sci. J.*, 2, 38–45, <https://doi.org/10.2174/1874282300802010038>, 2008.
- Stroud, C. A., Morneau, G., Makar, P. A., Moran, M. D., Gong, W., Pabla, B., Zhang, J., Bouchet, V. S., Fox, D., Venkatesh, S., Wang, D., and Dann, T.: OH-reactivity of volatile organic compounds at urban and rural sites across Canada: Evaluation of air quality model predictions using speciated VOC measurements, *Atmos. Environ.*, 42, 7746–7756, <https://doi.org/10.1016/j.atmosenv.2008.05.054>, 2008.
- 2720 Stroud, C. A., Makar, P. A., Moran, M. D., Gong, W., Gong, S., Zhang, J., Hayden, K., Mihele, C., Brook, J. R., Abbatt, J. P. D., and Slowik, J. G.: Impact of model grid spacing on regional- and urban- scale air quality predictions of organic aerosol, *Atmospheric Chem. Phys.*, 11, 3107–3118, <https://doi.org/10.5194/acp-11-3107-2011>, 2011.
- 2725 Su, Y., Sofowote, U., Debosz, J., White, L., and Munoz, A.: Multi-year continuous PM_{2.5} measurements with the Federal Equivalent Method SHARP 5030 and comparisons to filter-based and TEOM measurements in Ontario, Canada, *Atmosphere*, 9, 191, <https://doi.org/10.3390/atmos9050191>, 2018.
- Swall, J. L. and Foley, K. M.: The impact of spatial correlation and incommensurability on model evaluation, *Atmos. Environ.*, 43, 1204–1217, <https://doi.org/10.1016/j.atmosenv.2008.10.057>, 2009.
- 2730 Taylor, K. E.: Summarizing multiple aspects of model performance in a single diagram, *J. Geophys. Res. Atmospheres*, 106, 7183–7192, <https://doi.org/10.1029/2000JD900719>, 2001.
- Tesche, T. W., Morris, R., Tonnesen, G., McNally, D., Boylan, J., and Brewer, P.: CMAQ/CAMx annual 2002 performance evaluation over the eastern US, *Atmos. Environ.*, 40, 4906–4919, <https://doi.org/10.1016/j.atmosenv.2005.08.046>, 2006.
- Tessum, C. W., Hill, J. D., and Marshall, J. D.: Twelve-month, 12 km resolution North American WRF-Chem v3.4 air quality simulation: performance evaluation, *Geosci. Model Dev.*, 8, 957–973, <https://doi.org/10.5194/gmd-8-957-2015>, 2015.
- 2735 Thunis, P., Pederzoli, A., and Pernigotti, D.: Performance criteria to evaluate air quality modeling applications, *Atmos. Environ.*, 59, 476–482, <https://doi.org/10.1016/j.atmosenv.2012.05.043>, 2012.
- Toro, C., Foley, K., Simon, H., Henderson, B., Baker, K. R., Eyth, A., Timin, B., Appel, W., Luecken, D., Beardsley, M., Sonntag, D., Possiel, N., and Roberts, S.: Evaluation of 15 years of modeled atmospheric oxidized nitrogen compounds across the contiguous United States, *Elem. Sci. Anthr.*, 9, 00158, <https://doi.org/10.1525/elementa.2020.00158>, 2021.
- 2740 Toro, C., Sonntag, D., Bash, J., Burke, G., Murphy, B., Seltzer, K. M., Simon, H., Shephard, M., and Cady-Pereira, K. E.: Sensitivity of air quality to vehicle ammonia emissions in the United States, *Atmos. Environ.*, 120484, <https://doi.org/10.1016/j.atmosenv.2024.120484>, 2024.
- 2745 [U.S. EPA: Air Pollutant Emissions Trends Data: Criteria pollutants National Tier 1 for 1970 - 2024, Data set, U.S. Environmental Protection Agency, Research Triangle Park, North Carolina, \[https://www.epa.gov/system/files/other-files/2025-04/national_tier1_caps_21feb2025.xlsx\]\(https://www.epa.gov/system/files/other-files/2025-04/national_tier1_caps_21feb2025.xlsx\) \(last access: 6 April 2026\), 2025.](https://www.epa.gov/system/files/other-files/2025-04/national_tier1_caps_21feb2025.xlsx)
- Van Loon, M., Vautard, R., Schaap, M., Bergström, R., Bessagnet, B., Brandt, J., Builtjes, P. J. H., Christensen, J. H., Cuvelier, C., Graff, A., Jonson, J. E., Krol, M., Langner, J., Roberts, P., Rouil, L., Stern, R., Tarrasón, L., Thunis, P., Vignati, E., White, L., and Wind, P.: Evaluation of long-term ozone simulations from seven regional air quality models and their ensemble, *Atmos. Environ.*, 41, 2083–2097, <https://doi.org/10.1016/j.atmosenv.2006.10.073>, 2007.
- 2750 Vasilakos, P., Russell, A., Weber, R., and Nenes, A.: Understanding nitrate formation in a world with less sulfate, *Atmospheric Chem. Phys.*, 18, 12765–12775, <https://doi.org/10.5194/acp-18-12765-2018>, 2018.
- Vautard, R., Moran, M. D., Solazzo, E., Gilliam, R. C., Matthias, V., Bianconi, R., Chemel, C., Ferreira, J., Geyer, B., Hansen, A. B., Jericevic, A., Prank, M., Segers, A., Silver, J. D., Werhahn, J., Wolke, R., Rao, S. T., and Galmarini, S.: Evaluation of the meteorological forcing used for the Air Quality Model Evaluation International Initiative (AQMEII) air quality simulations, *Atmos. Environ.*, 53, 15–37, <https://doi.org/10.1016/j.atmosenv.2011.10.065>, 2012.
- 2755

Formatted: Font: (Default) +Body (Times New Roman), 10 pt, Font color: Text 1

Formatted: Hyperlink, Font: (Default) +Body (Times New Roman), 10 pt, Font color: Auto, English (United Kingdom), Ligatures: None

Field Code Changed

Formatted: Font: (Default) +Body (Times New Roman), 10 pt, Font color: Text 1

- Venkatram, A.: Inherent uncertainty in air quality modeling, *Atmospheric Environ.* 1967, 22, 1221–1227, [https://doi.org/10.1016/0004-6981\(88\)90352-6](https://doi.org/10.1016/0004-6981(88)90352-6), 1988.
- Venkatram, A., Karamchandani, P. K., and Misra, P. K.: Testing a comprehensive acid deposition model, *Atmospheric Environ.* 1967, 22, 737–747, [https://doi.org/10.1016/0004-6981\(88\)90011-X](https://doi.org/10.1016/0004-6981(88)90011-X), 1988.
- 2760 Vitali, L., Cuvelier, K., Piersanti, A., Monteiro, A., Adani, M., Amorati, R., Bartocha, A., D'Ausilio, A., Durka, P., Gama, C., Giovannini, G., Janssen, S., Przybyła, T., Stortini, M., Vranckx, S., and Thunis, P.: A standardized methodology for the validation of air quality forecast applications (F-MQO): lessons learnt from its application across Europe, *Geosci. Model Dev.*, 16, 6029–6047, <https://doi.org/10.5194/gmd-16-6029-2023>, 2023.
- 2765 Wagner, A., Blechschmidt, A.-M., Bouarar, I., Brunke, E.-G., Clerbaux, C., Cupeiro, M., Cristofanelli, P., Eskes, H., Flemming, J., Flentje, H., George, M., Gilge, S., Hilboll, A., Inness, A., Kapsomenakis, J., Richter, A., Ries, L., Spangl, W., Stein, O., Weller, R., and Zerefos, C.: Evaluation of the MACC operational forecast system – potential and challenges of global near-real-time modelling with respect to reactive gases in the troposphere, *Atmospheric Chem. Phys.*, 15, 14005–14030, <https://doi.org/10.5194/acp-15-14005-2015>, 2015.
- 2770 [Wang, H., Zhang, X. Y., Wang, P., Peng, Y., Zhang, W. J., Liu, Z. D., Han, C., Li, S. T., Wang, Y. Q., Che, H. Z., Huang, L. P., Liu, H. L., Zhang, L., Zhou, C. H., Ma, Z. S., Chen, F. F., Ma, X., Wu, X. J., Zhang, B. H., and Shen, X. S.: Chemistry-weather interacted model system GRAPES_Meso5.1/CUACE_CW_V1.0: Development, evaluation and application in better haze/fog prediction in China, *J. Adv. Model. Earth Syst.*, 14, e2022MS003222, <https://doi.org/10.1029/2022MS003222>, 2022.](#)
- 2775 Wang, K., Zhang, Y., and Yahya, K.: Decadal application of WRF/Chem over the continental U.S.: Simulation design, sensitivity simulations, and climatological model evaluation, *Atmos. Environ.*, 253, 118331, <https://doi.org/10.1016/j.atmosenv.2021.118331>, 2021.
- Watson, J. G., Chow, J. C., Chen, L.-W. A., and Frank, N. H.: Methods to assess carbonaceous aerosol sampling artifacts for IMPROVE and other long-term networks, *J. Air Waste Manag. Assoc.*, 59, 898–911, <https://doi.org/10.3155/1047-3289.59.8.898>, 2009.
- 2780 Wayland, R. A., White, J. E., Dye, T. S., Anderson, C. B., Chan, A. C., and D.E.B. Strohm: Future of AirNow and the Air Quality Index: beyond ozone mapping and forecasting, Sixth Conference on Atmospheric Chemistry, 12-14 January, Seattle, Washington, American Meteorological Society, <https://ams.confex.com/ams/pdfpapers/72556.pdf> (last access: 6 April 2026), 2004.
- Wetherbee, G. A., Shaw, M. J., Latysh, N. E., Lehmann, C. M. B., and Rothert, J. E.: Comparison of precipitation chemistry measurements obtained by the Canadian Air and Precipitation Monitoring Network and National Atmospheric Deposition Program for the period 1995–2004, *Environ. Monit. Assess.*, 164, 111–132, <https://doi.org/10.1007/s10661-009-0879-8>, 2010.
- 2785 Widziewicz-Rzońca, K. and Tytła, M.: First systematic review on PM-bound water: exploring the existing knowledge domain using the CiteSpace software, *Scientometrics*, 124, 1945–2008, <https://doi.org/10.1007/s11192-020-03547-w>, 2020.
- Williams, J. E., Huijnen, V., Bouarar, I., Meziane, M., Schreurs, T., Pelletier, S., Marécal, V., Josse, B., and Flemming, J.: Regional evaluation of the performance of the global CAMS chemical modeling system over the United States (IFS cycle 47r1), *Geosci. Model Dev.*, 15, 4657–4687, <https://doi.org/10.5194/gmd-15-4657-2022>, 2022.
- 2790 Willmott, C. J.: On the validation of models, *Phys. Geogr.*, 2, 184–194, <https://doi.org/10.1080/02723646.1981.10642213>, 1981.
- WMO: Training Materials and Best Practices for Chemical Weather/Air Quality Forecasting, Report no. ETR-26, World Meteorological Organization, Geneva, 576 pp., <https://library.wmo.int/idurl/4/54300> (last access: 6 April 2026), 2020.
- 2795 Yahya, K., Zhang, Y., and Vukovich, J. M.: Real-time air quality forecasting over the southeastern United States using WRF/Chem-MADRID: Multiple-year assessment and sensitivity studies, *Atmos. Environ.*, 92, 318–338, <https://doi.org/10.1016/j.atmosenv.2014.04.024>, 2014.
- Yahya, K., Wang, K., Gudoshava, M., Gtlofelty, T., and Zhang, Y.: Application of WRF/Chem over North America under the AQMEII Phase 2: Part I. Comprehensive evaluation of 2006 simulation, *Atmos. Environ.*, 115, 733–755, <https://doi.org/10.1016/j.atmosenv.2014.08.063>, 2015.
- 2800 Yu, S., Dennis, R., Roselle, S., Nenes, A., Walker, J., Eder, B., Schere, K., Swall, J., and Robarge, W.: An assessment of the ability of three-dimensional air quality models with current thermodynamic equilibrium models to predict aerosol NO_3^- , *J. Geophys. Res.*, 110, D07S13, <https://doi.org/10.1029/2004JD004718>, 2005.
- 2805 Yu, S., Mathur, R., Schere, K., Kang, D., Pleim, J., Young, J., Tong, D., Pouliot, G., McKeen, S. A., and Rao, S. T.: Evaluation of real-time $\text{PM}_{2.5}$ forecasts and process analysis for $\text{PM}_{2.5}$ formation over the eastern United States using the Eta-CMAQ forecast model during the 2004 ICARTT study, *J. Geophys. Res. Atmospheres*, 113, 2007JD009226, <https://doi.org/10.1029/2007JD009226>, 2008.

- Zhai, H., Huang, L., Emery, C., Zhang, X., Wang, Y., Yarwood, G., Fu, J. S., and Li, L.: Recommendations on benchmarks for photochemical air quality model applications in China — NO₂, SO₂, CO and PM₁₀, *Atmos. Environ.*, 319, 120290, <https://doi.org/10.1016/j.atmosenv.2023.120290>, 2024.
- 2810 Zhang, H., Yee, L. D., Lee, B. H., Curtis, M. P., Worton, D. R., Isaacman-VanWertz, G., Offenberg, J. H., Lewandowski, M., Kleindienst, T. E., Beaver, M. R., Holder, A. L., Lonneman, W. A., Docherty, K. S., Jaoui, M., Pye, H. O. T., Hu, W., Day, D. A., Campuzano-Jost, P., Jimenez, J. L., Guo, H., Weber, R. J., De Gouw, J., Koss, A. R., Edgerton, E. S., Brune, W., Mohr, C., Lopez-Hilfiker, F. D., Lutz, A., Kreisberg, N. M., Spielman, S. R., Hering, S. V., Wilson, K. R., Thornton, J. A., and Goldstein, A. H.: Monoterpenes are the largest source of summertime organic aerosol in the southeastern United States, *Proc. Natl. Acad. Sci.*, 115, 2038–2043, <https://doi.org/10.1073/pnas.1717513115>, 2018a.
- 2815 Zhang, J., Moran, M. D., Zheng, Q., Makar, P. A., Baratzadeh, P., Marson, G., Liu, P., and Li, S.-M.: Emissions preparation and analysis for multiscale air quality modeling over the Athabasca Oil Sands Region of Alberta, Canada, *Atmospheric Chem. Phys.*, 18, 10459–10481, <https://doi.org/10.5194/acp-18-10459-2018>, 2018b.
- Zhang, L., Moran, M. D., Makar, P. A., Brook, J. R., and Gong, S.: Modelling gaseous dry deposition in AURAMS: a unified regional air-quality modelling system, *Atmos. Environ.*, 36, 537–560, [https://doi.org/10.1016/S1352-2310\(01\)00447-2](https://doi.org/10.1016/S1352-2310(01)00447-2), 2002.
- 2820 Zhang, Y., Liu, P., Pun, B., and Seigneur, C.: A comprehensive performance evaluation of MM5-CMAQ for the summer 1999 southern oxidants study episode, Part II: Diagnostic and mechanistic evaluations, *Atmos. Environ.*, 40, 4856–4873, <https://doi.org/10.1016/j.atmosenv.2005.12.046>, 2006a.
- Zhang, Y., Liu, P., Pun, B., and Seigneur, C.: A comprehensive performance evaluation of MM5-CMAQ for the Summer 1999 Southern Oxidants Study episode—Part I: Evaluation protocols, databases, and meteorological predictions, *Atmos. Environ.*, 40, 4825–4838, <https://doi.org/10.1016/j.atmosenv.2005.12.043>, 2006b.
- 2825 Zhang, Y., Liu, P., Queen, A., Misenis, C., Pun, B., Seigneur, C., and Wu, S.-Y.: A comprehensive performance evaluation of MM5-CMAQ for the Summer 1999 Southern Oxidants Study episode—Part II: Gas and aerosol predictions, *Atmos. Environ.*, 40, 4839–4855, <https://doi.org/10.1016/j.atmosenv.2005.12.048>, 2006c.
- Zhang, Y., Wen, X., Wang, K., Vijayaraghavan, K., and Jacobson, M. Z.: Probing into regional O₃ and particulate matter pollution in the United States: 2. An examination of formation mechanisms through a process analysis technique and sensitivity study, *J. Geophys. Res. Atmospheres*, 114, 2009JD011900, <https://doi.org/10.1029/2009JD011900>, 2009a.
- 2830 Zhang, Y., Vijayaraghavan, K., Wen, X., Snell, H. E., and Jacobson, M. Z.: Probing into regional ozone and particulate matter pollution in the United States: 1. A 1 year CMAQ simulation and evaluation using surface and satellite data, *J. Geophys. Res. Atmospheres*, 114, 2009JD011898, <https://doi.org/10.1029/2009JD011898>, 2009b.
- 2835 Zhang, Y., Bocquet, M., Mallet, V., Seigneur, C., and Baklanov, A.: Real-time air quality forecasting, part I: History, techniques, and current status, *Atmos. Environ.*, 60, 632–655, <https://doi.org/10.1016/j.atmosenv.2012.06.031>, 2012a.
- Zhang, Y., Bocquet, M., Mallet, V., Seigneur, C., and Baklanov, A.: Real-time air quality forecasting, part II: State of the science, current research needs, and future prospects, *Atmos. Environ.*, 60, 656–676, <https://doi.org/10.1016/j.atmosenv.2012.02.041>, 2012b.
- 2840 Zhang, Y., Hong, C., Yahya, K., Li, Q., Zhang, Q., and He, K.: Comprehensive evaluation of multi-year real-time air quality forecasting using an online-coupled meteorology-chemistry model over southeastern United States, *Atmos. Environ.*, 138, 162–182, <https://doi.org/10.1016/j.atmosenv.2016.05.006>, 2016.
- Zhang, Y., Mathur, R., Bash, J. O., Hogrefe, C., Xing, J., and Roselle, S. J.: Long-term trends in total inorganic nitrogen and sulfur deposition in the US from 1990 to 2010, *Atmospheric Chem. Phys.*, 18, 9091–9106, <https://doi.org/10.5194/acp-18-9091-2018>, 2018c.
- 2845

Tables

Table 1. Comparison of Canadian, U.S., and Mexican annual anthropogenic and biogenic criteria-air-contaminant inventory emissions (tonnes/year) and model-ready anthropogenic and biogenic emissions for five years: 2013–2016 and 2021/22. Note that the U.S. inventory emissions are for all 50 U.S. states and other territories and the Mexican inventory emissions are for all 32 Mexican states. The “3 Country EIs” rows provide the sum of the three national emissions inventory amounts, while the “Total Anthro” rows correspond to the grid-limited-area, domain-total emissions that are input by the model after SMOKE emissions processing and TF scaling for fugitive PM emissions. The “Total Anthro” VOC emissions are the sum of 12 model VOC species, including EOTH (all unreactive or low-reactivity VOC species that are not considered by the gas-phase chemistry mechanism; see Moran et al, 2026⁵). The “Total Biogenic” emissions depend on hourly meteorology and are accumulated hourly predicted fields of soil NO emissions (in NO₂ units) and biogenic VOC emissions (as model VOC species) saved during each annual simulation.

Species	Region	Year					Relative Difference (%)		
		2013	2014	2015	2016	2021/22	2016-to-2013	2021/22-to-2016	2021/22-to-2013
SO ₂	Canada	1,245,629	1,196,925	1,067,133	1,050,048	720,937	-15.7	-31.3	-42.4
	U.S.A.	4,855,796	4,632,986	3,232,955	2,453,837	1,614,783	-49.5	-34.2	-66.7
	Mexico	1,907,119	1,955,040	1,955,789	1,956,538	1,963,766	2.6	0.4	3.0
	3 Country EIs	8,008,544	7,784,951	6,255,877	5,460,422	4,299,487	-31.8	-21.3	-46.3
	Total Anthro	6,788,380	6,566,599	5,008,720	4,248,067	2,683,021	-37.4	-36.8	-60.5
NO _x	Canada	1,859,213	1,812,458	1,749,885	1,689,466	1,534,067	-9.1	-9.2	-17.5
	U.S.A.	12,010,496	11,318,521	10,317,943	9,281,137	7,462,553	-22.7	-19.6	-37.9
	Mexico	2,633,018	2,613,843	2,628,180	2,642,516	2,722,692	0.4	3.0	3.4
	3 Country EIs	16,502,727	15,744,822	14,696,007	13,613,119	11,719,312	-17.5	-13.9	-29.0
	Total Anthro	15,286,803	14,565,303	13,489,658	12,425,458	9,759,000	-18.7	-21.5	-36.2
	Total Biogenic	613,443	613,133	637,436	649,609	653,066	5.9	0.5	6.5
	Total Anthr+Bio	15,900,246	15,178,436	14,127,094	13,075,067	10,412,066	-17.8	-20.4	-34.5
VOC	Canada	1,639,307	1,676,389	1,624,563	1,530,449	1,517,407	-6.6	-0.9	-7.4
	U.S.A.	11,060,472	11,016,641	10,803,994	9,906,147	9,693,686	-10.4	-2.1	-12.4
	Mexico	4,223,883	4,246,882	4,247,239	4,247,596	4,619,106	0.6	8.7	9.4
	3 Country EIs	16,923,662	16,939,913	16,675,796	15,684,193	15,830,199	-7.3	0.9	-6.5
	Total Anthro	13,528,480	13,532,330	13,282,897	12,374,426	12,292,800	-8.5	-0.7	-9.1
	Total Biogenic	47,373,454	47,372,280	49,734,073	51,315,450	52,655,466	8.3	2.6	11.1
	Total Anthr+Bio	60,901,934	60,904,610	63,016,970	63,689,876	64,948,266	4.6	2.0	6.6
CO	Canada	5,414,122	5,310,926	5,227,752	5,173,958	4,322,475	-4.4	-16.5	-20.2
	U.S.A.	40,865,160	39,613,006	37,758,763	34,539,607	29,945,990	-15.5	-13.3	-26.7
	Mexico	8,738,655	8,863,635	8,867,142	8,870,649	9,015,675	1.5	1.6	3.2
	3 Country EIs	55,017,936	53,787,568	51,853,657	48,584,214	43,284,139	-11.7	-10.9	-21.3
	Total Anthro	48,394,003	47,088,320	45,142,220	41,929,513	36,118,000	-13.4	-13.9	-25.4
NH ₃	Canada	496,282	490,436	491,656	490,675	543,154	-1.1	10.7	9.4
	U.S.A.	3,814,960	3,723,552	3,839,459	3,853,365	3,481,215	1.0	-9.7	-8.7
	Mexico	840,629	844,080	844,297	844,514	841,397	0.5	-0.4	0.1
	3 Country EIs	5,151,871	5,058,068	5,175,412	5,188,554	4,865,766	0.7	-6.2	-5.6
	Total Anthro	4,521,443	4,424,069	4,541,247	4,553,502	4,234,533	0.7	-7.0	-6.3
PM _{2.5}	Canada	817,212	814,398	793,598	780,950	804,186	-4.4	3.0	-1.6
	U.S.A.	3,421,551	3,580,536	3,287,999	3,359,590	3,614,926	-1.8	7.6	5.7
	Mexico	603,696	591,783	593,799	595,814	661,387	-1.3	11.0	9.6
	3 Country EIs	4,842,459	4,986,718	4,675,396	4,736,354	5,080,499	-2.2	7.3	4.9
	Total Anthro	3,101,173	3,076,508	2,932,475	2,855,582	2,889,000	-7.9	1.2	-6.8
PM ₁₀	Canada	3,548,631	3,543,931	3,515,237	3,495,289	3,746,529	-1.5	7.2	5.6
	U.S.A.	15,427,692	15,426,307	15,438,707	15,532,333	18,729,161	0.7	20.6	21.4
	Mexico	839,386	822,182	824,358	826,535	923,082	-1.5	11.7	10.0
	3 Country EIs	19,815,709	19,792,420	19,778,302	19,854,158	23,398,772	0.2	17.9	18.1
	Total Anthro	10,122,137	10,094,335	9,989,971	10,001,543	10,826,000	-1.2	8.2	7.0

Table 2. Total number of U.S. and Canadian measurement stations with complete hourly NO₂, O₃, and PM_{2.5} measurements for an annual evaluation vs. available measurements by network and year for 2013–2016 (AQS, NAPS) and 2021/22 (AirNow, NAPS).

Year	2013		2014		2015		2016		2021/22	
	Complete	Available	Complete	Available	Complete	Available	Complete	Available	Complete	Available
Variable										
	AQS								AirNow US	
NO ₂	327	405	338	412	341	412	331	402	162	193
O ₃	720	1310	733	1298	716	1285	755	1274	580	1085
PM _{2.5}	601	777	623	800	621	832	614	826	603	770
	NAPS								NAPS	
NO ₂	132	141	131	146	138	157	142	159	143	175
O ₃	171	187	175	192	174	193	180	200	175	209
PM _{2.5}	158	189	179	196	165	198	174	198	173	203

Formatted: Subscript

Formatted: Subscript

Formatted: Subscript

Formatted: Subscript

Formatted: Subscript

Formatted: Subscript

3865 Table 3. Summary table of all-station annual statistics for the RAQDPS-OP023 for hourly NO₂, O₃, and PM_{2.5} surface measurements for 2021/22 and 2013–2016. For dimensional statistics, units are ppbv for NO₂ and O₃ and µg·m⁻³ for PM_{2.5}.

Variable	Statistic	AirNow + NAPS Combined		AQS + NAPS Combined		
		2021/22	2013	2014	2015	2016
NO ₂	N	2,509,716	3,776,292	3,856,650	3,933,509	3,910,073
	Obs Mean	6.57	7.90	7.74	7.60	7.18
	Model Mean	5.30	8.80	8.53	8.32	7.74
	MB	-1.27	0.90	0.78	0.73	0.57
	NMB	-0.19	0.11	0.10	0.10	0.08
	RMSE	6.09	7.21	7.11	7.00	6.66
	CRMSE	5.96	7.15	7.07	6.96	6.63
	NMAE	0.56	0.58	0.58	0.58	0.58
	FACae2	0.52	0.59	0.58	0.58	0.57
	R	0.65	0.68	0.68	0.68	0.68
	NSD	0.84	1.05	1.05	1.06	1.05
	Obs SD	7.61	8.63	8.59	8.40	8.08
	Model SD	6.37	9.10	9.00	8.93	8.48
	O ₃	N	6,175,254	7,468,605	7,617,067	7,472,330
Obs Mean		29.64	29.50	29.14	28.95	29.42
Model Mean		27.60	25.87	26.03	26.34	26.68
MB		-2.04	-3.62	-3.11	-2.61	-2.75
NMB		-0.07	-0.12	-0.11	-0.09	-0.09
RMSE		10.77	12.15	11.66	11.60	11.35
CRMSE		10.57	11.59	11.24	11.30	11.01
NMAE		0.28	0.31	0.31	0.30	0.29
FACae2		0.83	0.78	0.79	0.79	0.80
R		0.72	0.71	0.71	0.71	0.72
NSD		0.88	0.99	0.99	0.98	0.97
Obs SD		14.76	15.34	14.97	15.03	14.89
Model SD		13.06	15.18	14.76	14.80	14.51
PM _{2.5}		N	6,374,875	6,280,280	6,635,531	6,471,206
	Obs Mean	8.02	8.67	8.34	8.37	7.44
	Model Mean	5.51	8.17	7.87	7.59	6.98
	MB	-2.51	-0.50	-0.46	-0.78	-0.46
	NMB	-0.31	-0.06	-0.06	-0.09	-0.06
	RMSE	9.73	11.62	11.33	11.39	13.43
	CRMSE	9.41	11.61	11.32	11.36	13.42
	NMAE	0.66	0.71	0.72	0.71	0.73
	FACae2	0.46	0.50	0.49	0.49	0.48
	R	0.24	0.29	0.27	0.26	0.17
	NSD	0.69	1.36	1.35	1.13	0.78
	Obs SD	8.78	8.11	7.83	8.73	11.54
	Model SD	6.06	11.02	10.60	9.89	9.05

Formatted Table

Table 4. Summary table of all-station annual statistics for the RAQDPS-OP023 for nine other ambient gas-phase chemistry measurements (NO, NO_x, CO, HNO₃, NH₃, SO₂, ETHE, ISOP, HCHO) for 2013–2016. For dimensional statistics, units are ppmv for CO, µg·m⁻³ for NH₃, and ppbv for other species. Sample duration used for all networks is hourly for NO, NO_x, CO, ETHE, and ISOP, daily for HCHO, weekly for HNO₃ and SO₂, and biweekly for NH₃.

Variable	Statistic	2013	2014	2015	2016
NO	N	3,562,348	3,721,353	3,680,583	3,564,269
	Obs Mean	4.09	3.89	4.01	3.61
	Model Mean	5.39	4.88	4.68	3.93
	MB	1.30	0.99	0.68	0.32
	NMB	0.32	0.25	0.17	0.09
	RMSE	16.44	15.21	14.65	12.90
	CRMSE	16.39	15.18	14.63	12.90
	NMAE	1.34	1.29	1.26	1.21
	FAC2	0.28	0.29	0.28	0.28
	R	0.41	0.42	0.41	0.41
	NSD	1.23	1.21	1.13	1.07
	Obs SD	13.36	12.61	12.60	11.46
	Model SD	16.49	15.30	14.20	12.26
NO _x	N	3,408,562	3,507,613	3,246,050	3,476,220
	Obs Mean	12.03	11.72	11.86	10.86
	Model Mean	14.38	13.40	12.69	11.67
	MB	2.35	1.68	0.83	0.82
	NMB	0.20	0.14	0.07	0.08
	RMSE	21.12	19.72	18.58	17.13
	CRMSE	20.98	19.65	18.56	17.11
	NMAE	0.79	0.77	0.73	0.74
	FAC2	0.53	0.53	0.53	0.53
	R	0.54	0.54	0.55	0.55
	NSD	1.19	1.15	1.04	1.05
	Obs SD	19.81	19.00	19.16	17.60
	Model SD	23.60	21.84	19.91	18.54
HNO ₃	N	4,766	4,946	4,874	4,788
	Obs Mean	0.25	0.24	0.23	0.22
	Model Mean	0.33	0.32	0.29	0.25
	MB	0.08	0.08	0.06	0.04
	NMB	0.33	0.32	0.25	0.16
	RMSE	0.19	0.19	0.18	0.14
	CRMSE	0.18	0.18	0.17	0.14
	NMAE	0.52	0.53	0.48	0.42
	FAC2	0.76	0.75	0.78	0.81
	R	0.69	0.64	0.66	0.69
	NSD	1.28	1.24	1.30	1.12
	Obs SD	0.19	0.18	0.17	0.16
	Model SD	0.24	0.22	0.22	0.18
NH ₃	N	1,705	1,731	2,417	2,464
	Obs Mean	1.54	1.71	1.62	1.73
	Model Mean	0.87	0.91	0.94	1.00
	MB	-0.67	-0.81	-0.68	-0.73
	NMB	-0.44	-0.47	-0.42	-0.42
	RMSE	2.54	2.86	3.10	2.66
	CRMSE	2.45	2.75	3.02	2.56
	NMAE	0.60	0.62	0.60	0.57

Non-classifié | Unclassified

	FAC2	0.50	0.47	0.54	0.57
	R	0.34	0.51	0.44	0.51
	NSD	0.44	0.41	0.36	0.44
	Obs SD	2.59	3.17	3.36	2.97
	Model SD	1.13	1.30	1.21	1.29
SO ₂	N	27,172	28,170	28,311	27,279
	Obs Mean	1.23	1.18	0.99	0.83
	Model Mean	1.96	1.78	1.42	1.22
	MB	0.74	0.60	0.43	0.39
	NMB	0.60	0.51	0.43	0.47
	RMSE	2.60	2.36	1.97	1.98
	CRMSE	2.49	2.28	1.92	1.94
	NMAE	1.11	1.00	0.99	1.10
	FAC2	0.45	0.49	0.47	0.45
	R	0.35	0.39	0.40	0.38
	NSD	1.43	1.35	1.29	1.37
	Obs SD	1.75	1.72	1.51	1.43
	Model SD	2.50	2.31	1.94	1.97
CO	N	2,413,310	2,313,412	2,263,157	2,207,060
	Obs Mean	0.27	0.27	0.27	0.28
	Model Mean	0.31	0.30	0.29	0.27
	MB	0.03	0.03	0.01	-0.01
	NMB	0.12	0.09	0.05	-0.05
	RMSE	0.29	0.27	0.25	0.56
	CRMSE	0.28	0.26	0.25	0.56
	NMAE	0.61	0.57	0.55	0.55
	FAC2	0.69	0.72	0.73	0.74
	R	0.42	0.43	0.43	0.14
	NSD	1.04	1.09	1.04	0.38
	Obs SD	0.26	0.24	0.23	0.55
	Model SD	0.27	0.26	0.24	0.21
ETHE	N	95,968	94,497	73,794	57,832
	Obs Mean	1.05	1.03	1.06	0.95
	Model Mean	1.77	1.80	2.01	2.08
	MB	0.72	0.77	0.95	1.13
	NMB	0.68	0.75	0.89	1.19
	RMSE	2.25	2.34	2.55	2.82
	CRMSE	2.13	2.21	2.36	2.58
	NMAE	1.24	1.27	1.42	1.66
	FAC2	0.41	0.42	0.39	0.35
	R	0.32	0.26	0.20	0.18
	NSD	1.05	1.08	1.12	1.13
	Obs SD	1.78	1.75	1.75	1.89
	Model SD	1.87	1.89	1.97	2.13
HCHO	N	4,909	5,063	4,889	4,826
	Obs Mean	2.38	2.07	2.27	2.37
	Model Mean	2.47	2.32	2.43	2.56
	MB	0.09	0.25	0.16	0.19
	NMB	0.04	0.12	0.07	0.08
	RMSE	3.71	2.13	2.09	2.34
	CRMSE	3.71	2.11	2.08	2.33
	NMAE	0.66	0.61	0.56	0.61

		Non-classifié Unclassified			
	FAC2	0.65	0.66	0.71	0.66
	R	0.26	0.43	0.46	0.41
	NSD	0.64	1.24	1.23	1.31
	Obs SD	3.59	1.75	1.78	1.83
	Model SD	2.28	2.17	2.19	2.39
ISOP	N	79,679	94,818	66,013	42,845
	Obs Mean	0.12	0.11	0.15	0.13
	Model Mean	0.39	0.38	0.56	0.48
	MB	0.27	0.27	0.41	0.35
	NMB	2.27	2.36	2.71	2.60
	RMSE	0.77	0.78	0.99	0.99
	CRMSE	0.73	0.73	0.90	0.93
	NMAE	2.81	2.85	3.12	3.20
	FAC2	0.18	0.19	0.18	0.19
	R	0.45	0.46	0.50	0.37
	NSD	3.37	3.25	3.13	3.69
	Obs SD	0.24	0.25	0.32	0.27
	Model SD	0.80	0.82	1.02	0.99

Table 5. Summary table of all-station annual statistics for the RAQDPS-OP023 for daily gravimetric and speciated PM_{2.5} measurements for 2013–2016. For dimensional statistics, units are µg·m⁻³.

Variable	Statistic	2013	2014	2015	2016
SO ₄	N	32,101	32,027	30,103	28,972
	Obs Mean	1.17	1.15	0.97	0.75
	Model Mean	0.84	0.82	0.73	0.63
	MB	-0.32	-0.33	-0.25	-0.12
	NMB	-0.28	-0.29	-0.25	-0.16
	RMSE	0.82	0.83	0.73	0.58
	CRMSE	0.75	0.76	0.69	0.57
	NMAE	0.46	0.46	0.47	0.49
	FA _{Cae2}	0.61	0.64	0.65	0.64
	R	0.71	0.69	0.65	0.61
	NSD	0.83	0.75	0.74	0.84
	Obs SD	1.05	1.05	0.90	0.69
	Model SD	0.87	0.79	0.67	0.57
	NO ₃	N	31,992	31,983	30,046
Obs Mean		0.75	0.79	0.68	0.54
Model Mean		0.67	0.61	0.58	0.49
MB		-0.08	-0.19	-0.10	-0.05
NMB		-0.11	-0.23	-0.15	-0.09
RMSE		1.40	1.25	1.00	0.91
CRMSE		1.40	1.23	1.00	0.91
NMAE		0.67	0.63	0.64	0.71
FA _{Cae2}		0.37	0.35	0.34	0.32
R		0.57	0.66	0.70	0.66
NSD		0.80	0.71	0.85	0.88
Obs SD		1.64	1.63	1.36	1.17
Model SD		1.32	1.16	1.16	1.02
NH ₄		N	14,828	14,711	13,283
	Obs Mean	0.64	0.69	0.54	0.33
	Model Mean	0.78	0.73	0.68	0.60
	MB	0.14	0.04	0.14	0.28
	NMB	0.22	0.06	0.26	0.85
	RMSE	0.75	0.69	0.61	0.60
	CRMSE	0.73	0.69	0.60	0.54
	NMAE	0.66	0.59	0.72	1.23
	FA _{Cae2}	0.58	0.60	0.52	0.34
	R	0.52	0.57	0.58	0.51
	NSD	0.81	0.71	0.82	0.92
	Obs SD	0.81	0.83	0.71	0.56
	Model SD	0.66	0.59	0.58	0.52
	EC	N	30,770	31,862	28,866
Obs Mean		0.34	0.33	0.32	0.30
Model Mean		0.52	0.50	0.47	0.40
MB		0.18	0.17	0.15	0.09
NMB		0.53	0.51	0.48	0.30
RMSE		0.74	0.66	0.67	0.55
CRMSE		0.71	0.64	0.65	0.55
NMAE		0.91	0.91	0.90	0.77
FA _{Cae2}		0.57	0.58	0.56	0.56
R		0.63	0.60	0.58	0.60
NSD		2.11	1.94	1.91	1.68
Obs SD		0.43	0.41	0.42	0.41
Model SD		0.90	0.80	0.80	0.69

Formatted: Subscript

Formatted: Subscript

Formatted: Subscript

Non-classifié | Unclassified

TOM	N	30,609	31,747	28,688	27,508
	Obs Mean	2.48	2.43	2.76	2.46
	Model Mean	2.74	2.54	2.61	2.41
	MB	0.26	0.11	-0.15	-0.05
	NMB	0.11	0.04	-0.05	-0.02
	RMSE	6.49	3.54	6.24	10.33
	CRMSE	6.48	3.54	6.24	10.33
	NMAE	0.75	0.68	0.72	0.74
	FACae2	0.54	0.55	0.51	0.50
	R	0.36	0.45	0.25	0.10
	NSD	2.52	1.44	1.54	0.54
	Obs SD	2.76	2.65	3.86	9.50
	Model SD	6.95	3.82	5.95	5.14
	CM	N	31,429	31,675	29,871
Obs Mean		0.58	0.63	0.61	0.56
Model Mean		0.83	0.85	0.83	0.83
MB		0.25	0.22	0.22	0.27
NMB		0.42	0.35	0.36	0.48
RMSE		1.60	1.67	1.53	1.46
CRMSE		1.58	1.65	1.52	1.43
NMAE		1.40	1.37	1.30	1.36
FACae2		0.31	0.30	0.32	0.32
R		0.12	0.13	0.17	0.22
NSD		1.30	1.19	1.27	1.59
Obs SD		1.02	1.14	1.03	0.85
Model SD		1.33	1.36	1.30	1.35
SS		N	31,860	31,852	30,185
	Obs Mean	0.26	0.25	0.29	0.23
	Model Mean	0.45	0.44	0.49	0.51
	MB	0.19	0.19	0.20	0.29
	NMB	0.74	0.78	0.71	1.25
	RMSE	1.02	1.12	1.09	1.16
	CRMSE	1.00	1.10	1.07	1.12
	NMAE	1.36	1.42	1.35	1.70
	FACae2	0.31	0.32	0.33	0.33
	R	0.62	0.58	0.61	0.60
	NSD	2.55	2.74	2.66	3.03
	Obs SD	0.48	0.48	0.48	0.44
	Model SD	1.23	1.31	1.29	1.33
	PM _{2.5}	N	104,944	104,095	111,150
Obs Mean		8.19	8.12	7.94	7.24
Model Mean		8.72	8.10	8.10	7.47
MB		0.54	-0.02	0.16	0.23
NMB		0.07	0.00	0.02	0.03
RMSE		8.24	7.86	7.65	7.15
CRMSE		8.22	7.86	7.65	7.14
NMAE		0.54	0.51	0.53	0.54
FACae2		0.70	0.70	0.70	0.68
R		0.47	0.44	0.45	0.43
NSD		1.61	1.50	1.41	1.53
Obs SD		5.69	5.67	5.81	5.04
Model SD		9.19	8.49	8.20	7.70

Formatted: Subscript

2885

Table 6. Summary table of all-station annual statistics for the RAODPS-OP023 for weekly precipitation-chemistry measurements for 2013–2016. For dimensional statistics, units are mg·L⁻¹ for concentration in precipitation, mm·week⁻¹ for precipitation, and mg·m⁻²·week⁻¹ for wet deposition. Note that daily CAPMoN measurements have been aggregated to weekly values for consistency with NADP measurements.

Variable	Statistic	2013	2014	2015	2016
SO ₄ ²⁻ conc	N	9,115	8,997	9,759	9,193
	Obs Mean	0.81	0.74	0.65	0.62
	Model Mean	0.82	0.84	0.74	0.61
	MB	0.02	0.10	0.09	-0.01
	NMB	0.02	0.14	0.14	-0.01
	RMSE	0.91	0.91	0.87	1.19
	CRMSE	0.91	0.90	0.87	1.19
	NMAE	0.59	0.65	0.68	0.61
	FAC _{ae2}	0.64	0.65	0.63	0.65
	R	0.41	0.38	0.37	0.25
	NSD	0.89	1.00	1.09	0.50
	Obs SD	0.88	0.81	0.74	1.19
	Model SD	0.78	0.81	0.80	0.60
	NO ₃ ⁻ conc	N	9,115	8,995	9,752
Obs Mean		0.96	0.93	0.91	0.90
Model Mean		0.94	0.91	0.90	0.78
MB		-0.02	-0.01	-0.01	-0.12
NMB		-0.02	-0.02	-0.01	-0.14
RMSE		0.97	0.93	1.02	0.94
CRMSE		0.97	0.93	1.02	0.93
NMAE		0.55	0.54	0.57	0.52
FAC _{ae2}		0.69	0.70	0.68	0.69
R		0.49	0.52	0.48	0.46
NSD		1.06	1.03	1.06	0.80
Obs SD		0.92	0.94	0.97	0.98
Model SD		0.98	0.97	1.03	0.78
NH ₄ ⁺ conc		N	9,103	8,980	9,727
	Obs Mean	0.37	0.36	0.39	0.39
	Model Mean	0.46	0.46	0.54	0.52
	MB	0.09	0.09	0.16	0.13
	NMB	0.23	0.25	0.41	0.35
	RMSE	0.65	0.65	0.91	0.79
	CRMSE	0.65	0.65	0.90	0.78
	NMAE	0.78	0.80	0.95	0.89
	FAC _{ae2}	0.60	0.59	0.57	0.58
	R	0.47	0.41	0.38	0.39
	NSD	1.62	1.54	1.98	1.75
	Obs SD	0.45	0.44	0.49	0.47
	Model SD	0.72	0.68	0.96	0.83
	PR	N	13,732	13,874	14,050
Obs Mean		19.48	20.27	19.77	19.38
Model Mean		21.72	21.64	19.63	20.11
MB		2.25	1.37	-0.14	0.73
NMB		0.12	0.07	-0.01	0.04
RMSE		19.62	20.63	17.60	18.91
CRMSE		19.49	20.58	17.60	18.90
NMAE		0.54	0.53	0.49	0.52
FAC _{ae2}		0.57	0.57	0.57	0.56
R		0.72	0.71	0.78	0.75
NSD		1.07	1.06	0.99	1.03

Formatted: Subscript

Formatted: Superscript

Formatted: Subscript

Formatted: Superscript

Formatted: Subscript

Formatted: Superscript

Non-classifié | Unclassified

	Obs SD	25.24	26.33	26.65	26.40
	Model SD	26.91	27.90	26.52	27.18
SO ₂ dep	N	9,115	8,997	9,759	9,193
	Obs Mean	15.65	14.41	11.41	10.71
	Model Mean	15.91	15.18	11.36	10.08
	MB	0.26	0.78	-0.06	-0.63
	NMB	0.02	0.05	0.00	-0.06
	RMSE	16.29	16.85	12.91	12.58
	CRMSE	16.29	16.83	12.91	12.56
	NMAE	0.61	0.65	0.65	0.62
	FAC _{ae} 2	0.55	0.56	0.53	0.56
	R	0.58	0.49	0.53	0.58
	NSD	0.90	0.85	0.83	0.76
	Obs SD	18.55	17.85	14.33	15.04
	Model SD	16.72	15.09	11.84	11.38
	NO _x dep	N	9,115	8,995	9,752
Obs Mean		16.48	15.64	13.71	14.12
Model Mean		16.16	14.76	12.35	11.65
MB		-0.33	-0.88	-1.35	-2.47
NMB		-0.02	-0.06	-0.10	-0.18
RMSE		14.46	16.49	12.16	13.00
CRMSE		14.46	16.47	12.09	12.76
NMAE		0.54	0.54	0.55	0.52
FAC _{ae} 2		0.63	0.64	0.62	0.62
R		0.59	0.46	0.56	0.56
NSD		0.89	0.72	0.85	0.72
Obs SD		16.84	17.81	13.76	15.13
Model SD		14.97	12.86	11.68	10.93
NH ₃ dep		N	9,103	8,980	9,727
	Obs Mean	6.60	6.26	5.85	6.14
	Model Mean	7.65	7.28	6.75	6.94
	MB	1.05	1.02	0.90	0.80
	NMB	0.16	0.16	0.15	0.13
	RMSE	8.88	9.54	7.78	8.33
	CRMSE	8.82	9.48	7.73	8.29
	NMAE	0.69	0.72	0.72	0.68
	FAC _{ae} 2	0.56	0.57	0.55	0.57
	R	0.59	0.47	0.55	0.56
	NSD	1.08	1.01	1.05	1.06
	Obs SD	9.32	9.20	7.90	8.53
	Model SD	10.06	9.29	8.33	9.03

Formatted: Subscript

Formatted: Superscript

Formatted: Subscript

Formatted: Superscript

Formatted: Subscript

Formatted: Superscript

Table 7. Comparison of RAQDPS-OP023 and RAQDPS-FW023 all-station seasonal scores for predicted hourly surface NO₂, O₃, and PM_{2.5} abundances for 2021/22. For dimensional statistics, units are ppbv for NO₂ and O₃ and µg·m⁻³ for PM_{2.5}.

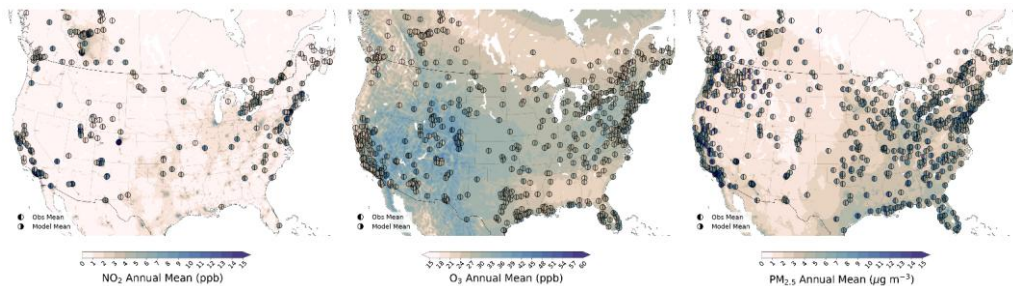
Variable	Statistic	Winter		Spring		Summer		Autumn	
		OP023	FW023	OP023	FW023	OP023	FW023	OP023	FW023
NO ₂	N	618,274	618,274	635,685	635,685	633,977	633,977	621,780	621,780
	Obs Mean	9.42	9.42	5.53	5.53	4.57	4.57	6.82	6.82
	Model	7.32	7.32	4.50	4.50	3.98	4.02	5.45	5.46
	MB	-2.10	-2.10	-1.03	-1.03	-0.59	-0.55	-1.38	-1.37
	NMB	-0.22	-0.22	-0.19	-0.19	-0.13	-0.12	-0.20	-0.20
	RMSE	7.69	7.69	5.69	5.69	4.62	4.64	6.00	6.00
	CRMSE	7.40	7.40	5.60	5.60	4.59	4.60	5.84	5.84
	NMAE	0.52	0.52	0.60	0.60	0.60	0.61	0.55	0.55
	FACae2	0.56	0.56	0.48	0.48	0.49	0.50	0.54	0.54
	R	0.66	0.66	0.62	0.62	0.56	0.56	0.64	0.64
	NSD	0.85	0.85	0.87	0.87	0.89	0.90	0.78	0.79
	Obs SD	9.54	9.54	6.76	6.76	5.14	5.14	7.49	7.49
	Model SD	8.14	8.14	5.89	5.89	4.57	4.62	5.88	5.89
O ₃	N	1,523,37	1,523,37	1,567,17	1,567,17	1,570,21	1,570,21	1,514,48	1,514,48
	Obs Mean	26.37	26.37	34.78	34.78	31.34	31.34	25.83	25.83
	Model	27.56	27.57	30.59	30.61	27.09	27.93	25.07	25.31
	MB	1.19	1.19	-4.19	-4.17	-4.25	-3.41	-0.76	-0.52
	NMB	0.05	0.05	-0.12	-0.12	-0.14	-0.11	-0.03	-0.02
	RMSE	9.65	9.65	11.02	11.01	12.36	11.95	9.76	9.67
	CRMSE	9.57	9.57	10.19	10.19	11.60	11.46	9.73	9.66
	NMAE	0.28	0.28	0.25	0.25	0.31	0.30	0.28	0.28
	FACae2	0.82	0.82	0.88	0.88	0.82	0.83	0.81	0.82
	R	0.68	0.68	0.66	0.66	0.75	0.76	0.75	0.76
	NSD	0.88	0.88	0.93	0.93	0.90	0.93	0.89	0.91
	Obs SD	12.50	12.50	12.82	12.82	16.94	16.94	14.42	14.42
	Model SD	11.06	11.06	11.92	11.93	15.32	15.79	12.88	13.12
PM _{2.5}	N	1,574,82	1,574,82	1,616,88	1,616,88	1,622,57	1,622,57	1,560,59	1,560,59
	Obs Mean	8.03	8.03	6.20	6.20	10.39	10.39	7.41	7.41
	Model	7.00	7.04	4.56	4.69	5.06	10.82	5.47	7.06
	MB	-1.04	-0.99	-1.64	-1.52	-5.34	0.42	-1.94	-0.35
	NMB	-0.13	-0.12	-0.26	-0.24	-0.51	0.04	-0.26	-0.05
	RMSE	8.38	8.37	5.93	5.88	14.14	19.92	8.48	10.26
	CRMSE	8.32	8.31	5.70	5.68	13.09	19.92	8.25	10.25
	NMAE	0.66	0.66	0.63	0.62	0.69	0.65	0.65	0.64
	FACae2	0.49	0.49	0.46	0.47	0.43	0.56	0.48	0.54
	R	0.40	0.41	0.37	0.38	0.09	0.55	0.28	0.49
	NSD	1.16	1.17	0.94	0.96	0.35	1.87	0.76	1.50
	Obs SD	7.00	7.00	5.21	5.21	12.74	12.74	7.68	7.68
	Model SD	8.14	8.17	4.91	5.01	4.46	23.79	5.83	11.54

Formatted: Subscript

Formatted: Subscript

Formatted: Subscript

Figures



1900 Figure 1. Spatial distribution of RAQDPS-OP023-predicted 2021/22 mean-annual-mean abundance fields of hourly (a) NO₂ VMR, (b) O₃ VMR, and (c) PM_{2.5}-noSS concentration with NRT observed and predicted NRT-station annual abundances superimposed (shown as filled-in divided circles, same colour bar). Units are ppbv, ppbv, and µg·m⁻³, respectively.

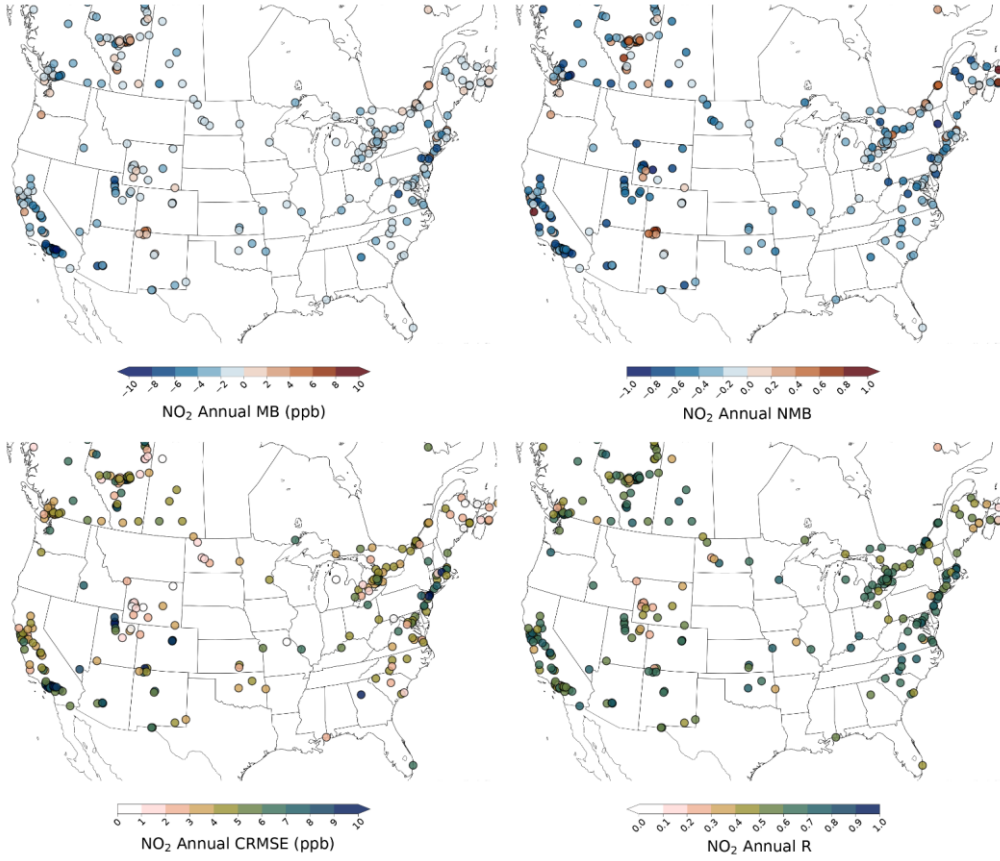


Figure 2. Spatial distribution of 2021/22 annual (a) MB, (b) NMB, (c) CRMSE, and (d) R scores for the RAQDPS-OP023 at all NRT stations for hourly NO₂ VMR measurements (ppbv).

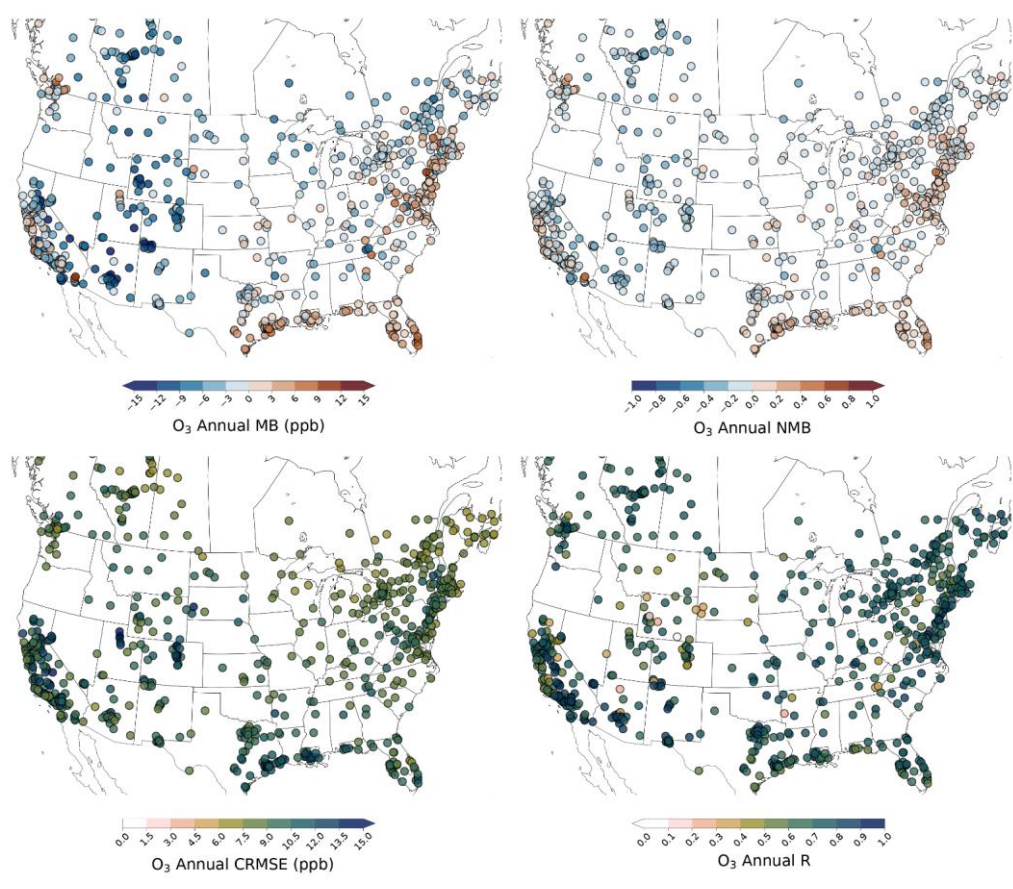


Figure 3. Spatial distribution of 2021/22 annual (a) MB, (b) NMB, (c) CRMSE, and (d) R scores for the RAQDPS-OP023 at all NRT stations for hourly O₃ VMR measurements (ppbv).

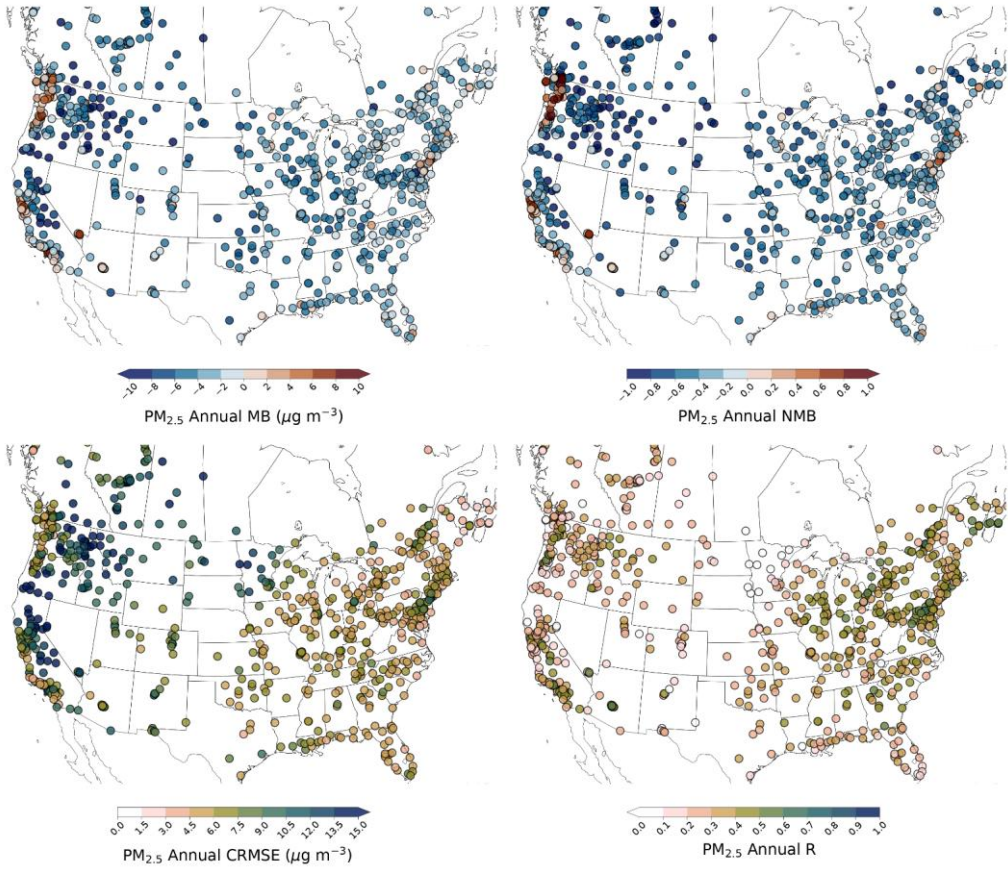


Figure 4. Spatial distribution of 2021/22 annual (a) MB, (b) NMB, (c) CRMSE, and (d) R scores for the RAQDPS-OP023 at all NRT stations for hourly $\text{PM}_{2.5}$ concentration measurements ($\mu\text{g}\cdot\text{m}^{-3}$).

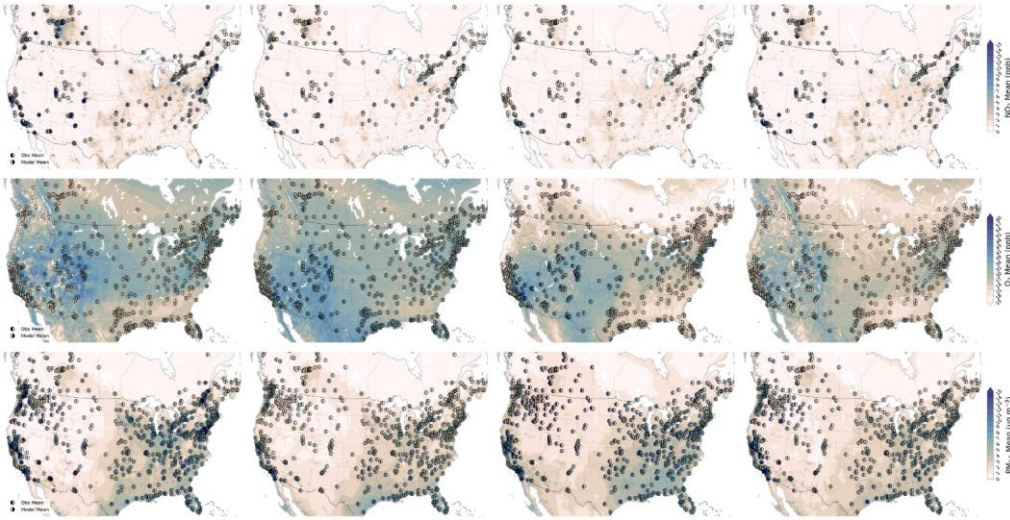


Figure 5. Spatial distribution of **RAQDPS-OP023**-predicted 2021/22 **mean**-seasonal-**mean** abundance fields (from left to right: winter [DJF], spring [MAM], summer [JJA], autumn [SON]) of hourly (top row) **NO₂ VMR**, (middle row) **O₃ VMR**, and (bottom row) **PM_{2.5}-noSS concentration** with **NRT** observed and predicted station seasonal abundances superimposed (shown as filled-in divided circles, same colour bar). Units are ppbv, ppbv, and $\mu\text{g}\cdot\text{m}^{-3}$, respectively.

Formatted: Not Superscript/ Subscript

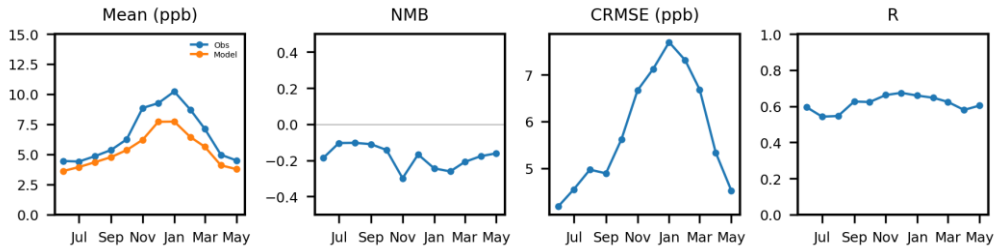


Figure 6. Time series of (a) observed and **RAQDPS-OP023**-predicted monthly means of hourly **NO₂ volume-mixing ratio VMR** (ppbv) and monthly (b) **NMB**, (c) **CRMSE**, and (d) **R** scores for 2021/22 for all **NRT measurement** stations.

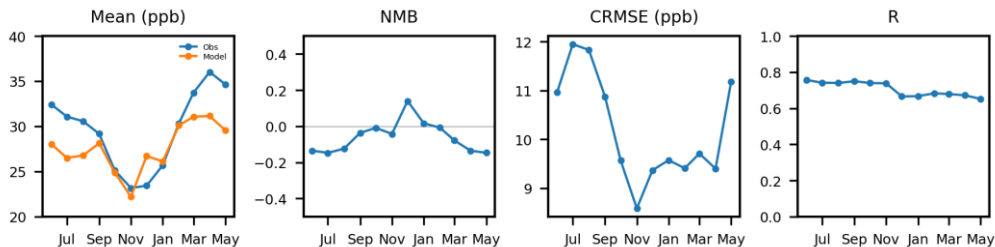


Figure 7. Time series of (a) observed and [RAQDPS-OP023](#)-predicted monthly means of hourly O_3 ~~volume mixing ratio~~ VMR (ppbv) and monthly (b) NMB, (c) CRMSE, and (d) R scores for 2021/22 for all NRT measurement stations.

2935

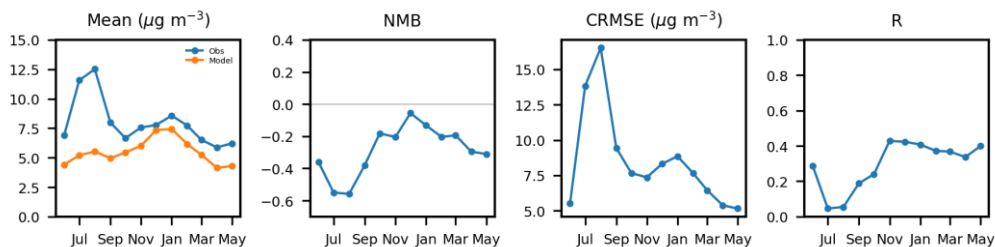


Figure 8. Time series of monthly (a) observed and [RAQDPS-OP023](#)-predicted mean hourly $PM_{2.5}$ concentration ($\mu g \cdot m^{-3}$) and (b) NMB, (c) CRMSE, and (d) R scores for 2021/22 for all NRT measurement stations.

2940

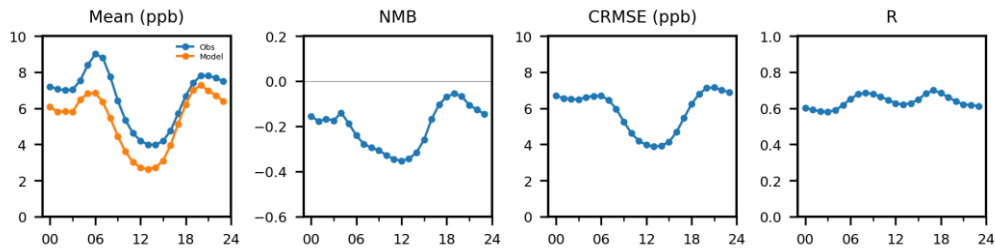
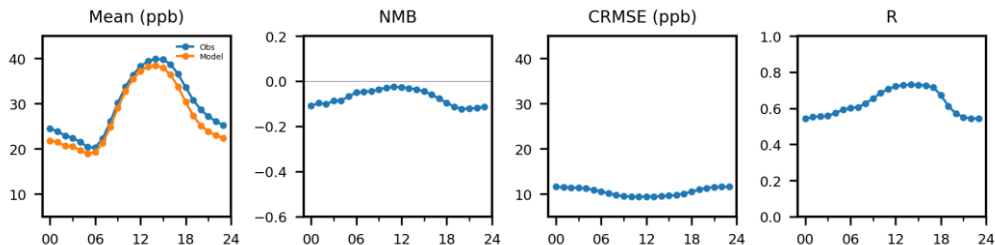
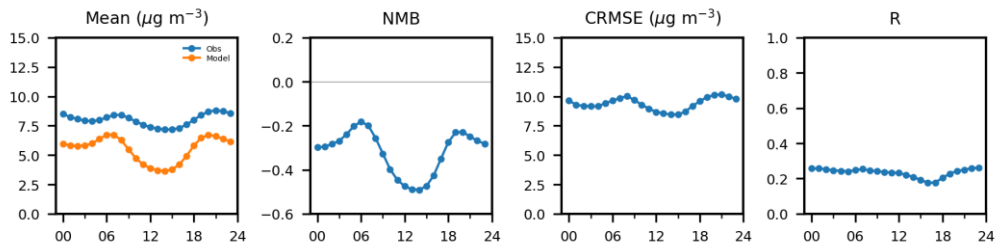


Figure 9. Time series of diurnal (a) observed and [RAQDPS-OP023](#)-predicted ~~annual-mean~~ hourly NO_2 ~~volume mixing ratio~~ VMR (ppbv) and (b) NMB, (c) CRMSE, and (d) R scores for all of 2021/22 for all NRT stations. Time is in hours LT.

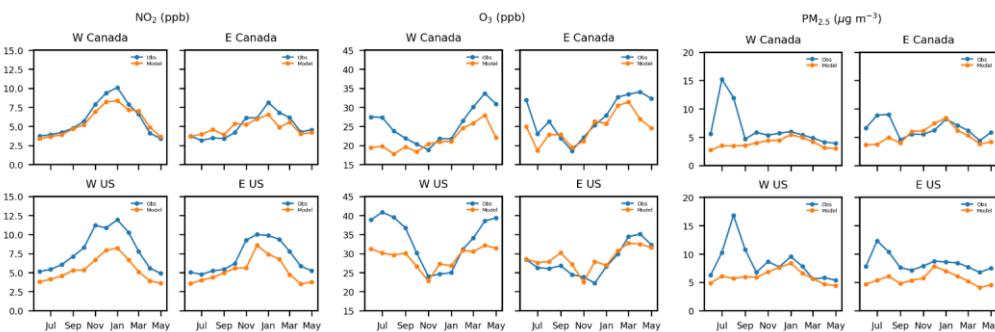
2945



2950 Figure 10. Time series of diurnal (a) observed and RAQDPS-OP023-predicted annual-mean hourly O₃ volume mixing ratio (ppbv) and (b) NMB, (c) CRMSE, and (d) R scores for all of 2021/22 for all NRT stations. Time is in hours LT.

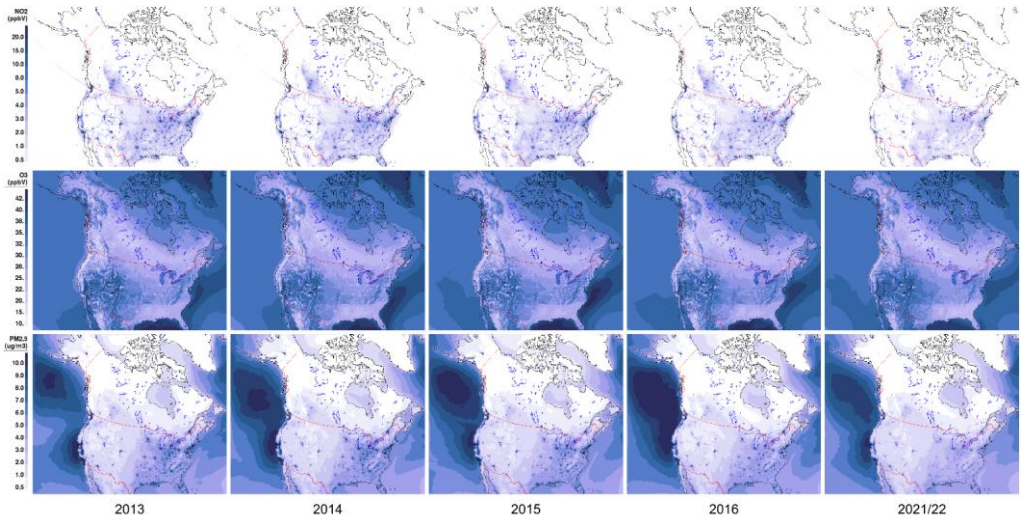


2955 Figure 11. Time series of diurnal (a) observed and RAQDPS-OP023-predicted annual-mean hourly PM_{2.5} concentration (µg·m⁻³) and (b) NMB, (c) CRMSE, and (d) R scores for all of 2021/22 for all NRT stations. Time is in hours LT.



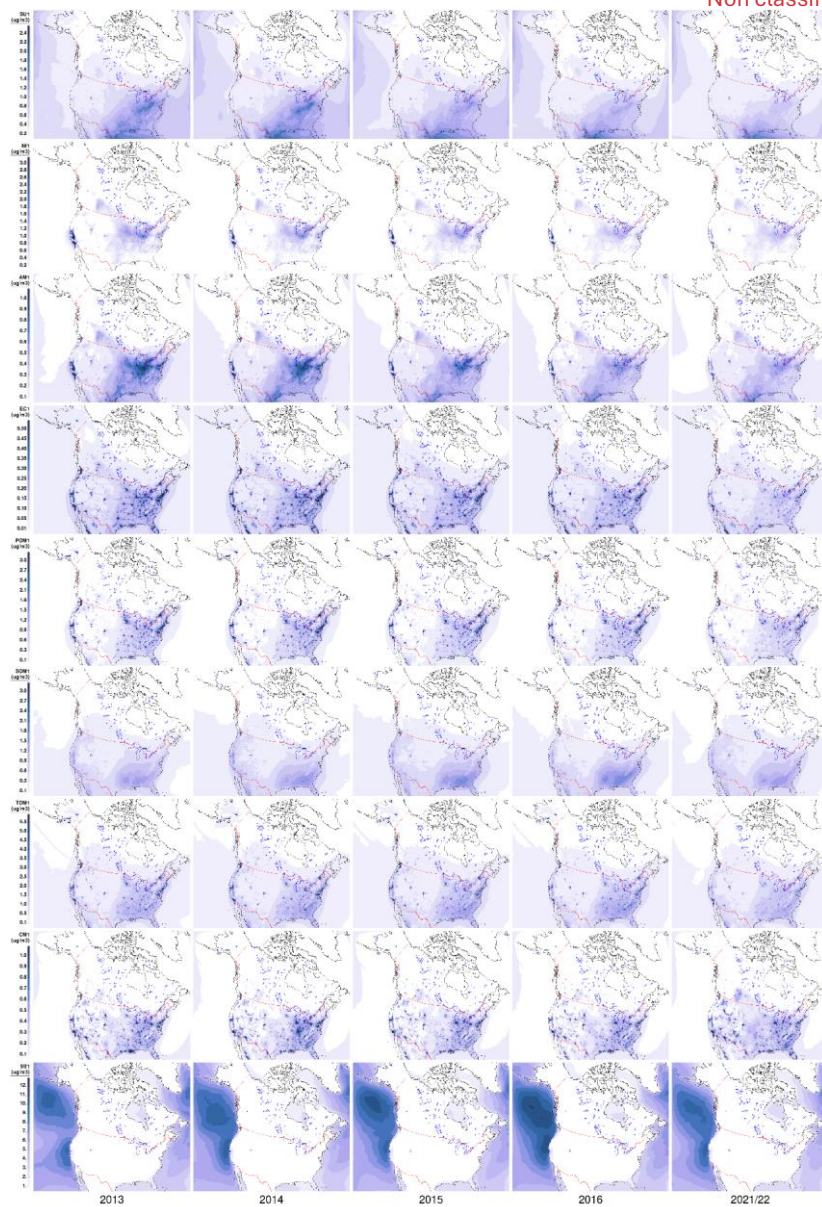
2960 Figure 12. Time series of monthly observed and RAQDPS-OP023-predicted annual-mean hourly (left) NO₂ volume mixing ratio (ppbv), (centre) O₃ volume mixing ratio (ppbv), and (right) PM_{2.5} concentration (µg·m⁻³) for all NRT stations in LT but stratified into four regions [see Fig. S7] for 2021/22. Orange curves denote predicted monthly values and blue curves denote observed monthly values.

2970



2975

Figure 13. Spatial distribution of **RAQDPS-OP023**-predicted **mean annual-mean** abundances of hourly (top row) NO₂, (middle row) O₃, and (bottom row) PM_{2.5} total mass for five years (from left to right, 2013–2016 and 2021/22). Units are ppbv, ppbv, and µg·m⁻³, respectively.



4980 Figure 14. Spatial distribution of RAQDPS-OP023-predicted mean-annual-mean ambient surface concentrations of nine daily PM_{2.5} chemical components ($\mu\text{g}\cdot\text{m}^{-3}$) for five years (from left to right, 2013–2016 and 2021/22). These components are SO₄, NO₃, NH₄, EC, POM, SOM, TOM, CM, and SS (in rows ordered from top to bottom).

Formatted: Subscript

Formatted: Subscript

Formatted: Subscript

CSN+IMPROVE+NAPS Speciated $PM_{2.5}$ ($\mu g m^{-3}$)

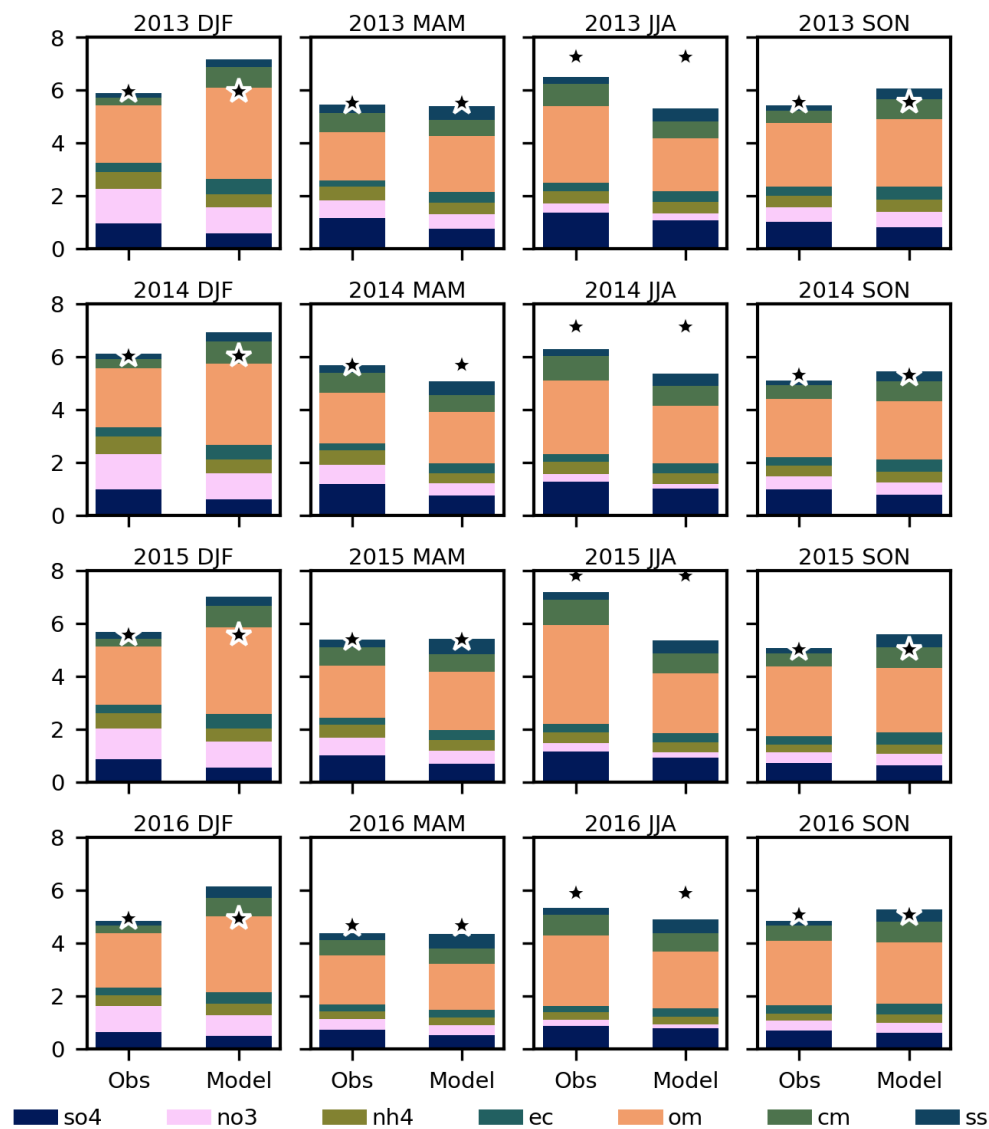


Figure 15. Stacked bar graphs of observed vs. **RAQDPS-OP023**-predicted domain-wide season-mean $PM_{2.5}$ chemical component concentrations ($\mu g m^{-3}$) based on combined CSN, IMPROVE, and NAPS $PM_{2.5}$ speciation daily measurements and hindcasts for four consecutive years. The top row corresponds to 2013 seasons, the next two rows below to 2014 and 2015 seasons, and the bottom row to 2016 seasons. Each row has four seasonal bar-graph pairs (observed and predicted), starting with winter (DJF) on the left, and then spring (MAM), summer (JJA), and autumn (SON) on the right. The stars mark the measured or predicted season-mean gravimetric $PM_{2.5}$ total mass.

Formatted: Font: 11 pt

2985

2990

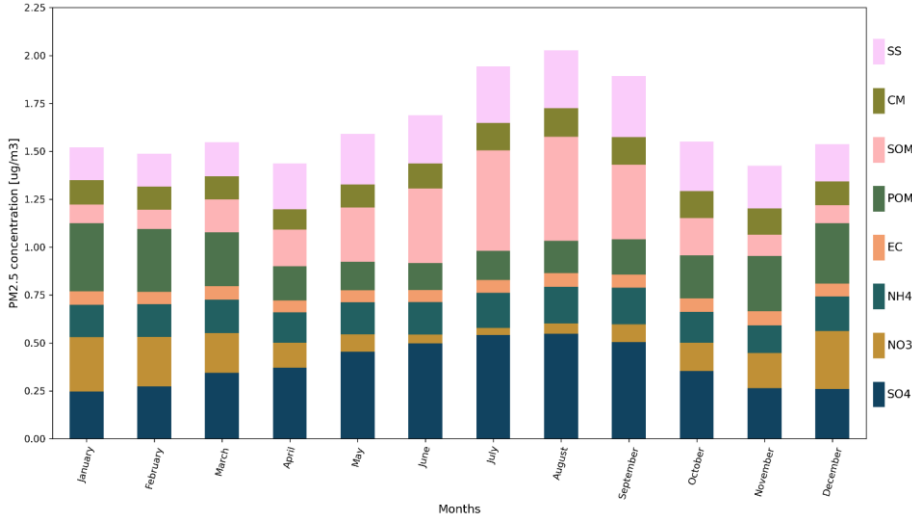


Figure 16. Time series of **RAQDPS-OP023**-predicted monthly mean variation of eight daily PM_{2.5} chemical component concentrations ($\mu\text{g}\cdot\text{m}^{-3}$) area-weighted averaged over North American continent grid cells and 2013 to 2016 simulations. These components are SO₄, NO₃, NH₄, EC, POM, SOM, CM, and SS (shown ordered from bottom to top in stacked bar graphs).

Formatted: Subscript
 Formatted: Subscript
 Formatted: Subscript

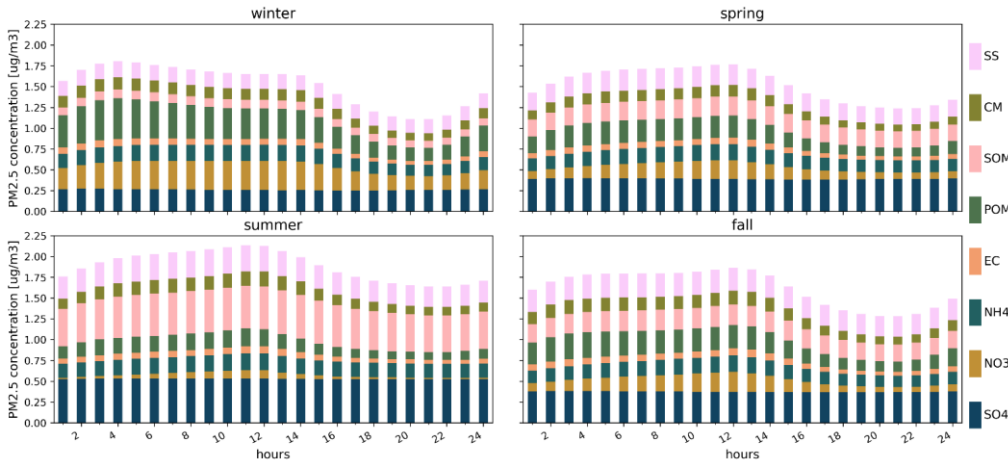
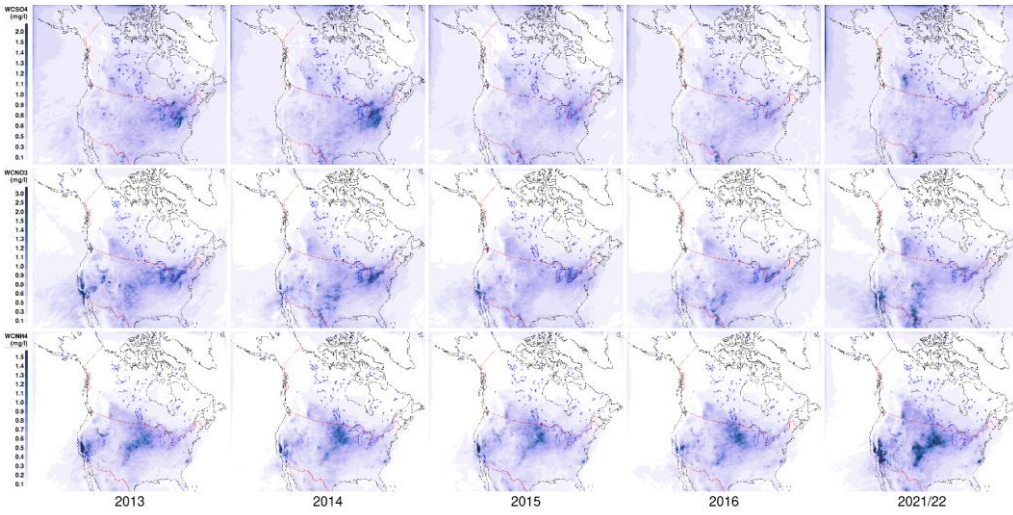


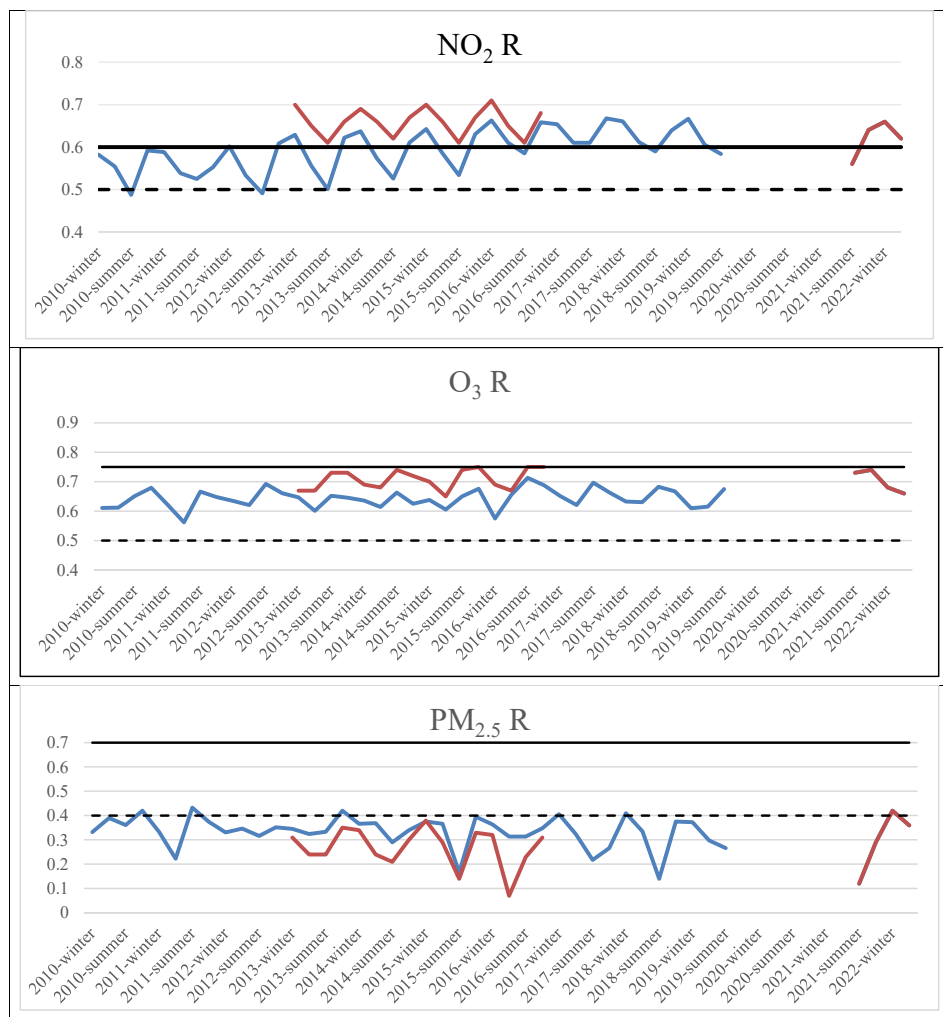
Figure 17. Time series of **RAQDPS-OP023**-predicted **season**-mean diurnal (UTC) variation of eight hourly PM_{2.5} chemical component concentrations ($\mu\text{g}\cdot\text{m}^{-3}$) area-weighted averaged over North American continent grid cells and 2013 to 2016 simulations for each of four seasons: (a) winter; (b) spring; (c) summer; and (d) autumn. These components are SO₄, NO₃, NH₄, CM, SS, EC, POM, and SOM (shown ordered from bottom to top in stacked bar graphs).

Formatted: Subscript
 Formatted: Subscript
 Formatted: Subscript



3010 Figure 18. Spatial distribution of RAQDPS-OP023-predicted mean annual-mean concentrations in precipitation ($\text{mg}\cdot\text{L}^{-1}$) of (top row) SO_4^{2-} , (middle row) NO_3^- , and (bottom row) NH_4^+ for five years (from left to right, 2013–2016 and 2021/22).

3015



3020

Figure 19. Time series of season-mean correlation coefficient (R) scores for surface (top) NO₂, (middle) O₃, and (bottom) PM_{2.5} hourly abundances for all available North American NRT measurement stations for the periods Jan. 2010–June 2019 and June 2021–May 2022. The solid blue line denotes scores for the operational RAQDPS at the time while the solid orange-red line denotes scores for the RAQDPS-OP023 forecasts and hindcasts. The dashed and solid black lines mark the “acceptable” and “good” benchmark thresholds, respectively, taken from Emery et al. (2017) for O₃ and PM_{2.5} and from Zhai et al. (2024) for NO₂.